

https://dspace.org/

Raw material sourcing and economy from the Acheulean Open-Air Site of Maropeng, Cradle of Humankind, South Africa.

Tasker, Daniel

2020
https://hdl.handle.net/10539/31057

Downloaded from a DSpace repository. https://dspace.org/

Raw Material Sourcing and Economy from the Acheulean Open-Air Site of Maropeng, Cradle of Humankind, South Africa.

Daniel Tasker

940079

A Dissertation submitted to the Faculty of Science, University of the Witwatersrand, Johannesburg, in fulfilment of the requirements for the degree of Master of Science

FACULTY OF SCIENCE UNIVERSITY OF THE WITWATERSRAND, JOHANNESBURG

2020

Declaration

I, Daniel Tasker, declare that this dissertation “Raw Material Sourcing and Economy from the Acheulean Open-Air Site of Maropeng, Cradle of Humankind, South Africa” is my own unaided work. It is being submitted for the Degree of Master of Science in Archaeology at the University of the Witwatersrand, Johannesburg. It has not been submitted before for any degree or examination at any other University.



_____

Daniel Tasker

5 October 2020, Johannesburg

Abstract

The Earlier Stone Age lithic assemblage discovered on the Maropeng property is a palimpsest of Acheulean stone tool materials and is one of only two published open-air Earlier Stone Age sites within the Cradle of Humankind World Heritage Site. Research on excavated lithics found that quartzite dominates as the raw material of choice in the assemblage, represented by 65.4% of the pieces. To date, no investigations have attempted to provenance the quartzite artefacts, nor explore the landscape-use behaviours. To determine the raw material source locations and transport distances, geochemical testing was applied to a subsample of cores from the Maropeng excavated assemblage and the quartzite outcrops within a three kilometre radius of the Maropeng property. Thereafter, reduction intensity data, calculated from 22 Large Cutting Tools and 60 cores, were compared to the geochemically determined possible origins. In turn, statistical correlations between outcrop distance and reduction intensity were used to interpret mobility and landscape-use behaviours. Results indicate the area hosts a multitude of quartzite outcrops, providing a broad variety of quartzite lithologies from which hominins around one million years ago could choose. Utilising variation and clustering statistical techniques, 12 of the 14 artefacts analysed through geochemical methods were linked to geological samples and probable outcrops. This research suggests hominins accessed quartzites from various locations across the landscape up to a range of 2.8 kilometres from the site of discovery. This study presents preliminary insights into the abilities of Acheulean tool manufacturing, the economy thereof, and early hominin behaviour in this region, at a landscape scale.

Acknowledgements

First and foremost, may my supervisors Dominic Stratford and Matt Caruana, be thanked beyond belief. Both of you don't understand the amount of mentorship, leadership, faith, values and strength I draw from your inspiration. These years have not been the easiest, and you have sat with me through the storm. I always knew that I could count on you. I will treasure you for the rest of my life. Your precious time you have invested in me I swear will not be wasted. Both of you are the best researchers I know, and I want for you to know that you are making a difference in furthering humanities knowledge with every discovery you make. You deserve all the success you have and way more.

My funding bodies: The Palaeontological Scientific Trust, and the Department of Science and Technology – National Research Foundation, deserve a huge thanking for their support in paying for my tuition and the ICPMS. Without their support I would not have been able to afford a Masters degree. Lastly, not to forget Dom and your gracious funding for the P-XRF results.

I would like to thank Prof. Robert Bolhar for your guidance, you go beyond just a professional and truly do help those in need. I would like to thank Zubair Jinnah for his wonderful insight. I would also like to thank the Earth lab team Marlin, Allan and Sarah for all their help.

I would like to thank Peter, Kelitha and Rosa as my older and wiser peers.

I would love to thank Heidi, my partner, my "whatever I do, we do" partner. Thank you for bringing me out of the dark times and making my life the happiest it's ever been. Thank you for making me live life to the fullest again and happily spending long nights with me, in the lab.

My Mom, my Dad and Talitha. Your ever-loving selves and interest in me will not go unforgotten. Your sacrifices are not in vain and I will make sure to carry your love and thoughts wherever I go. Thank you for your understanding and effort put into my growth. I love you.

I would love to thank Jessi, Brad, Luke and Omi for your ever-giving love and resources. There is a really lovely reason that we are so close and it's because of you.

I would love to thank everyone in my life that has gotten me this far, my family and friends. You are my reason.

Table of Contents

Declaration……..……..……..ii

Abstract……...……iii

Acknowledgements……..iv

Table of Contents……v

List of Figures……..……..…....viii

List of Tables…….……...x

Chapter 1: Introduction……..…1

1.1 Introduction……1

1.2 Rationale……..…3

1.3 Research Questions……4

1.4 Aims……...4

1.5 Organisation of Thesis…….…..5

Chapter 2: Literature Review……6

2.1 The Acheulean Industry……6

2.2 Earlier Acheulean Sites South Africa…….…….……..9

2.2.1 Canteen Kopje……9

2.2.2 Rietputs 15……10

2.2.3 Lower Sundays River……...…11

2.2.4 Wonderwerk Cave……..…..11

2.3 Open-air Acheulean sites in the Cradle of Humankind Region……...…12

2.3.1 Wonderboom……...….12

2.3.2 Elandsdrift Farm…….…..12

2.4 Acheulean cave sites in the Cradle of Humankind……...13

2.4.1 Sterkfontein Cave……13

2.4.2 Swartkrans Cave……...14

2.4.3 Linking open-air sites to karstic sites……...15

2.5 The Maropeng Acheulean Site……16

2.5.1 Geology and geomorphology…….…..17

2.6 Raw material sourcing……..20

2.6.1 Quartzite sourcing……...…….21

2.6.2 Solution/Acid Digestion-Inductively Coupled Plasma- Mass Spectrometry artefact provenance sourcing……..…..29

2.6.3 Portable X-ray Fluorescence artefact provenance sourcing…….……30

2.7 Hominin mobility and the raw material economy…….……31

2.7.1 Landscape Use and Raw Material Economy…….……..31

2.7.2 Reduction intensity……..33

Chapter 3: Methodology……35

3.1 Materials……...….35

3.1.1 The Assemblage……...35

3.1.2 Geological Surveying……...36

3.1.3 Biases……...37

3.2 Methods……...……..37

3.2.1 Macroscopic Lithological Quantification Methods……..37

3.2.2 Geochemical Methods…….……...…..38

3.2.3 Technological Methods……...…41

3.2.4 Reduction Intensity Analysis……...……..….46

3.2.5 Statistical Methods for Provenance…….……47

3.2.6 Digital Mapping……..48

Chapter 4: Results……..49

4.1. Surveyed Quartzite Outcrops……...53

4.2 Macroscopic lithological analysis……68

4.2.1 Texture……...…….69

4.2.2 Grain Visibility……72

4.2.3 Banding……72

4.2.4 Colour……..……76

4.3 Technological analysis…….82

4.3.1 Cores…….……82

4.3.2 Large Cutting Tools..……...85

4.4 Reduction intensity……..……..…..86

4.4.1 Scar Density Index…….…..87

4.5 Geochemistry……..…….91
4.5.1 Calculating variance……94
4.6 Quartzite provenance predictions…….…..102
Chapter 5: Discussion ……103
5.1 Geochemical characterisation of the landscape……..103
5.1.1 The landscape……103
5.1.2 Outcrops……104
5.1.3 Macroscopic lithological traits in artefacts and geological samples…….105
5.1.4 Geochemical characteristics……..106
5.2 Landscape-use and raw material economy characterisation……..107
5.2.1 Reduction intensity at Maropeng……..107
5.2.2 Comparison to Moll (2017)……...……107
5.2.3 Raw material economy of Maropeng……109
Chapter 6: Conclusion ……...….111
6.1 Further research……..112
Reference List……...……113
Appendix…….……..130

List of Figures

Figure 1.1: Acheulean sites of South Africa…….……1

Figure 1.2: The Cradle of Humankind, Gauteng, South Africa…….……2

Figure 2.1: Quartzite outcroppings plotted upon a geological map…….……....18

Figure 3.1: Core typologies based on reduction strategies…….....…..43

Figure 3.2: An example of basic characteristics on lithic morphology……44

Figure 3.3: Edge angles of flaked pieces……..……....45

Figure 4.1: The geological map of 2527DC, with Maropeng indicated……..…50-51

Figure 4.2: Maropeng Inland Outcrop 1, looking north across the exposure……...54

Figure 4.3: Maropeng Inland Outcrop 2, looking south in front of the exposure…….…..…..55

Figure 4.4: Maropeng Inland Outcrop 3, looking north behind the exposure……..56

Figure 4.5: Maropeng Inland Outcrop 4, looking north across the exposure…….……..57

Figure 4.6: Maropeng Inland Outcrop 5, southern portion of the outcrop, looking east…....58

Figure 4.7: Maropeng Inland Outcrop 5, northern portion of the outcrop, looking west.....…59

Figure 4.8: Quartzite Mountain shown from far, looking north……...……....60

Figure 4.9: Visagie Mountain Outcrop shown from far, looking north…..…….....61

Figure 4.10: Mogales Gate Quartzite Outcrop, looking south towards the exposure……..62

Figure 4.11: Fynbos Farm Outcrop 1, looking south across the exposure……..….63

Figure 4.12: Fynbos Farm Outcrop 2, looking north towards the exposure……....64

Figure 4.13: Grazing Outcrop 1, looking north across the exposure…….…..65

Figure 4.14: Grazing Outcrop 2, looking east across the exposure……..……...66

Figure 4.15: Quantification of geological sample textures …….……69

Figure 4.16: Quantification of artefact textures…….…….……70

Figure 4.17: Quantification of LCT textures……..……..71

Figure 4.18: Quantification of core textures…….……...…72

Figure 4.19: Quantification of geological sample banding …….……..……..73

Figure 4.20: Quantification of artefact banding …….……..…74

Figure 4.21: Quantification of LCT banding ……..……..…75

Figure 4.22: Quantification of core banding …….……..…76

Figure 4.23: Colours present in geological samples ……..……..77

Figure 4.24: Colours present in artefacts ……..……...78

Figure 4.25: Colours present in LCT samples ……..……...79

Figure 4.26: Colours present for bifacial flaking strategies …….……..…..80

Figure 4.27: Colours present in multifacial flaking strategies …….……...81

Figure 4.28: Colours present in unifacial flaking strategies……..……...82

Figure 4.29: SDI values calculated across reduction strategies …….……...…..88

Figure 4.30: SDI values across LCT types……..…….89

Figure 4.31: LCT and core SDI variability within the Maropeng assemblage……....90

Figure 4.32: A linear regression plotting SDI by volume in flaked objects….....91

Figure 4.33: Parts per million values of elements across geological and archaeological samples, detected through AD-ICMPS…….……...93

Figure 4.34: Percentage values of elements across geological and archaeological samples detected though P-XRF……...…….94

Figure 4.35: Geological AD-ICPMS samples displayed in hierarchical cluster dendrograms…….95

Figure 4.36: Geological P- XRF samples displayed in a hierarchical cluster dendrogram…..97

Figure 4.37: Archaeological and geological AD-ICPMS samples displayed in a hierarchical cluster dendrogram…….…….….99

Figure 4.38: Archaeological and geological P-XRF samples displayed in a hierarchical cluster dendrogram…….……..…..101

Figure 4.39: Line regression scatter plotting SDI by distance of geochemically artefacts…102

List of Tables:

Table 2.1: Summary of quartzite provenance studies…….…….24

Table 3.1: Examples of core technological attributes……..……....42

Table 3.2: Example of LCT technological attributes…….……..45

Table 4.1: Quartzite outcrops tabulated by size, GPS locations, bearing and distance from source……...53

Table 4.2: Geological samples by macroscopic properties…….…….66

Table 4.3: Descriptive analysis of core technologies attribute……..……...84

Table 4.4: Descriptive analysis of LCT technological attributes…….……84

CHAPTER 1: Introduction

1.1 Introduction

Maropeng (25°58'0.83"S, 27°39'7.45"E, Figure 1.1), the main interpretive museum of the Cradle of Humankind World Heritage Site (COHWHS) was built in the early 2000s and during its construction, an open-air, Acheulean tool-bearing deposit was discovered near the eastern border of the property (Pollarolo *et al.* 2010). This deposit is a clast-supported, artefact-rich, palimpsest known as the artefact-bearing horizon (ABH) (Pollarolo *et al.* 2010; Morrisey 2015), containing lithics attributed to the Earlier Acheulean industry (Pollarolo *et al.* 2010; Moll 2017). The ABH was formed through the gradual colluvial accumulation of artefacts and sediments into the shallow topographic depressions of the Maropeng landscape (Pollarolo *et al.* 2010; Morrisey 2015). So far, due to the burial depth and formation processes, absolute dating techniques (i.e., optically stimulated luminescence, cosmogenic nuclide dating) would have been unsuccessful in determining an age for the artefact-bearing unit or the underlying and overlying sediments. Instead, relative dates of more than one million years old have been suggested based on the typology of the ABH-derived lithic assemblage (Pollarolo *et al.* 2010; Moll 2017).

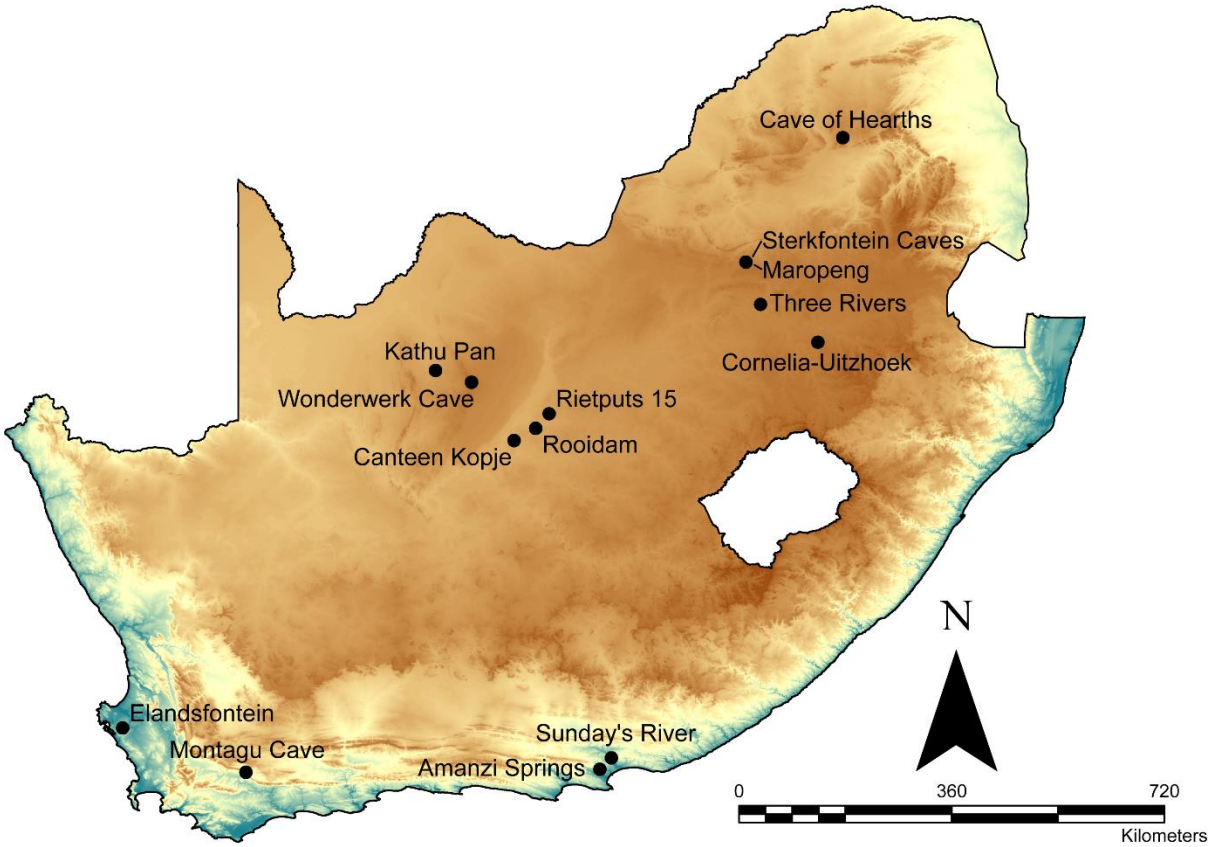


Figure 1. Selected Acheulean sites of South Africa

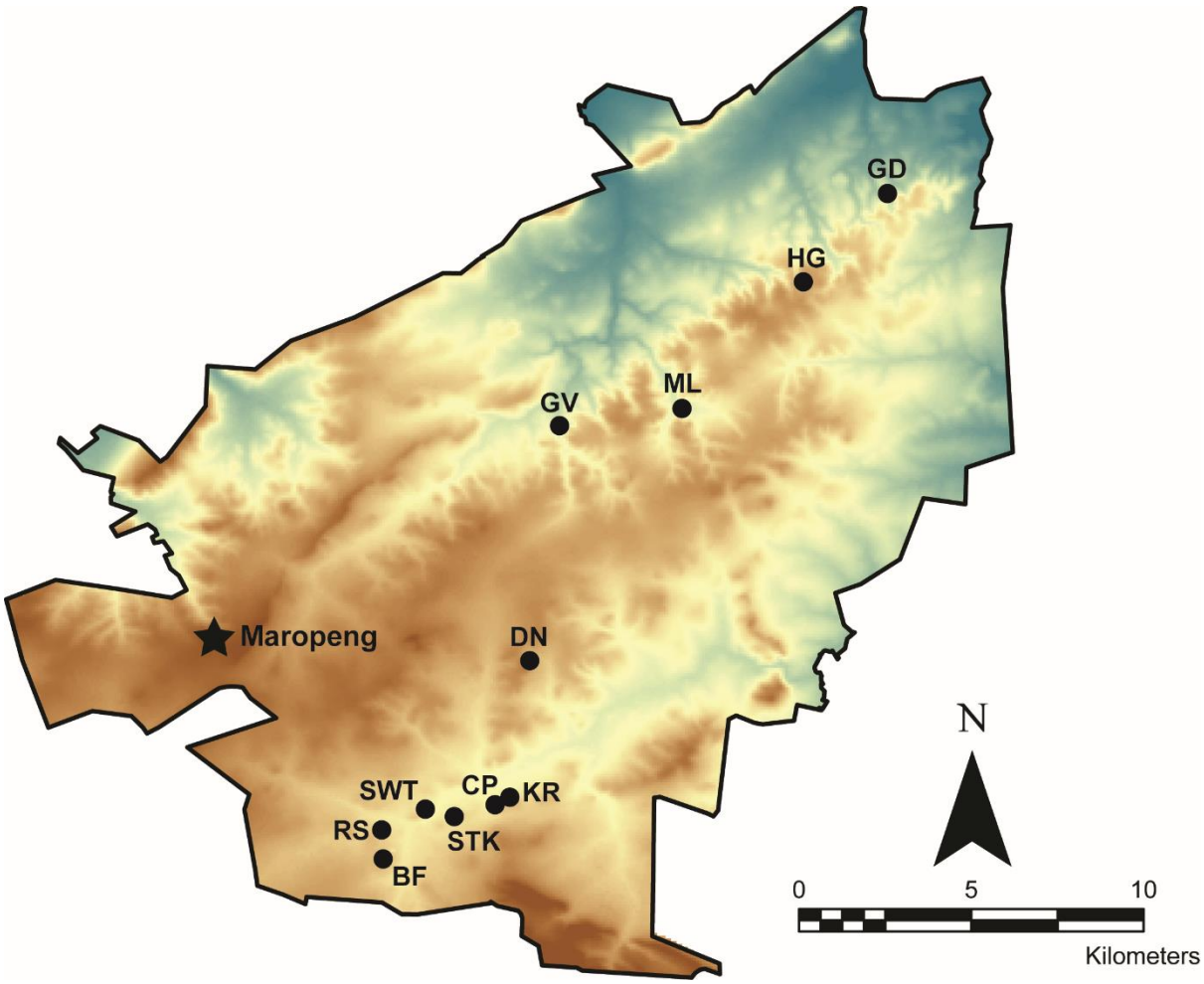


Figure 2. The Cradle of Humankind World Heritage Site, Gauteng, South Africa, showing the location of Maropeng in relation to the other prominent fossil- and lithic-bearing sites. Abbreviations: STK= Sterkfontein, SWT= Swartkrans, GV= Gladysvale, DN= Drimolen, KR= Kromdraai, CP= Coopers, BF= Bolt's Farm, RS= Rising Star, HG= Hasgaat, GD= Gondolin.

Three investigations have been undertaken at Maropeng. The first was a preliminary study with the goal of describing the site's formation and the technology (Pollarolo et al. 2010). This concluded that long periods of deflation contributed to the accumulated colluvial pavement. Colluvium, containing clasts and artefacts, were proposed to have accumulated from the large quartzite outcrop south of the site, which, during accumulation, collected artefacts discarded on the landscape (Pollarolo *et al.* 2010). Descriptive and comparative analysis of the artefacts suggested the buried assemblage dated to the Earlier Acheulean (Pollarolo *et al.* 2010). In the second study, Morrissey (2015) undertook a landscape-scale, geomorphological investigation of the Maropeng property, focusing on sedimentological characteristics of the ABH-bounding sediments, and spatial distributions of the ABH, with

the goal of characterising the formation and spatial variability of the ABH across the Maropeng landscape. Sedimentological and clast characteristics in relation to the local geomorphology suggested that multiple sediment sources contributed to the accumulation of the ABH from various local highpoints on the landscape (Morrissey 2015). The varied accumulation of materials was further clarified through suggested evidence of local lithic discard, as several artefacts unaffected by the characteristics of slope-wash, were discovered (Morrissey 2015). The third investigation by Moll (2017) conducted a more detailed technological study of the lithics based on an assemblage from expanded excavations, with the goal aimed at characterising the lithic technocomplex and by extension, the likely age of the lithic assemblage. Her techno-typological analysis used core flaking patterns to conclude that the time-averaged palimpsest accumulated through the Earlier Acheulean, ~1.76- 1 Mya (Moll 2017).

Maropeng's ABH lithic assemblage is characterized by raw materials such as quartzite, quartz, andesite, dolerite and chert (Pollarolo *et al.* 2010; Moll 2017). Initial research on lithics from *ex situ* and test pit contexts indicated a dominance of quartzite in the assemblage (Pollarolo *et al.* 2010), and an expanded excavation at Maropeng confirmed that 65.4% of 693 artefacts were made on this material (Moll 2017). Recent investigations have observationally identified differences in quartzite types within the ABH assemblage based on colour and texture (i.e., grain size), a darker (brown to red) fine-grained quartzite and a lighter, coarser-grained type (Moll 2017). Moll also observed that these lithological qualities may link to possible differences in flaking properties, exploitation strategies and selection behaviours, which has yet to be explored at Maropeng.

1.2 Rationale

Raw material transport and reduction behaviours are important factors for understanding foraging strategies and landscape use of Acheulean hominins. Investigating these processes are also important for reconstructing technological, cultural, and cognitive evolution (Plummer 2004; Stout 2011). Transport distances have been closely linked to reduction intensity in retouched tools and cores (Kuhn 1991; Marks *et al.* 1991; Brantingham 2003; Braun & Harris 2003; Kuhn 2004; Braun 2005; Wallace & Shea 2006; Blumeschine *et al.* 2008; Braun *et al.* 2008a; 2009; Caruana *et al.* 2019). At some archaeological sites, a linear

relationship between the reduction of raw materials and distances to sources has been detected, suggesting that toolmakers conserved raw materials according to the distance travelled to sources (Wallace & Shea 2006; Braun *et al.* 2008a; Shipton & Clarkson 2015; Caruana *et al.* 2019). This research has used such data to outline 'raw material economies', where the relationship between raw material transport and reduction represents adaptive behaviours aiming to mitigate the energetic costs of producing stone tools (Kuhn 1991, 2004; Braun & Harris 2003; Braun 2005; Wallace & Shea 2006; Braun *et al.* 2008a; 2009; Caruana *et al.* 2019 Investigating these relationships helps contextualise Acheulean hominin adaptations, cognitive capacities and how they interact with the landscape. Few studies have focused on landscape-scale research questions in the COHWHS, and additionally most of our understanding of the archaeology of this region has focused on cave sites (Kuman 2003). The focus on Maropeng as an open-air site in the COHWHS region lends itself to examining aspects of raw material procurement and lithic production that will provide insight into foraging strategies and landscape use.

1.3 Research Questions

The dissertation attempts to answer the following research questions:

1. Is there a correlation between the proximity of raw material sources and reduction intensity at Maropeng?

2. What do these trends reveal about the economy of lithic production processes?

1.4 Aims

Two overall aims and 4 subordinate objectives were established:

1. Geochemically characterise artefacts and potential sources.
    - Objective 1. Survey possible raw material sources within a three km radius of the Maropeng archaeological site, geochemically distinguish different outcrops, and model distance using Geographic Information System (GIS) modelling.

- Objective 2. Compare geochemical characteristics between raw material sources and artefacts, through statistical methods.

2. Identify patterns of landscape-use through the assessment of reduction intensity.

- Objective 3. Determine reduction intensity values within the Maropeng large cutting tools (LCTs) (i.e., handaxes, cleavers, picks and bifaces) and cores (N=80) between quartzite types and then, compare raw material source distances to reduction intensities through statistical methods.

- Objective 4. Compare results with Moll's (2017) descriptions of core exploitation patterns at Maropeng to further characterise the economy of raw material use on a landscape-scale.

1.5 Organisation of thesis

This thesis is arranged into six chapters, the first being a brief introduction to the site, research history and the summary of the projects research questions and aims. Chapter two addresses the relevant literature surrounding the Earlier Acheulean within South Africa and investigates literature corresponding to open-air sites in the COHWHS. It further digresses into the geology and geomorphology, linking into literature discussing raw material sourcing methods. The chapter finally moves onto the concept of 'raw material economy' and hominin mobility, situating the research within current archaeological theory. The third chapter describes the methods used to attain results and is divided into three parts: 1) the collecting of the quartzite samples from outcrop source, 2) the analysis of the excavated artefacts, and 3) geochemical analyses. The fourth chapter presents the results of the morphological, geochemical and statistical analyses, which will be used to investigate evidence of hominin mobility and land use. The fifth chapter presents a discussion of these results in relation the raw material economy constricted to the Maropeng landscape. Chapter six will provide conclusions and suggest further research avenues.

CHAPTER 2: Literature Review

Lithic analysis studies offer a wide variety of approaches and methods for examining tool production processes in the past (Andrefsky Jr. 2005). Understanding behaviours in Acheulean tool production through different approaches allows for the examination of cognitive evolution (Deacon 1997; Coolidge & Wynn 2005; Stout *et al.* 2006; Amati & Shallice 2007; Stout 2010), raw material economies (Kuhn 1991; 2004; Braun *et al.* 2008a; Li *et al.* 2016; Presnyakova *et al.* 2018; Caruana *et al.* 2019) and organised tool-reduction strategies (de la Torre *et al.* 2003; de la Torre 2009; 2011; de la Torre & Mora 2018). By studying lithics and their production, important sites in southern Africa and the COHWHS (Cradle of Humankind World Heritage Site) hold the key to addressing vital research gaps regarding hominin cognitive capacities and landscape-use. This chapter outlines the conceptual and methodological framework for this study, by reviewing literature that addresses the following research fields. Section 2.1 discusses the emergence of the Acheulean industry in Africa. Following that, section 2.2 contextualises Earlier Acheulean open-air sites contained in the South African interior. Sections 2.3 and 2.4 introduce and characterise the Acheulean open-air and karstic sites located within the COHWHS. Section 2.5 introduces the importance of the Maropeng archaeological site, as well as its geology and geomorphology. The research field of raw material sourcing is discussed in section 2.6, with particular reference to quartzite sourcing, Portable X-Ray Fluorescence (pXRF) and Acid Digestion-Inductively Coupled Plasma Mass Spectrometry (AD-ICPMS) applications to source artefact raw materials. Finally, section 2.7 discusses approaches to reduction intensity, landscape-use and raw material economies to understand adaptive behaviours.

2.1 The Acheulean industry

The Acheulean industry, first described by Leakey (1971), is found at least 1.76 Million years ago (Mya) at the site of Kokiselei, Kenya (Lepre *et al.* 2011). The Acheulean is preceded by the Oldowan (2.6 Mya and 2.58 Mya) (Semaw 2000; Braun *et al.* 2019), where complex sourcing behaviours (Braun 2008a; 2008b) and multiple core reduction patterns emerge (De la Torre 2011), and the Lomekwian, the oldest known stone tool industry with simple flaked tools (3.3 Mya) (Harmand *et al*. 2015), however the context of the artefacts is disputed (Archer *et al.* 2020). During the Acheulean techno-complex, hominins first shape Large Cutting Tools (LCTs) like handaxes, picks, bifaces and cleavers, while regularly producing

flakes larger than 10cm (Kleindienst 1962; Sharon 2010). The Acheulean lasted until ~300 thousand years ago (Kya) in Africa when the Middle Stone Age (MSA) emerges (Deino & Mcbrearty 2002; Sahle *et al.* 2014). At certain sites in Africa, Acheulean technology continues after the development of the Middle Stone Age, such as at Middle Awash, Ethiopia, at 154 Kya (Clark *et al.* 2003).

Formalised tools initiate a fundamental change in technology, moving away from expedient behaviours (Hodgson 2015), to enlarged efforts in production, like resharpening (Bienenfeld & Andrefsky 1984; Shipton 2011). The LCTs are usually defined through partial or full bifacial edge working on large flakes (<10 cm), however unifacial examples are also observed (e.g., de la Torre *et al.* 2008; Li *et al*, 2014; Kuman *et al.* 2014). Through use-wear studies, LCTs are thought to be used in activities such as woodworking, digging, and animal butchery (Keely & Toth 1981; Schick & Toth 1993; Beyene *et al.* 2013; Solodenko *et al.* 2015; Toth & Schick 2019). LCTs are the first standardized formal tools to appear in the archaeological record, with many of them exhibiting bilateral symmetry and thinning, especially during the later parts of the Acheulean (Roe 1994; Clark 1999; McNabb *et al.* 2004; Lycett 2008; Hodgson 2015; McNabb & Cole 2015). The symmetry of handaxes (i.e., convergent, shaped tips and standardised symmetrical forms) is potentially not just a bi-product of bifacial flaking and more than likely represents intentional processes of tool shaping (McNabb *et al.* 2004; Hodgson 2015), which has been recorded through East African, European, and Asian assemblages (Shipton *et al.* 2019). East Africa plays a vital role in tracing the cognitive developments through analysing the production of LCTs, and with it, the rise of new *chaine operatiores* characterising Acheulean toolmaking from 1.76 – 1.3 Mya, as such, much inter/intra-site variability is witnessed (Gallotti & Mussi 2018).

Previously mentioned, Kokiselei 4 (1.76 Mya) represents the earliest presence of Acheulean LCTs (Lepre *et al.* 2011). This site was dated through argon-argon ($^{40}A/^{39}A$) methods on tephra layers, which were used to develop a complex chronostratigraphy at the site (Lepre *et al.* 2011). The lithic assemblage is made mostly on locally available basalt and aphiric phonolite and contains trihedral or quadrangle-like picks and uni/bifacially flaked handaxes, and a limited number of flakes and cores (Lepre *et al.* 2011). LCT production is seen to be crude and cores were inefficiently flaked (Lepre *et al.* 2011). The inability to manage core mass can be described as a partially exploitative reduction technique that exhibits no platform rejuvenation and artefacts are therefore abandoned early (de la Torre *et al.* 2011). The basic

toolmaking and poor formal tool manufacture at Kokiselei 4 encapsulates the upper limits of intellect, and speak to the gradual cognitive evolution during the Oldowan to Earlier Acheulean transition (Lepre *et al.* 2011).

Another Earlier Acheulean site potentially preserving the earliest evidence of LCTs is FLK West at Olduvai Gorge (Tanzania), dated to 1.7 Mya through $^{40}A/^{39}A$ techniques (Diez-Martin *et al.* 2015). The assemblage comprises of 2120 artefacts, made predominantly on Naibor Soit quartz as well as some on volcanic rocks and chert (Diez-Martin *et al.* 2015). LCTs are crude and lack distinct forms, while flake scars are non-invasive (i.e., do not penetrate into the central mass of the tool) (Diez-Martin *et al.* 2015). However, highly symmetrical handaxes co-occur within the same assemblage, contrasting the assumed simple knapping strategies of the Earlier Acheulean (Diez-Martin *et al.* 2015). Thus, shape variability within LCTs at FLK West, is likely correlated to behavioural aspects as opposed to cognitive capacities underlying stone-knapping skill (Diez-Martin *et al.* 2015). Witnessing symmetrical shaping behaviours at the beginning of the Acheulean speaks to the previously mentioned site variability (Gallotti & Mussi 2018), and helps characterise mental evolution in LCT production.

The Acheulean industry is marked by an advancement in hominin cognitive abilities, paralleled by the appearance and evolution of *Homo ergaster* (Gowlett 1986; Bar-Yosef & Belfer-Cohen 2001; Klein 2009). This period of human evolution in *Homo ergaster* is defined by encephalisation as average brain size expanded to 800 – 1250 cubic centimetres (Holloway 2000; Rightmire 2004). Increased consumption of animal tissue within the Acheulean is thought be an important aspect of human evolutionary patterns, including encephalization and the development of complex social structures (Shipman & Walker 1989; Schick & Toth 1993; Stanford 1996; Ambrose 2001). The increase in brain size was likely, in part, related to the development of larger, socially-complex groups that were dependent on high meat and animal fat diets, which in turn led to the development of more complex technologies (Schick & Toth 1993; Stanford 1996).

Geographically, the Acheulean is distributed across Africa, Middle East, Europe and Asia through dispersals from East Africa (Lycett & Cramon-Taubadel 2008).The spread of the Acheulean industry reached out of Africa initially at Ubediya (1.4 Mya, Bar-Yosef & Goren-Inbar 1993; Belmaker *et al.* 2002) and continued into Asia at places such as Attirampakkam

(1.5-1.1 Mya, Pappu *et al.* 2011) and Bose, (~0.8 Mya, Wang & Bae 2015) and finally Europe, at La Noira (0.7 Mya, Moncel *et al.* 2013). The earliest Acheulean appear in South Africa at sites such as Rietputs 15 (~1.3 Mya) (Gibbon *et al.* 2009; Kuman & Gibbon 2017; Leader *et al.* 2018) and Sterkfontein Member 5 West (Acheulean infill) (1.7- 1.4 Mya) (Kuman and Clarke 2000), which follow the appearance of this industry in East Africa (Kuman and Clarke 2000; Gibbon *et al.* 2009; Kuman & Gibbon 2017).

2.2 Earlier Acheulean Sites in South Africa

The Acheulean archaeological record in South Africa mainly consists of open-air sites on fluvial landscapes that are often difficult to date (Lotter and Kuman 2018). Large scale erosion across South Africa remains the main cause for poor site preservation and high abundance of deflated surface scatters (Kuman 1998; Lotter & Kuman 2018). Dated Earlier Acheulean sites outside the COHWHS include: Canteen Kopje, dating to ~1.5-1 Mya (Gibbon *et al.* 2013); the previously mentioned Rietputs 15; Lower Sundays River complex, dated to 1.37-0.65 Mya (Lotter & Kuman 2018); and Wonderwerk Cave dating to 1.5-1 Mya (Matmon *et al* 2012; Chazan 2015). Three Rivers is technologically thought to belong to the Earlier Acheulean as well but remains undated (Mason 1962), therefore it will not be discussed. Many other Acheulean sites dated to <1 Mya, exist across South Africa such as Amanzi Springs, Pniel, Doornlaagte, Cave of Hearths, Montagu Cave, Kathu Pan 1, Rooidam, Bestwood, Elandsfontein, Kudu Kopie and Cornelia-Uitzoek (for a review see Lotter & Kuman 2018). However, it should be noted, recent hominin remains were dated and they indicated that the oldest Acheulean occurrences of Cornelia-Uitzoek is 1.07-0.99 Mya (Brink *et al.* 2012). These sites will not be discussed due to their later chronology, as Maropeng has been attributed to the Earlier Acheulean (Pollorolo *et al.* 2010; Moll 2017).

2.2.1 Canteen Kopje

Canteen Kopje was discovered by diamond miners digging the river gravels along the Vaal, near the town of Barkly West (De Wit 2008). The site consists of two separate artefact bearing deposits, the Vaal River gravels, containing the Acheulean industry dating to ~1.5-1 Mya (Gibbon *et al.* 2013) and the overlying Hutton Sands, containing a Later Stone Age technocomplex (Chazan *et al.* 2013). The Acheulean at Canteen Kopje has seen numerous studies, however, controlled excavations only began in 1997 (Beaumont 1990; Beaumont & McNabb 2000; McNabb & Beaumont 2011; Lotter *et al.* 2016). The most recent excavations

at Canteen Kopje (Area 1 and 2, Pit 6) have provided finer details on the assemblage characteristics (McNabb & Beaumont 2011; Leader 2014). There was a clear preference for andesite, along with diabase, quartzite and minimal hornfels use (McNabb & Beaumont 2011; Leader 2014). Within Pit 6, the lowermost layer containing Earlier Acheulean, is characterised by the absence of prepared and organised core reduction strategies (Leader 2014). The Pit 6 Acheulean assemblage is mostly made up of flakes and debris, while the LCTs (N= 33) are dominated by cleavers (Leader 2014). The Victoria West industry, first described in 1929 (Goodwin 1929; Van Riet Lowe 1929) is also represented at the site, it dates to 1.3 Mya at Rietputs 15 (Leader *et al.* 2018), which is seen as the earliest prepared core technology (Li *et al.* 2017). The Victoria West industry is found in the uppermost gravel layers of Pit 6 with larger frequencies of LCTs (N= 113) and prepared core reduction strategies (Leader 2014). LCTs are preferably made on flakes as opposed to cobbles and are mostly cleavers, followed by handaxes (McNabb & Beaumont 2011; Leader 2014). Overall, most cores appear to be casually produced and represented by irregular, radial, chopper, and polyhedral core types (Leader 2014). A record of cognitive knapping limitations is seen in the record as Earlier Acheulean basal levels contain organised/unorganised and unprepared cores while, Victoria West Earlier Acheulean levels have highly organised, and prepared cores.

2.2.2 Rietputs 15

Rietputs 15 is located in Windsorton, Northern Cape just 1.5 km from the Vaal River (Leader 2009). Here, in the Vaal gravels, numerous ESA lithics have been collected from diamond mining activities (Leader 2009). The site has been dated through cosmogenic nuclide burial techniques, which produced ages from five different pits ~1.3 Mya (Gibbon *et al.* 2009; Kuman & Gibbon 2018: Leader *et al.* 2018). Ventersdorp lava and hornfels are the most common raw material type found in this assemblage across both Pit 5 and ACP (Artifact Collection Pit), while chalcedony and quartzite make up a smaller portion of toolstone use (Kuman & Gibbon 2018; Leader *et al.* 2018). ACP pit core types are seen as "simple" due to the larger proportions of bipolar reduction strategies, as well as multifacial and bifacial cores (Kuman & Gibbon 2018). This is contrasted by more organised cores of Pit 5, with 17% showing organised surfaces and even rare cases of preparation (Leader *et al.* 2018). LCTs at ACP appear to be smaller and on the low end of the dimension scale when compared to African Earlier Acheulean sites while LCT's at Pit 5 vary in size (Kuman & Gibbon 2018).

Handaxe shape variability across both pits seen in the Rietputs 15 formation attests to multi-purpose functions for these tools and site variability (Kuman & Gibbon 2018; Leader *et al.* 2018).

2.2.3 Lower Sundays River

Lower Sundays River complex contains three sites: Atmar, Penhill and Bernol, all preserved in alluvial river terrace deposits (Lotter & Kuman 2018). Atmar Farm is characterized by the poor preservation of artefacts that are highly abraded and dates to ~0.65 Mya (Granger *et al.* 2013; Lotter & Kuman 2018). Bernol Farm (~1 Mya) is characterized by better preservation with minimally abraded artefacts, as well as minimal fossil materials (Granger *et al.* 2013; Lotter & Kuman 2018). Penhill Farm (1.37 Mya) has 9904 artefacts, most being flaking debris while large amounts of formal tools (N= 510), cores (N= 206) and flakes (N= 469) were also recovered (Granger *et al.* 2013; Lotter & Kuman 2018). Quartzite (85%) is the most abundant raw material found in the Penhill assemblage followed by hornfels, silcrete, and an assortment of rarer materials (Lotter & Kuman 2018). This assemblage shows an emphasis on the utilisation of cobbles, due to its proximity to the river (Lotter & Kuman 2018). Casual, discoidal, and chopper cores are most frequently represented in the reduction strategies at Penhill (Lotter & Kuman 2018). Handaxes and cleavers are predominantly made on quartzite/siltstone and show little attention to the refinement of edges (Lotter 2016; Lotter & Kuman 2018). The less extensive shaping, thinning and edge working in LCTs, point to the early nature of the assemblage (Lotter & Kuman 2018). However, LCTs are only a small percentage of the formal tools at 9.6%, while scrapers (34%), denticulates (16%) and miscellaneously retouched pieces (22%) were more abundant (Lotter 2016; Lotter & Kuman 2018). Overall, cores and LCTs follow simple reduction sequences and a low reduction intensity suggesting that the assemblage may technologically be associated with the Earlier Acheulean (Lotter 2016; Lotter & Kuman 2018). Interestingly in LCT production flake blanks were preferred over abundant cobble sources and show a preference for core working to obtain large flakes.

2.2.4 Wonderwerk Cave

The only cave site preserving Earlier Acheulean assemblages outside of the COHWHS is Wonderwerk Cave (Chazan *et al.* 2008). The stratigraphic sequence at Wonderwerk preserves Oldowan, Acheulean, MSA and LSA (Chazan *et al.* 2008; Chazan 2015; Horwitz & Chazan 2015). The Earlier Acheulean comes from Strata 5-11 and has been dated to 1.78->1.07 Mya through paleomagnetic and cosmogenic burial methods (Matmon *et al* 2012; Chazan 2015). Most of the Acheulean materials are made on banded ironstone while chert and igneous rocks make up a small percentage of the raw material profile (Chazan 2015). Only small numbers of cores have been found, ~35 per Strata, with no core reduction trends published (Chazan 2015). Handaxes are the most represented LCT, they are non-invasively flaked and highly variable in shape meanwhile, in later stratigraphic levels there is a rise in handaxe flaking invasiveness, indicating reduction behaviours that are more complex (Chazan 2015).

2.3 Open-air Acheulean sites in the Cradle of Humankind Region

The COHWHS is of particular interest to this chapter, understanding the neighbouring Acheulean contexts and assemblages herein, enables the contextualisation of the Maropeng tool production and landscape.

2.3.1 Wonderboom

Wonderboom was discovered in the 1950s and lies approximately 30 km out of the COHWHS in Pretoria (Mason 1957, 1958). Excavations have yielded one of the largest Acheulean assemblages in the area (>5000 artefacts) (Mason 1957, 1958). The site was formed by the erosion of a diabase intrusion and local quartzites along a hillside, forming a talus of at least 12 m deep (Mason 1957, 1958). These materials appear to be mostly *in situ*, while some appear slightly weathered, due to them eroding from the hillsides into the valley floor (Mason 1957, 1958). Sediment acidity has led to an absence of faunal assemblages (Mason 1957, 1958). Preliminary observations of the LCTs and other lithic materials suggest that this assemblage may be affiliated with the Later Acheulean, although this requires further investigation (Mason 1957, 1958). Since the 1950s no work has been done on the site nor the lithic assemblage.

2.3.2 Elandsdrift Farm

Elandsdrift Farm was discovered in 2014, and is one kilometre west of the COHWHS boundary (Tasker 2017; Caruana, *et al*. 2019). The site has yielded a large, time averaged palimpsest of Acheulean and MSA artefacts (approximately 3000), formed through accretional colluvial processes (Tasker 2017; Caruana, *et al.* 2019). A selected sample was randomly chosen for analysis, numbering 204 flake elements, 134 cores and 55 LTC's (Tasker 2017; Caruana, *et al.* 2019). This sampled assemblage was dominated by quartzite (68%) use, followed by local diabase and quartz (20%), and chert (11%) (Tasker 2017; Caruana, *et al.* 2019). Bifacial and multifacial core reduction strategies predominate in the core sample, indicating a high frequency of core rotation in this assemblage (Tasker 2017; Caruana, *et al.* 2019). LCT flaking patterns and the overall absence of cleavers suggest the assemblage may also be affiliated with the Later Acheulean (Tasker 2017; Caruana, *et al.* 2019). Even though dating wasn't attempted, valuable information regarding raw material sourcing and the lithic production strategies were extrapolated (Tasker 2017; Caruana *et al.* 2019). Comparisons between raw material distance and reduction intensity allowed for landscape-scale behaviours to be investigated (Tasker 2017; Caruana *et al.* 2019). A 'ruggedness index' was also developed to understand true distance based on the amount of ascent and descent across the terrain to specific materials sources. Results found that possible source distance is linearly correlated to flaking intensity and that managing core mass through reduction was likely correlated with the energy spent in collecting raw materials (Tasker 2017; Caruana *et al.* 2019).

2.4 Acheulean cave sites in the Cradle of Humankind

Archaeological sites within the COHWHS are important for understanding the prehistory of South Africa, as karstic cave infills preserve archaeological and fossil assemblages. Being able to link and compare literature with direct associations to fossil hominins further aids in contextualising the mental capacity and raw material behaviours that characterise the area. Of cave sites in the COHWHS, only two have known, large Acheulean assemblages: Sterkfontein and Swartkrans.

2.4.1 Sterkfontein Cave

Sterkfontein is one of the most famous COHWHS sites and excavations in the younger Member 5 deposits yielded a *Homo ergaster* fossil directly associated with Acheulean stone tools (StW 80) (Kuman & Clarke 2000). Member 5 West formed as an underground talus of debris inflowing from cave openings in the roof of the chamber, which accumulated Earlier Acheulean materials from the landscape above (Kuman & Clarke 2000; Stratford 2011). Sterkfontein Member 5 West has yielded 701 Earlier Acheulean artefacts, comprised mostly of cores and pieces (72%), and dates to 1.7-1.4 Mya through relatively associated technology (Field 1999; Kuman & Clarke 2000; Kuman 2003; 2007), although this is debated for example, recent U-Pb dating has suggested an age of <1.8 Mya (Pickering & Kramers 2010) and paleomagnetic dating has suggested an age of 1.4-1.07 Mya (Herries & Shaw 2011). The Blaauwbank River is located within 500 m from the site where river cobbles were collected and knapped close to the site (82% of lithic show river-cobbles cortex) (Field 1999; Kuman & Clarke 2000; Kuman 2003). Large manuports and partly flaked cobbles were also brought to the site (Kuman 1994; Kuman & Clarke 2000). Most of the assemblage is made on quartzite in sharp contrast to the predominance of quartz in the Oldowan infill (>90%) (Field 1999; Kuman & Clarke 2000). Most cores show a range of 4-16 removals are made on fine-grained quartzite (Field 1999; Stratford 2008) The Member 5 West Acheulean assemblage is comprised of a small number of "crude" handaxes, large flakes (which LCTs were typically made from) and cleavers (Kuman 1994). The LCTs are considered to not be refined or unstandardized and their mass was inefficiently managed (i.e., limited thinning), as many handaxes are trihedal (i.e., 'pick-like') in shape (Kuman & Gibbon 2018). The simple nature of knapping separates it cognitively from the more advanced core reduction techniques seen in assemblages 1.5 Mya and onward (Kuman & Gibbon 2018).

2.4.2 Swartkrans Cave

Swartkrans Cave is located ~1.2 km away from Sterkfontein and is comprised of five stratigraphic units or Members, with Acheulean assemblages yielded from Members 2 and 3 (Brain 1993; Field 1999; Sutton 2012). Member 2 at Swartkrans has yielded the largest assemblage of Earlier Acheulean artefacts in the COHWHS (N= 887), although no LCTs have been found in situ at the site (Brain 1993). U-Pb dating of fossil bovid teeth from Member 2 have restricted its age to ~1.3 Mya (Balter *et al.* 2008). Gibbon *et al.* (2014) infer the age range of Member 2 could be between 1.8 ±0.09 and 0.96 ±0.09 Mya due to under- and over-lying cosmogenic nuclide burial dating of Members 1 and 3. Quartz, diabase,

quartzite and chert were utilised in the Members 2 and 3 Acheulean assemblages (Field 1999; Sutton 2012; Sherwood 2013). Sherwood (2013) was able to determine that raw material quality selection during the Acheulean slightly improved from previous Oldowan behaviours at Swartkrans. She also found a large increase (18.1%) in the use of quartzite within the Acheulean deposit, similar to Sterkfontein (Sherwood 2013). Sherwood (2013) concludes that Acheulean hominins in the Swartkrans area had a complex understanding of toolstone lithologies relating to knapping characteristics, opting for higher quality raw materials. Swartkrans Cave is closer to the Blaauwbank River than Sterkfontein and allows for easier access to plentiful quantities, suggesting variations in raw material procurement between the sites (Kuman & Clarke 2000; Caruana 2017). While karstic sites such as Kromdraai (sites A and B) and Gladysvale have provided other Acheulean deposits within the COHWHS, their artefact samples have been very limited (Kuman *et al.* 1997; Kuman 2003; Hall *et al.* 2006; Sutton *et al.* 2017). As such, Sterkfontein and Swartkrans with their adequate sample sizes and preservation conditions, remain important time capsules of Acheulean hominin behaviour.

2.4.3 Linking open-air sites to karstic sites

At the dawn of the Earlier Acheulean, simple and variable core reduction behaviours emerge (eg de la Torre *et al.* 2008; Lepre *et al.* 2011; Diez-Martin *et al.* 2015), this practice continues through the spread of the technology into southern Africa, where similar traits are seen at Swatrkrans, Sterkfontein and Rietputs 15 (Pollorolo *et al.* 2010; Kuman & Gibbon 2018). Simple flaking, limited rotation of the core mass and lack of organised cores reflect the Earlier Acheulean behaviours stated in this section, the only deviation from this is represented through later technology (e.g., Elandsdrift Farm). It should be noted however, that intra- and inter-site variability does play a role in differentiating between assemblages, alongside the introduction of prepared, (e.g., Li *et al.* 2017) and more organised core reductions (e.g., de la Torre 2009). Through technological studies of the Earlier Acheulean insight has been brought into a multitude of behaviours including knapping capabilities (e.g., de la Torre *et al.* 2008; de la Torre 2009; Sharon 2010; White *et al.* 2011; Gallotti & Mussi 2018; Leader *et al.* 2018), and intention (e.g., Beyene *et al.* 2013; Beyene 2013). The discussion of the Earlier Acheulean sets the framework for reviewing Maropeng, as technological behaviours have already been analysed (e.g., Pollorolo *et al.* 2010; Moll 2017). However, the research gap evident in South African Earlier Acheulean assemblages presents

itself of behaviours inferred through landscape-use. Landscape archaeology has long been used in open-air contexts (Isaac 1981; Blumenschine & Masao 1981; Stern 1991;1994; Blumenschine *et al.* 2003; 2008; Caruana *et al.* 2019) and does not confine to spatial limitations applied by 'site' conceptions (Barton *et al.* 1999; Cowan 1999; Bailey 2007). In archaeological literature, the focus on well stratified sites and layers with clear temporal and spatial resolutions has created a study bias (Bailey 2007), often ignoring open-air lithic scatter (Cowan 1999; Arrizabalaga *et al.* 2015; Caruana & Stratford 2018) and palimpsest sites (Barton *et al.* 1999; 2004; Fernández-López de Pablo and Barton, 2013). Palimpsests have been described as a reduction of the temporal aspects, through the reworking and superpositioning of material (Lucas 2005), however they hold vital importance in ascribing generalized long term archaeological processes to assemblages (Foley 1981; Bailey 2007). Karstic sites in the COHWHS have a limited catchment area, preserving only a portion of the lithics i.e., keyhole preservation (Kuman 2003; Kuman & Field 2009). Palimpsests are able to capture comparatively larger quantities of lithics due to increased catchment zones and time spans (Bailey 2007). The time-averaged accumulation of artefacts can equally be used to infer mobility and land use patterns (Stern 1994; Holdaway *et al.* 1998; Doelman *et al.* 2001). Therefore, through landscape-scale approaches, the temporally-generalised trends contained in the ABH at Maropeng, may be reconstructed.

2.5 The Maropeng Acheulean Site

Maropeng is the only open-air site located within the border of the COHWHS and was discovered by archaeologists Kathy Kuman and Ron Clarke when an interpretive museum was constructed on the property (Pollarolo *et al.* 2010). Earlier Acheulean artefacts (N = 512) were recovered from *ex situ* dumps, while another 200 were recovered from controlled excavations (Pollarolo *et al.* 2010). More recent excavations from five trenches (M1, M2, M3, M4, and South Pit) have increased this assemblage by another 693 artefacts, bringing the total to 1405 artefacts (Moll 2017). Only 12 LCTs were recovered but reflect low LCT recovery rates across the COHWHS (Moll 2017). Maropeng's assemblage is predominantly comprised of quartzite (65.4%) materials (Moll 2017), with lower counts of andesite, quartz and dolerite (Pollarolo *et al.* 2010; Moll 2017). Stone tools are found in a clastic artefact-bearing horizon (ABH) underneath up to 1 m of lateritic matrix, while the ABH reaches thickness measurements of up to 15 cm (Morrissey 2015). Sediment and clast transport

followed the natural low-energy slope-wash processes from the eastern quartzite ridge (later referred to as Quartzite Mountain), accumulating the ABH north and south of the geomorphological low relief depression or 'saddle' (Morrissey 2015). During the sediment flow, artefacts from various locations on the surface were entrained and deposited, after which surface flow winnowed and deflated the ABH into a clast-supported pavement. This created the time-averaged palimpsest that was further disturbed through varying turbatory processes, mixing and displacing artefacts from the ABH (Morrissey 2015). Stone tool abrasion rates were calculated to determine the degree of transportation undergone, and the heterogeneity of the results indicates local artefact discard (very fresh surfaces) and longer distance geogenic transport (heavy abrasion) (Morrissey 2015). LCTs exhibit primary and secondary shaping to create tips or working edges, and while thinning was attempted sparsely, it remained unsuccessful (Moll 2017). Blank shapes most often recorded were equant, tabular, and cobble-like, and had an influence in shaping thereof (Moll 2017). Maropeng cores exhibited expedient knapping, the inability to rejuvenate platforms and large numbers of unused flaking platforms (Moll 2017). Overall, cores and LCTs depict a preference for limited shaping and low reduction intensities and thus are in line with Earlier Acheulean lithic patterns (Moll 2017). However, the flakes exhibited larger reduction intensities in relation to cores, through a greater number of dorsal scars, reduced remaining cortex percentages and radial rotations (Moll 2017). This contrasting behaviour, usually seen in later assemblages, indicates the appearance of intense reduction sequences (Moll 2017). Molls (2017) results are further discussed in comparison with the results of this landscape-scale study in chapter five.

2.5.1 Geology and geomorphology of Maropeng

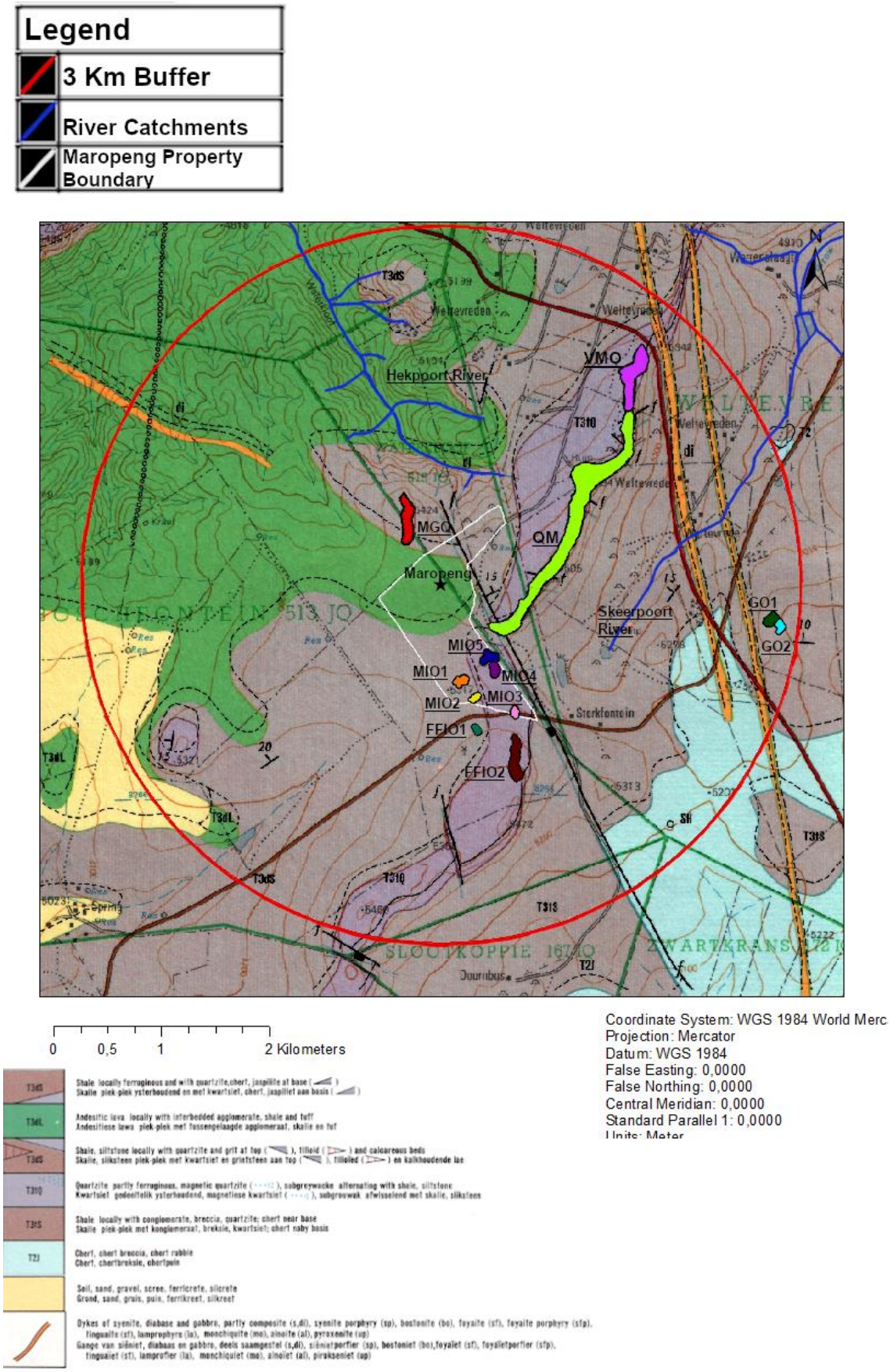


Figure 2.1 Quartzite outcroppings (underlined) plotted upon a geological map. Abbreviations: MIO1= Maropeng Inland Outcrop 1 (orange), MIO2= Maropeng Inland Outcrop 2 (yellow), MIO3= Maropeng Inland

Outcrop 3 (pink), MIO4= Maropeng Inland Outcrop 4 (dark purple), MIO5= Maropeng Inland Outcrop 5 (dark blue), QM= Quartzite Mountain (light green), VMO= Visagie Mountain Outcrop (purple), MGQ= Mogales Gate Quartzite (red), FFIO1= Fynbos Farm Outcrop 1 (green), FFIO2= Fynbos Farm Outcrop 2 (brown), GO1= Grazing Outcrop 1 (dark green), GO2= Grazing Outcrop 2 (light blue).

Geomorphologically, the landscape in the immediate vicinity of Maropeng is dominated by a saddle, sloping from east-west and then down either side in the north-south direction. Its elevation is around 1660 m above sea level with various sloping and rising elements present in different intensities (Morrisey 2015). There is a watershed that runs along the span of the saddle and a large quartzite outcrop forms a hill (1975 m) at the top of the east slope (Morrisey 2015). A river (Figure 2.1) courses in the valley one km north of the property, a valuable resource bringing rounded cobbles (this is seen in the archaeological record as previously mentioned blanks indicated some LCTs/cores are made on river cobbles). Another intermittent river (Figure 2.1) is situated about 1.5 km west and behind the later mentioned Quartzite Mountain outcrop. There are multiple quartzite outcroppings inside the Maropeng property that also extend just outside its borders (Figure 2.1). The largest outcropping of quartzite is a large hill to the west of the property (Quartzite Mountain, Figure 2.1) and was proposed to be the source of lithics by Pollarolo *et al.* (2010). The soil is largely of lateritic origin, formed through the decay of the local diabase intrusions that are present across the property.

Numerous lithologies are found exposed within three kilometres of the Maropeng property (Figure 2.1). The local geological sequence is part of the Transvaal Basin (Pretoria Group) just west of the lithological contact with the cave bearing, Malmani dolomites (Obbes 2000; Martini *et al.* 2003). Locally, the following Members are of particular relevance to the outcropping lithologies and geomorphology. The Timeball Hill Formation (2316 Mya) overlies the Rooihoogte Formation and contains mainly shales, quartzose sandstones that locally recrystalise into quartzites, lesser conglomerate lenses and diamictites (Catukeanu & Eriksson 2002; Hannah *et al.* 2004; Lenhardt *et al.* 2012). The Bushy Bend Lava Member within this Formation is represented by diabase intrusions (Lenhardt *et al.* 2012), that are present on the landscape. Figure 2.1 demonstrates the appearance of ferruginous shales and ferruginous quartzites dominating the stretch of Timeball Hill Formation exposed around the Maropeng property. The Rooihoogte Formation (2300 Mya), underlain by the previously mentioned Timeball Hill Formation, is mainly comprised of chert, silicious breccia and conglomerate (Button 1986; Lenhardt *et al.* 2012), represented in Figure 2.1 by chert. The

Hekpoort Formation which is exposed on the property and is mainly comprised of balsitic andesites and shales formed around 2250 Mya (Erikson *et al.* 1993; Lenhardt *et al.* 2012). Quaternary sediments, >2.6 Mya (Catukeanu & Eriksson 2002; Lenhardt *et al.* 2012), are also present around the Maropeng landscape. This geologically diverse zone holds multiple sources of varied quartzites in and around the area, which this study seeks to further understand.

2.6 Raw material sourcing

Raw material sourcing remains a vital component to understanding lithic assemblages and hominin behaviours related to lithic production. Raw material sourcing studies have been used to ascertain information regarding raw material quality selection behaviours (e.g.,, Stout *et al.* 2005; Goldman-Neuman & Hovers 2012; Sherwood 2013; McHenry & de la Torre 2018; Egeland *et al.* 2019) and raw material economy behaviours (e.g., Kuhn 2004; Wallace & Shea 2006; Blumenschine *et al.* 2008; Braun *et al.* 2009; Caruana *et al.* 2019). Geochemical analysis has been used within archaeology for interpreting raw material selection behaviours, by distinguishing specific outcrop sources and thus determining lithic transport ranges (e.g., Jercher *et al.* 1998; Braun *et al.* 2008a, 2008b, Prieto *et al.* 2018). In Africa, most sourcing studies have concentrated in East Africa along with the emergence of the lithic technology (e.g., Stout *et al.* 2005; Blumenschine *et al.* 2008; Braun *et al.* 2008a; Goldman-Neuman & Hovers 2012). In southern Africa, there a limited number of studies on raw material provenance, and most of it concentrates on MSA sites (e.g., Ambrose 2006; Nash *et al.* 2013a; 2013b; 2016). Examples of Later Acheulean assemblage provenance like the Elandsfontein dunes, have reported potential raw material source distances of 40 km and upwards (Braun *et al.* 2013). In the COHWHS, raw material landscape sourcing studies have not been able to provide complex ranges as the Blaauwbank river (the source of most lithics) is situated in such close proximity. Hominin ranges for raw material sourcing vary, but during the South African Earlier Acheulean, the quartz/quartzite river cobbles at Sterkfontein and Swartkrans (within 1 km) indicate a tethering to the raw material source (Kuman 2003). As outlined above, raw material sourcing can provide information of mobility, selection and raw material economies, section 2.6.1 focuses on quartzite provenance but yields insights into the techniques required to provide the aforementioned behaviours.

2.6.1 Quartzite sourcing

Quartzite is defined as a sedimentary or metamorphic rock with around 90% silica or quartz content (Howard 2005). Quartzite can metamorphosize to the extent that the individual quartz grains fracture straight through rather than break around their structures (Howard 2005). Within archaeology the term quartzite generally refers to both orthoquartzite and metaquartzite (Pitblado *et al.* 2008; Cnudde *et al.* 2013; Dalpra & Pitblado 2016; Prieto *et al.* 2018). Orthoquartzite is from sedimentary origin, while metaquartzite is from a metamorphic origin, only through petrography are these distinctions possible, due to variable petrogenesis exhibited within both types (Howard 2005). The term quartzite is used here as broad encompassing term of both types, as petrography will be a focus of further publications.

Quartzites are also characterized by a high degree of variation in homo- and heterogeneity that is often localised and intra-formational (Howard 2005; Cnudde *et al.* 2013; Prieto *et al.* 2018). Depending on high levels of homogeneity and petrogeneity, it can reach a value of 7 on the Mohs scale of hardness, making it a preferable material for knapping, which produces robust edges (Hay 1976; Ebright 1987; Braun *et al.* 2009; Sherwood 2013; Soto *et al.* 2020). On the other hand, low levels of petrogeneity (the amount of metamorphic processes the rock has undergone) and apparent flaws in non-homogenous quartzites have been a determining factor in their selection or lack thereof (Prieto *et al.* 2018). Sherwood (2013) tested multiple raw materials present in the COHWHS and found medium- and fine-grained quartzite was very high in durability, edge sharpness, and flake predictability. Quartzites despite being found in assemblages across the world, have been largely ignored in archaeological studies focused on raw material provenience (Pitblado *et al.* 2008; Cnudde *et al.* 2013; Dalpra & Pitblado 2016; Prieto *et al.* 2018). However, recently headway has been made in addressing the issue of sourcing quartzite, as discussed below. All presented studies in this section speak to the utilisation of quartzite across time and region, each presenting their unique challenges and their unique approaches to accurately provenance the quartzite.

Prieto *et al.* (2018) examined Northern Spain's Mousterian archaeological sites to determine differing mineralogical properties of quartzite, and traced varieties thereof, back to their source locations (Prieto *et al.* 2018). This preliminary study set out to understand the raw material use centred around two sites in the Cantabrian area, El Arteu and El Habario, both

technologically dated to the Mousterian 160-40 Kya (Prieto *et al.* 2018; 2020). El Arteu rock shelter is described as a hunting post with a high-frequency of non-cortical lithic elements and a majority of quartzite exploitation (93%) (Prieto *et al.* 2018). El Habario is described as an open-air, workshop site, with an abundance of unretouched, cortical pieces and a predominance of quartzite use (99%) (Prieto *et al.* 2018; 2020). Both assemblages are part of a larger network of regional sites and display abundant discoid core reduction patterns in quartzite (Prieto *et al.* 2018: 2020). XRF, petrography, and digital image processing were used in this study to differentiate quartzites (Prieto *et al.* 2018). Seventeen lithologically representative quartzites from the previously mentioned groups, were chosen for destructive thin sectioning where petrography and software such as *ImageJ* found identifying features to characterise the quartzite types (Prieto *et al.* 2018). Six quartzite groups present within the El Arteu and El Habario sites, were then identified based on their petrogenetic characteristics (Prieto *et al.* 2018). XRF data did not confirm the groupings the petrography depicted, which indicated the preferred use of primary sources at El Arteu while El Habario preferred higher quality secondary sources (Prieto *et al.* 2018). Landscape-scale conclusions show different occupations, utilising different quartzites based on location and material preference, yet further work is needed in establishing behaviours of the Northern Spanish Mousterian (Prieto *et al.* 2018).

In Belgium, Rheine-Meuse-Scheldt area quartzites used in the Mesolithic (10000-5000 BP) were geochemically distinguished (Cnudde *et al.* 2013). Within the same geological formation, two quartzite varieties (the coarse-grained Tienen and fine-grained Wommersom) were exploited for lithic production during the previously mentioned time period (Cnudde *et al.* 2013). The Tienen and Wommersom quartzites can potentially inform on landscape-use behaviours, covering a huge network distance of 80000m^2 during the European Mesolithic (Cnudde *et al.* 2013). This preliminary study examined which methods would allow characterisation of these two quartzite varieties and aids in setting up a method for eventual linkage of artefacts to their provenance (Cnudde *et al.* 2013). Cnudde *et al.* (2013) utilised the techniques of petrography, cathodoluminescence, x-ray micro-computed tomography scanning, and scanning electron microscopy with energy dispersive x-ray analysis, which allowed the study to determine the difference between quartzite varieties. While each test could not achieve accurate results alone, when combined, structural and chemical differences were detected (Cnudde *et al.* 2013). Further investigations into these approaches are needed

as only a small portion of observationally-distinct sample sizes were used (Cnudde *et al.* 2013).

Ongoing research since into North American quartzite use within the Upper Gunnison Basin has found that 90% of all artefacts during the Paleo-American occupation of this area (11000 – 8000 BP) were made of quartzite (Pitblado *et al.* 2013; Dalpra & Pitblado 2016). After vast surveying of 48 potential sources, petrographic methods were able to preliminarily establish five different quartzite varieties within the Paleo-American quartzite outcrops (Dalpra & Pitblado 2016). In this study, destructive thin sectioning and the 100 point 'point-count' method for petrography were carried out on 50 randomly selected thin sections (Dalpra & Pitblado 2016). These five varieties identified will then be linked in future research to lithics and help to establish Paleoindian behavioural aspects (Dalpra & Pitblado 2016). The data on the previous LA-ICP-MS results mentioned within the study (Pitblado *et al.* 2013), speak to the necessity of geochemical methods, as a geochemically tested carbonite crystalline limestone, was misidentified as quartzite in the field even with a 10x magnification (Dalpra & Pitblado 2016).

A preliminary case study by Sciuto *et al.* (2019) examined quartz and quartzite varieties during the Mesolithic in Lillsjön, Northern Sweden (7200-5800 BP). The Mesolithic in the Angermanland is dominated by the use of poor materials like quartz and quartzite (Sciuto *et al.* 2019). Large numbers (2612) of lithics, with 39 being formal tools, were scanned using hyperspectral wavelengths, in order to distinguish quartzite and quartz varieties (Sciuto *et al.* 2019). The determined varieties were further backed up by Energy Dispersive X-ray Fluorescence (ED-XRF) results to validate the categories created by the hyperspectral scanning and statistical groupings (Sciuto *et al.* 2019). This was the first time that hyperspectral signatures were used in an archaeological context correctly identifying two types of quartz and two types of quartzite, through multivariate statistical models of the scanned samples (Sciuto *et al.* 2019). The early phase of the settlement was characterized by bright grey-shaded quartz and coarse, light coloured quartzite (Sciuto *et al.* 2019). The later phase of occupation was characterised by white, opaque quartz and scarce dark, fine quartzites and these trends mirror documented use of raw materials in the Mesolithic of Sweden (Sciuto *et al.* 2019). High variability of the local quartz and quartzite geology made sourcing very difficult and this study stands to show that geological characterization of raw materials is still attainable even when sources are not observable (Sciuto *et al.* 2019).

Quartzite in the COHWHS, is a major component of Acheulean assemblages (Field 1999; Kuman 2003; Pollarolo *et al.* 2010; Sutton 2012; Moll 2017). Soto *et al*. (2020) is the only African example of quartzite provenance attempts, and this study attains a preliminary insight into ESA quartzite sourcing, relevant to this project. Along the Mozambique Belt adjacent to the Oldupai Gorge, quartzite is a main component of the ESA assemblages in this region (McHenry & de la Torre 2018; Soto 2020), so tracing them back to their specific origin was of importance in assessing raw material sourcing behaviours (Soto *et al.* 2020). Consulting geological maps and local knowledge, the authors identified and sampled five different outcrops for a total of 257 samples (Soto *et al.* 2020). Macroscopic traits, petrography as well as Energy Dispersive- X-Ray Flourescence (ED-XRF) were all methods utilised to characterize the quartzites of the Oldupai Gorge region (Soto *et al.* 2020). Initially four groups were established through macroscopical traits, which were later grouped into 12 raw material groups through petrography (Soto *et al.* 2020). This was based on characteristics such as gloss, colour, grain size, texture, morphology, transparency, impurities, post-depositional alterations, and mineral composition (Soto *et al.* 2020). Thirty representative samples were sent for ED-XRF analysis in order to obtain chemical profiles of the raw material groups (Soto *et al.* 2020). Through this combination of physical and geochemical approaches, quartzites were able to be statistically identified per outcrop, through Coefficients of Variation (Soto *et al.* 2020). Despite bulk geochemical overlap, discussed above, at least three raw material groups were found to belong to specific outcrops (outcrops: Naisuisui, Naibor Soit Ndogo, Naibor Soit Kubwa) (Soto *et al.* 2020). This study allows for the fingerprinting of quartzite outcrops, so regional ESA site researchers may use the data in interpreting sourcing behaviours, as well as acting as a stepping-stone for future fingerprinting research (Soto *et al.* 2020).

As seen through this discussion in section 2.6.1, a successful 'blanket approach' to quartzite provenance has yet to be established, each new region requires different methodology to enable the fingerprinting of outcrops. This is relevant to the aim of this thesis, and the initial preliminary look into geochemically characterising quartzites in the COHWHS as such, future research will draw from the results presented here. A summary of the studies presented above, as well as further studies of quartzite sourcing, are described below in Table 2.1.

Table 2.1. Summary of quartzite provenance studies.

Site	Age	Sourcing Methods	Conclusions	Authors

Upper Gunnison Basin, USA	10500-8000 BP	UVF, LA-ICPMS, AD-ICPMS, WD-XRF, INAA and petrography	Pitblado *et al. (*2008) was a pilot study into the sourcing and discrimination of quartzites. This study found that a combination of ICP-MS and petrography work the best to discriminate Upper Gunnison Basin quartzite artefact and sources.	Pitblado *et al.* 2008
Upper Gunnison Basin, USA	10500-8000 BP	LA-ICPMS	Pitblado et al. (2013) utilised LA-ICPMS, PCA's and hierarchical clustering, to discriminate cobble and outcrop sources from another. These methods were used to tackle chemical overlap of quartzites, calling for the use of petrography to improve sourcing accuracy.	Pitblado et al. 2013
Upper Gunnison Basin, USA	10500-8000 BP	Petrography: 50 point-count under a petrographic microscope	Dalpra & Pitblado (2016) utilised petrography to initialise later studied comparisons of geochemical data. The study found five different petrographical groups that could be identified within the Upper Gunisson Basin quartzites.	Dalpra & Pitblado 2016
St. Huibrechts-	Belgian Pre-history	Petrography: Optical polarising and CCL	This was a pilot study into discriminating different	Veldeman *et al.*

Hern and Tienen Formations, Belgium		microscopy, energy-dispersive microscopy and back-scatter electron imaging	quartzites from the St. Huibrechts-Hern and Tienen Formations. Six quartzite varieties were mircoscopically distinguished through mineralogy, cement types, micro-textures and microstructures, to formatively shape lithic sourcing studies of the Belgium Mesolithic. Two quartzites remained macroscopically identical and called for Oxygen isotope analysis and LA-ICPMS to increase fingerprinting accuracy.	2012
Various Mesolithic sites, Flemmish region, Belgium	Mesolithic, 10000-5000 BP	Petrography: optical scanning electron and hot-cathodoluminescnce mircoscopy, P-XRF and ICP-OES	Three geological quartzite varieties were tested against 20 archaeological lithic samples to determine their origin. Two groupings were found where one correlated to fine-grained Wommerson quartzite while the other came from an unidentified source. This study emphasised the contribution of destructive petrographical and geochemical means, over non-destructive means for	Blomme *et al.* 2012

			fingerprinting.	
Rheine-Meuse-Scheldt, Belgium	Mesolithic, 10000-5000 BP	Petrography: point-count, cathodoluminescence, x-ray microCT scanning, and scanning electron microscopy with energy dispersive x-ray analysis	This study attempted to distinguish the geological Tienen and Wommersom quartzites, to characterise their extensive use throughout the Mesolithic. Only through the multi-scalar approach of various methods were these two groups fingerprinted, enabling further research into the Mesolithic.	Cnudde *et al.* 2013
Lillsjön, Northern Sweden	7200-5800 BP	Hyperspectral imaging, ED-XRF	Large numbers (2612) of quartz and quartzite artefacts were scanned with hyperspectral imaging. This study piloted the use of hyperspectral imaging in discriminating varieties of quartz and quartzite, ED-XRF results backed up hyperspectral methods. It established two phases of settlements utilising different varieties of quartzite to different extents.	Sciuto *et al.* 2019
Roca Dels Bous, South Eastern Pyrenesse,	MIS 3 60-25000 BP	Petrography: macroscopic and thin-section	Eighty-five % of the assemblage (quartzites) from level 12 of Roca Dels Bous were petrographically linked to secondary,	Sunyer *et al.* 2017

Spain			Pleistocene cobble sources. The selection of specific raw material groups within the cobbles reflected behaviors of local selection.	
El Habario and El Arteu, Spain	160-40000 BP	Petrography and binocular characterisation	This study set out to link destructive petrography with non-destructive stereoscope microscopy to characterise whole assemblages. Through the description of petrographical data and raw material properties, petrogenetic raw material groups were formed. They were then used to characterise lithic production behaviours pertaining to quartzite varieties at the two sites.	Prieto *et al.* 2020
El Habario and El Arteu, Spain	160-40000 BP	Petrography, digital image processing and WD-XRF	Six raw material groups were established through petrography and showed a variety of usage behaviours across location, preference and occupation. XRF data did not produce definite distinctions between metamorphic textures.	Prieto *et al.* 2018
Oldupai Gorge, Tanzania	ESA	Macroscopic trait characterisation, petrography and ED-	This study served as the pilot for assessing ESA quartzite sources in the	Soto *et al.* 2020

		XRF	Oldupai Gorge. A multi-scalar approach reduced the found chemical overlap between quartzite and 12 raw material groups were established. Three of which could be linked to specific outcrops.	

2.6.2 Solution/Acid Digestion-Inductively Coupled Plasma- Mass Spectrometry artefact provenance sourcing

Solution Inductively Coupled Plasma Mass Spectrometry or also known as Acid-Digestion-ICP-MS (AD-ICP-MS) was developed in the early 1980s and has a wide range of uses in the material fields (e.g., geology, water and chemistry) (Becker 2002). Archaeological uses for provenance through ICPMS have been documented since the 1990's (Tykot & Young 1996; Gratuze 1997, 1999; Neff *et al.* 2003; Barca *et al.* 2008; Pitblado *et al.* 2008, 2013; Ma *et al.* 2011; Shoval 2018) AD-ICP-MS can be used as a geochemical technique to measure most periodic elements, up to parts per trillion (Rollinson 1993). Ions are directed through a mass spectrometer that allows 'mass to charge' measurements, producing trace elemental makeup (Rollinson 1993).

Pitblado *et al*.'s (2008) comprehensive study of geochemical testing on quartzite examined multiple analyses and evaluated their accuracy in relation to artefact provenance (namely: petrography, Laser Ablation Inductively Coupled Plasma Mass Spectrometry [LA-ICP-MS], AD-ICP-MS, Ultraviolet Fluorescence [UVF], Wavelength Dispersive XRF [WDXRF] and Instrumental Neutron Activation Analyses [INAA]). Using the Paleoindian Upper Gunnison Basin sites, they found that INAA, LA-ICP-MS and AD-ICP-MS were well suited for distinguishing and mapping quartzite, namely due to their ability to detect large arrays of elements (Pitblado *et al.* 2008). Bivariate plots depicted well grouped variability within the geochemical profiles of artefacts and geological sources, indicating the large possibility of eventual provenance (Pitblado *et al.* 2008). Pitblado *et al.* (2008) further suggested that the best way to source archaeological quartzites would be a combination of petrography and LA-ICP-MS due to the relatively small amount of sample destruction. Yet, this study does prove

that AD-ICP-MS is the most accurate method for quartzite sourcing as it is able to identify the highest number of trace elements (Pitblado *et al.* 2008).

Ten Bruggencate *et al*. (2015) assessed Paleo-Eskimo mobility in the southern Baffin Island through the provenance of chert artefacts, using AD-ICP-MS. Milled samples were compared from chert outcrop sources labelled: LdBt-1 and LdBx-2 (n = 15), thereafter artefacts from the interior site LeDx-42 (n = 9), as well as nearby glacially deposited cobbles (n = 3) were sent for AD-ICP-MS trace element analysis (ten Bruggencate *et al.* 2015). Variations between the sources were observed in the values of Molybdenum (Mo) and Barium (Ba), lending to the fingerprinting of sources, but statistically the variations were too low to definitively source the archaeological material (ten Bruggencate *et al.* 2015). Ten Bruggencate *et al.* (2018) suggest that tracing land-use patterns of Paleo-Eskimos through chert provenancing is currently unattainable due to accidental laboratory contamination.

2.6.3 Portable X-ray Fluorescence artefact provenance sourcing

Portable X-ray Fluorescence (P-XRF) is a known method for artefact provenancing (Kristmanson 2004; Shackley 2005; Meierhoff *et al.* 2010; Vásquez *et al.* 2011; Williams *et al.* 2012). X-ray fluorescence (XRF) is a geochemical method that determines the chemical compositions of materials (Mantler & Schreiner 2000; Shackley 2011). It enables the researcher to uncover elemental compositions of materials in a destructive manner due to sample homogenisation (Rollinson 1993; Mantler & Schreiner 2000; Shackley 2011). An X-ray is sent to the object exciting the electron, and when a new electron takes its place, the fluorescence given off is measured and calibrated to determine its chemical composition (Rollinson 1993; Shackley 2011). It is able to measure and analyse the compounds found in raw materials and provide an in-depth analysis of mineralogical composition (Rollinson 1993; Wess *et al.* 2001; Mantler & Schreiner 2001). Portable-XRF, on the other hand, produces non-destructive elemental composition readings (major and minor) through weight (%) and is time efficient as no sample homogenisation is needed (Vásquez *et al.* 2011).

Land use and mobility patterns of Patagonian hunter-gatherer groups in Argentina have been investigated through obsidian artefact source provenance using XRF analyses (Vásquez *et al.* 2011). Fifty-three samples from 15 archaeological sites, as well as 23 samples from four outcrop sources related to the Asceret Formation in northwest Patagonia, were chosen for analysis. Obsidian was geochemically analysed using energy dispersive x-ray fluorescence

(ED-XRF) as well as P-XRF (Vásquez *et al.* 2011). Twenty-two major, minor and trace elements were observed through lab-based ED-XRF while only eight minor and trace elements were detected through the P-XRF (Vásquez *et al.* 2011). The results were then run through a principle component analysis (PCA) to define three groupings and then plotted against known archaeometric studies of obsidian sourcing within the area (Vásquez *et al.* 2011). Sourcing these artefacts provided insight into the long-distance trade-routes (more than 100 km) involving Patagonian obsidian (Vásquez *et al.* 2011). This study also found that there is no difference between Lab-based ED-XRF and P-XRF in attaining reliable geochemical results for the purpose of obsidian provenancing (Vásquez *et al.* 2011).

2.7 Hominin mobility and the raw material economy

2.7.1 Landscape Use and Raw Material Economy

Landscape-scale studies in Earlier Stone Age archaeology focus on raw material procurement patterns and transport distances involved in provisioning tool stone (Braun 2005; Blumenschine *et al.* 2008; Braun *et al.* 2008a, 2008b; Caruana *et al* 2019). The distance of raw material sources to archaeological sites is compared with measures of reduction intensity and frequencies of raw material use, to model predictive relationships. While karstic sites are only able to capture a certain portion of lithic assemblages, limiting interpretations to intra-site perspectives, the increased catchment areas of open-air sites lend themselves to landscape-scale interpretations in the COHWHS region (Caruana *et. al* 2019). Landscape archaeological approaches are significant in this context, because they can provide perspective on past knowledge or perception of raw material distributions and the flaking properties of rocks. The relationship between raw material source distances, their lithological flaking properties, and the core and flake reduction intensities can potentially reveal a 'raw material economy' or patterns relating to the conservation of materials and energy expenditure required for toolstone transport (e.g., Braun 2005; Blumenschine *et al.* 2008; Braun *et al.* 2008a, 2008b; Li *et al.* 2015; Caruana *et al.* 2019).

Previous research comparing reduction intensity and raw material source distances has found a general trend that materials located further away are typically more reduced (Braun *et al.* 2008a; 2009a). Braun *et al.* (2008a) looked at single-platform cores from 'Developed

Oldowan' sites within the Okote Member (1.6-1.4 Mya) of the Koobi Fora Formation (Kenya). Examining unifacial scraper reduction methods, Braun *et al*. (2008a) took measurements of the platform area versus flake mass to indicate reduction intensity: higher mass-platform ratios meant lesser reduction. Three hundred and sixty-three flakes were metrically measured using *ImageJ* digital imaging, and then using Mann-Whitney U tests, relationships were compared across sites closer and further away from a paleo-stream, which was the proposed raw material source (Braun *et al.* 2008a). They found that transport and reduction intensity of single-platform cores were linked to raw material availability and proximity (Braun *et al.* 2008a). The study also found cores with higher knapping longevity potential (i.e., larger) were transported into areas scarce of raw material (Braun *et al.* 2008a). Lithic production strategies were implemented to conserve resources and in turn the energy expended during transport, mitigating the need to return to the source (Braun *et al.* 2008a).

Blumenschine *et al.* (2008) used landscape-scale approaches to understand frequencies of raw material types in Oldowan assemblages from the Lowermost Bed II of the Eastern Olduvai Gorge Basin. One hundred excavations extending over 7 km produced >8000 artefacts, which allowed them to examine potential relationships between raw material use and transport distances across landscapes (Blumenschine *et al.* 2008). The excavation sites were grouped according to distance to raw material sources, the closest being 1.28 km and the furthest being 5.37 km away from the expected source (Blumenschine *et al.* 2008). Quartzite (n=7359) from the Naibor Soit hill was the most abundant raw material within the assemblages, albeit its frequency lowered with distance to sources. They developed a 'distance-decay' model that suggest raw material use is proportionally related to its transport distance (Blumenschine *et al.* 2008). Further, the size of whole flakes, weight thereof, and relative abundance in the assemblage, also decreased relative to transport distances (Blumenschine *et al.* 2008).

2.7.2 Reduction intensity

Clarkson (2013) used 3D scanning to attain accurate surface area measurement of cores, which he compared with the number of flake scars on cores to assess reduction intensity on a diachronic (i.e., temporal) scale at Klassies River Mouth. He created the Scar Density Index (SDI), which compares the number of flake scars to surface area measurement to quantify how intensely cores were knapped (Clarkson 2013). Here, Clarkson (2013) compared 25

experimental cores, knapped to the point of exhaustion, utilising five different reduction methods, including discoidal, bifacial, levallois, blade and multiplatform strategies on quartzite, obsidian, and flint cores (Clarkson 2013). Utilising a NextEngine scanner, surface area was calculated and samples were weighed after ~25% (of the core mass) was removed, until cores were exhausted (Clarkson 2013). Through this experiment, Clarkson (2013) found that the SDI results were highly correlated to mass loss in cores throughout reduction, thus validating this calculation as a measurement of reduction intensity. This method was then applied to the Klassies River Mouth assemblage, showing a change in core reduction patterns during Howiesons Poort (HP) industry (Clarkson 2013). The HP industry introduces exotic fine-grained material that is specifically collected to produce smaller MSA artefacts, like blades (Clarkson 2013). Higher levels of reduction are observed here during the HP and may be linked to behaviours regarding effort and exotic lithic sourcing (Clarkson 2013).

Shipton and Clarkson (2015) further adapted the SDI calculation to measure the reduction intensity of handaxes, and to examine the effects of resharpening on size and shape. Handaxes from Kariandusi (977 Kya) and Isenya (974 Kya) (Kenya) (Durkee & Brown 2014), as well as from Patpara (150 Kya) and Bhimbetka (106-94 Kya) (India) (Bednarik *et al.* 2005; Haslam *et al.* 2011) were compared along with 57 experimental handaxes made from chert, quartzite, silcrete, volcanic, flint and obsidian materials (Shipton & Clarkson 2015). At several stages during experimental production of handaxes, pieces were weighed, 3D scanned, and scars were counted to compare reduction and resharpening measurements (Shipton & Clarkson 2015). They found that resharpening had no effect on the relationship between SDI and mass lost, although blank type accounted for 30% of shape variation as cobbles required more shaping (Shipton & Clarkson 2015). Their study generally found the higher SDI score equated to more intense resharpening (Shipton & Clarkson 2015). At Kariandusi (~1 Mya) raw materials that were located further away were more heavily reduced (Shipton & Clarkson 2015). Isenya (700 Kya) showed the same pattern as Kariandusi in that local materials had the smallest SDI; however, cleavers also had low SDI scores due to their morphology (Shipton & Clarkson 2015). Both East African assemblages had very low SDI's compared to the final stages of experimental resharpening, indicating behaviours of discard despite resharpening potential (Shipton & Clarkson 2015). In the Indian Acheulean-to-Middle Palaeolithic assemblages, handaxes from Patpara produced high SDI scores while Bhimbetka had no resharpening (Shipton & Clarkson 2015). These data speak to the variability in Acheulean behaviours and across landscapes (Shipton & Clarkson 2015).

Reduction patterns in connection to distances to raw material sources can further indicate selectivity and transport behaviours related to the surrounding environment (Schick 1987; Braun 2005; Braun *et al.* 2008a; 2008b; Blumenschine *et al.* 2008; 2012). This has become a way for understanding landscape-use within the COHWHS (e.g., Caruana *et al.* 2019). Both aforementioned authors in the previous section (Blumenschine *et al.* 2008; Braun *et al.* 2008a) utilised metric-based methods to calculate reduction intensity, and, as presented, both 3D methods (Clarkson 2013; Shipton & Clarkson 2015) and metric methods are able to provide data indicating landscape use and raw material economies.

CHAPTER 3:Materials and Methodology

Within the Cradle of Humankind World Heritage Site (COHWHS), quartzite is a favoured material for LCT production in the Acheulean (Field 1999; Kuman 2003; 2007; Sherwood 2013). Maropeng's landscape is characterised by a wealth of potential quartzite sources, and it is possibly a reason a large surface scatter of Acheulean stone tools has been preserved in this area. As such, the characterisation of the archaeological quartzite to the landscape is crucial for examining the raw material selection behaviours of hominins. Raw material sourcing characterises the cognition behaviours related to lithological properties, quality, and selection thereof (e.g., Stout *et al.*2005; Braun *et al.* 2009; Goldman-Neuman & Hovers 2012), as well as hominin mobility (e.g., Wallace & Shea 2006; Braun *et al.* 2013; Presnyakova *et al.* 2018). As previously discussed in section 2.6, geological surveying and geochemical analyses allow for this characterisation to occur, by linking sources to their provenance (e.g., Jercher *et al.* 1998; Shackley 1998; Negash *et al.* 2005; Braun *et al.* 2008a; 2009; Sunyer 2017; McHenry & de la Torre 2018; Prieto *et al.* 2018; 2020). Reduction intensity studies allow insight into the skill and effort expenditure put into the knapping process (e.g., Kuhn 1991; de la Torre & Mora 2005; Marwick 2008; de la Torre 2009; de la Torre *et al.* 2011; Clarkson 2013; Shipton & Clarkson 2015). When looked at in conjunction, raw material sourcing and reduction behaviours allow for the characterisation of the raw material economy in relation to the landscape (Kuhn 2004; Braun 2008a), see section 2.7.2.

Materials are described from the lithic assemblage and the three km geological survey in section 3.1. Methods are examined in section 3.2. Here, macroscopic lithological quantification methods are discussed and followed by geochemical methods: P-XRF and AD-ICP-MS, followed by the technological analytical methodology. Thereafter, statistical approaches to calculating reduction intensities and raw material provenance are detailed in section 2.3.3 and 2.3.4. Finally, section 2.3.5 describes the methods used to create the maps of raw material availability at Maropeng.

3.1 Materials

3.1.1 The Assemblage

The Maropeng assemblage used in this study consisted of 60 quartzite cores and 22 LCTs (see Tables 1 and 2, Appendix). All available LCTs and a random selection of cores from *in*

situ and *ex situ* assemblages were chosen to represent the flaked pieces. Flakes were not used as they can often overrepresent raw material usage (Goldman-Neuman & Hovers 2009). While most of the samples analysed here come from controlled excavations (Moll 2017), surface finds from building dumps augmented the materials discussed below (Pollorolo *et al.* 2010). Following the current understanding of the ABH formation, discussed earlier (Pollorolo *et al.* 2010; Morrisey 2015), it is likely that processes such as erosion, sediment slope-movement, and winnowing have affected this assemblage (Morrisey 2015). It is acknowledged that the assemblage is biased by erosional processes, although landscape-scale methods, discussed earlier, can overcome some of the limitations that challenge the analysis of open-air sites (e.g., time-averaging and spatial displacement).

3.1.2 Geological Surveying

After consulting geological maps made by the Counsel for Geoscience (Figure 4.1), a ground survey was completed sampling quartzites exposures within a three km radius, collecting samples from every identifiable quartzite outcropping, following methods adapted from Braun, et al. (2008b) and Sherwood (2015). Three kilometres was chosen due to the relatively close proximities of three large quartzite sources of the Hekpoort and Timeball Hill Formations. In addition, Earlier Stone Age raw material ranges have been shown to link to relatively short distances: one to five km (Toth 1982; Potts 1994; Potts *et al.* 1999), therefore a distance of three kilometres was chosen to fit into the time constraints of a Masters thesis. Property access permission from residents was acquired and walks and drives provided verification of quartzite outcrops, as well as new identifications. For sampling, a hammer was used to break pieces off quartzite clasts (Sherwood 2015). This was carried out across an entire outcrop. Depending on colour/grain size variety (Braun *et al.* 2008a) and on the size of the outcrop, several samples were recorded and taken (variations from N= 5 to N= 15). Sizeable samples larger than 50 mm maximum dimension were removed to ensure future studies can use the same material. A handheld GPS unit (Garmin 60s) was used to record the spatial positioning of samples and photographs were taken. Each piece was given a sample number and grain size, and colour was recorded. After, the entire outcrop was photographed and documented using GPS tracks. Lithological and geomorphological descriptions of each outcrop enabled its distinction across the landscape. Features documented of each outcrop included size, location, bearing, shape, *in situ* clast descriptions, detached clast maximum

length, colour and grain size of hammered, detached clasts, clast shapes and surfaces, banding, and general observations warranting note. Cobbles from river sources were ignored for sampling due to the river systems potentially bringing in exotic quartzites (Barrientos *et al.* 2018). Characterising them would require far more research, unattainable within the time frame of a Masters thesis. However, understanding and fingerprinting the quartzite cobbles from river sources is important considering the presence in the artefact assemblage at Maropeng and will be the focus of further research. It should be noted that artefacts U5 and 504p may be from river sources but still provide valuable information regarding quartzite sourcing. A total of 12 quartzite outcrops were identified, sampled (total: 103 samples) and taken for analysis (see Table 7, Appendix).

3.1.3 Biases

The limitation of sampling via macroscopic variation is that it reflects only captured variance and not abundance, hence why outcrops are described in an effort to capture such. Not every quartzite clast was hammered for inspection, therefore minor variance of colour or grain within outcrops may not be represented and may skew results. Bias may also be introduced in which some outcrops may have not been identified due to the long grass covering large portions of the landscape. Excluding outcrops not identified through ground survey can potentially categorise local materials as exotic materials, nonetheless meaningful information regarding the quartzites of Maropeng can still be extracted.

3.2 Methods

3.2.1 Macroscopic Lithological Quantification Methods

Both artefacts and geological samples were described qualitatively (see Table 7, Appendix) in terms of banding, grain visibility, colour and groundmass texture, using a hand lens at 10x magnification (Stout *et al.* 2005; Goldman-Neuman & Hovers 2009). It is noted that the most dominant colour within the sample was used for categorisation. The generalisation of properties such as colour limit the potential for outcrop distinction and therefore required the use of geochemical methods.

Many studies include petrography as a way of distinguishing quartzite groups (e.g., Pitblado *et al*. 2008; Prieto *et al.* 2018). Not using this method in this study will include biases for "ground-truthing" the quartzites, macroscopic lithological properties are used instead. The purpose of this study is to be as minimally destructive as possible, petrography is comparatively more damaging, meaning it is not included. Therefore, this research aims to identify whether just the methods employed here are enough to source Maropeng quartzites. Geochemical observations allow for distinctions between quartzite types within the Maropeng lithic assemblage and the complex geological layout. Due to the monetary costs of geochemical work not all samples were tested, and this means there is a selective bias present. This is rectified through the selection of averaging the sample's lithological properties, to identify averages as well as maximums and minimums within the data. It should be noted averaging may not wholly represent the quartzite upon the Maropeng landscape. Nonetheless, while bias may be present, meaningful information from this landscape-scale approach is presented.

Limited funding meant just 26 sample spaces were available to geochemically define 12 outcrops and 14 spaces to define 82 artefacts. Selection of these samples for geochemical processing was therefore necessary and was done through statistical methods. Qualitative descriptions were assigned numbers in order to perform the quantitative analysis (see Table 7, Appendix). First, variance analysis plots were performed on all of the previously mentioned lithological categories, to determine which displayed the most variance. The colour category accounted for ~90% variance across all geological samples, therefore it was used as the determining factor for artefact and geological sample selection (see Table 7, Appendix). The maximum, minimum and mean colour quantifications were then calculated of each outcrop and across all artefacts. The reason was to provide information of geological samples by their average as well as their variance. The mean sample, as well as the minimum or maximum sample that varied the most from the mean, was chosen for analysis. Large outcrops such as Quartzite Mountain and Visagie Mountain Outcrop were sampled to have both maximum and minimum variables, due to their size. For artefact geochemical testing, a destruction permit (ID: 2887) was received from the South African Heritage and Resource Agency (SAHRA). Unfortunately, the selective sampling limits the accuracy of the data when trying to provenance artefacts but could not be avoided due to funding limitations. Increased sampling will be the focus of further publications of Maropeng.

3.2.2 Geochemical Methods

AD-ICPMS

Fourteen archaeological samples and 26 geological samples were ground into a fine powder for analysis (see Tables 3 and 4, Appendix). AD-ICPMS was chosen due to its ability to detect large amounts of trace elements in quartzites (Rollinson 1993; Pitblado *et al.* 2008), even up to the parts per trillion level (Rollinson 1993; Elmer 2001), and requires minimal sample destruction (Ma *et al.* 2011). LA-ICPMS is however less destructive (Pitblado *et al.* 2008), but the sizes of the ESA artefacts do not fit into the machine and therefore, acid digestion of drilled samples was the chosen method. Samples were taken to a rock-crushing room, located at the University of the Witwatersrand, with an extractor fan for ventilation, in an effort to stop contamination of elements between samples (Rollinson 1993). Here, samples were drilled using an AEG drill, size ten masonry drill bit with a tungsten carbide tip, to produce a homogenised sample (Attas *et al.* 1984; Ma *et al.* 2011). Homogenisation of samples was undertaken to represent average compositions (Rollinson 1993). After every procedure completion, the drill and the bit, new samples and table were wiped with acetol to further prevent contamination between samples (Rollinson 1993). Samples were also put on a new sheet of white paper every time for anti-contamination purposes (i.e., fresh surface devoid of previous workings) and the ease of transfer into their separate labelled Ziplock bags. Six geological samples were too hard to penetrate with the drill and were milled instead using a steel carbide ring mill. The milling machine uses a steel carbide mill to crush samples to a fine powder. The machine is checked regularly according to laboratory standards and thus contamination from the steel carbide rings is negligible. Milling was not done on any artefacts as this would cause large scale destruction. One geological sample was also milled as well as drilled, providing two similar samples, to look at what contamination drill bits bring into the sample. Archaeological samples were drilled on parts where little technologically diagnostic information about the piece could be obtained (typically on, and straight through the original cortex). This is the least destructive method and prevents breaking the artefacts during drilling. It is noted that major elements are prone to becoming mobile during weathering and could potentially alter results, though the misrepresentation of chemical abundance (Gautheir and Burke 2011), therefore all artefacts and geological samples were drilled into, past the outer chemical weathering to create homogenised

representative samples. Due to the nature of drilling samples and the relative hardness of the quartzite, elements that aren't part of the quartzites were introduced. The use of a tungsten carbide bit introduces variable quantities of tungsten, cobalt (clearly visible in the results, see Tables 3 and 4, Appendix) and tantalum (Attas *et al.* 1984). As such, these elements were left out of the analysis.

The prepared samples were sent to the Earth laboratory at the University of the Witwatersrand, where a dissolution of 50 mg of each sample was carried out. Past ICP-MS studies using homogenised materials found that 10, 50 and 100 mg all allowed reliable average chemical composition results (Ma *et al.* 2011), corroborating the legitimacy of these ICP-MS results. Dissolution of the samples was completed with high purity HF-HNO3, using a MARS microwave digester. This digested all Silica (Si) present within the sample. Forty-one trace elements were determined using the Perkin Elmer DRC-e and analysed against certified primary solution standards. All measured elements are visible in Tables 3 and 4, Appendix. During every measurement international reference materials BCR-1, BR-1 and AGV-2 were analysed, taking their ppm values, to determine the accuracy of geochemical measurements. All elements measured had a variance between accepted values of up to ten percent, while many instances of five percent or less occurred, further legitimising the accuracy of the results.

P-XRF

Portable X-ray fluorescence (P-XRF) is a geochemical method that determines the chemical compositions of materials (Rollinson 1993; Mantler and Schreiner 2000; Shackley 2011). It enables the researcher to uncover elemental compositions of materials in a destructive/non-destructive manner and measured in weight (Rollinson 1993; Mantler and Schreiner 2000; Shackley 2011). An X-ray is sent to the object exciting the electron, and when a new electron has taken its place the fluorescence given off is measured and calibrated to determine its chemical composition (Rollinson 1993; Shackley 2011). P-XRF is the portable version of XRF. This method was selected because it gives an elemental exposure of silica (previously digested in the ICPMS) and other major trace elements (Rollinson 1993), enlarging the potential for chemical identification, which will aid in accurately differentiating between types of quartzite (Piblado *et al.* 2008; Prieto *et al.* 2018). The surplus homogenised powdered sample from the drilling underwent P-XRF using lab standards at the Earth Lab,

University of the Witwatersrand. The powder was taken and laid across a mylar sheet, as this allows elemental detection to go on without huge interference from the material it is laid onto. A cup was formed with mylar sheet to spread the sample evenly across the area of the P-XRF's aperture. The cup was placed in a mobile P-XRF stand with lead lining to hold the sample still for the analysis duration. The sample was analysed for 120 seconds, using the Thermo Scientific Niton XL3t P-XRF machine. The P-XRF analysed: four oxide weights Al2O3, FeO, MgO, Cr2O3 and 32 major element weights: Mg, Al, Si, P, S, K, Ca, Ti, V, Cr, Mn, Fe, Co, Ni, Cu, Zn, As, Se, Rb, Sr, Zr, Nb, Mo, Pd, Ag, Cd, Sn, Sb, Ba, W, Au, Pb and Bi (see Table 5, Appendix). The aperture was completely covered to ensure scientific accuracy and a majors detection mode was selected to analyse the samples. Acetone was used to clean surfaces and instruments to ensure no contamination took place after every analysis. Following every daily session with the P-XRF machine, a system check was performed where known concentrations were analysed, and all fell within industry detection standards.

3.2.3 Technological Methods

Technological methods were utilised to analyse this archaeological assemblage. Technological analyses contribute to the understanding of approaches adopted, the limitations therein (de la Torre & Mora 2009), cultural practices (inter- and intra-site) (Kelly 1998; de la Torre & Mora 2009) or ecological constraints (de la Torre & Mora 2009). All variables were chosen in an effort to aid contextualisation of the intended reduction intensity calculations, section 3.2.2 (Adapted from Andrefsky 2005; Marwick 2008). LCTs and cores received slightly different methods (Table 3.1) due to their differing natures of reduction and are discussed below. The results of the quantification of these traits are discussed specifically by core and LCT type in Section 4.3 and the subsequent technological data are presented in Tables 1 and 2, Appendix.

Cores

Metric measurements

Digital callipers were used to calculate measures of maximum length, thickness and width, in millimetres (mm), in order to understand size variation (Andrefsky 2005). Mass was measured in grams (g), on a digital scale to understand artefact size (Andrefsky 2005). An example of the technological measurements is seen below in Table 3.1.

Table 3.1: Example of core technological attributes.

Accession#	**Type**	**Length**	**Width**	**Thick**	**Mass (g)**	**Scars**	**Edge Angle**	**Cortex %**
21	bsp	128.60	106.50	48,60	1054.26	7	<45°	75
32	bsp	78.60	67.30	38.70	234.65	19	<45°	40

Core Types

Core type was determined by assessing the core exploitation pattern, following the work of de la Torre (2011) and de la Torre and Mora (2018). Core exploitation patterns were best fit into the ESA patterns seen in Figure 3.1 (de la Torre 2011; de la Torre & Mora 2018). This method of classifying core types was implemented to understand and compare exploitation patterns across sources and to compare with Moll's (2017) results.

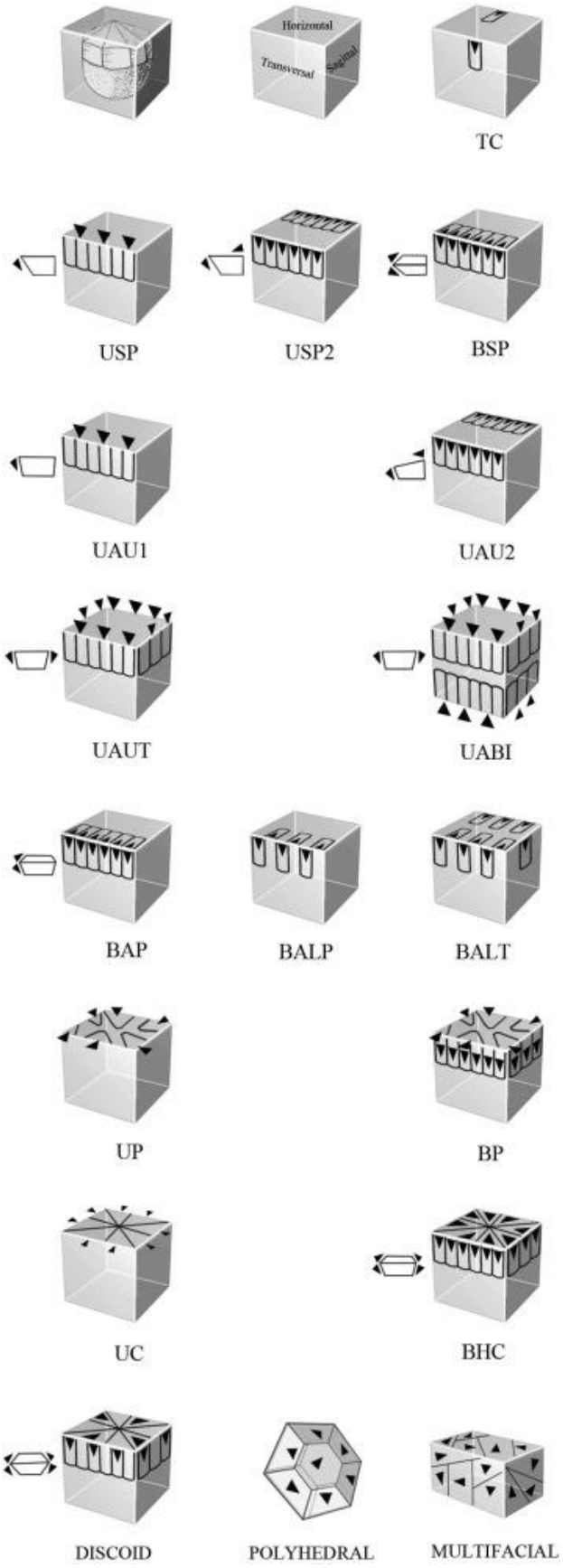


Figure 3.1. Core typologies based on reduction strategies (taken from De La Torre & Mora 2018: pg.5) Abbreviations: TC: Test core. USP: Unifacial simple partial exploitation. USP2: Unifacial simple partial

exploitation on two independent knapping surfaces. BSP: Bifacial simple partial exploitation. UAU1: Unidirectional abrupt unifacial exploitation on one knapping surface. UAU2: Unidirectional abrupt unifacial exploitation on two independent knapping surfaces. UAUT: Unifacial abrupt unidirectional total exploitation. UABI: Unifacial abrupt bidirectional exploitation. BAP: Bifacial abrupt partial exploitation. BALP: Bifacial alternating partial exploitation. BALT: Bifacial alternating total exploitation. UP: Unifacial peripheral exploitation. BP: Bifacial peripheral. UC: Unifacial centripetal exploitation. BHC: Bifacial hierarchical centripetal.

Number of dorsal flake scars

Flake scars measuring over 10 mm (see Figure 3.2) were counted on all core surfaces (Andrefsky 2005). Flake scars found on the core-mass further than 10 mm from the edge, were an exception to the 10 mm rule, as they are indications of flake scars that were partially erased (Braun *et al.* 2008a). Flake scar counts are indicative of reduction intensity (see section 2.7.1) when compared to the overall size of the flaked piece (Braun *et al.* 2008a; De la Torre 2011).

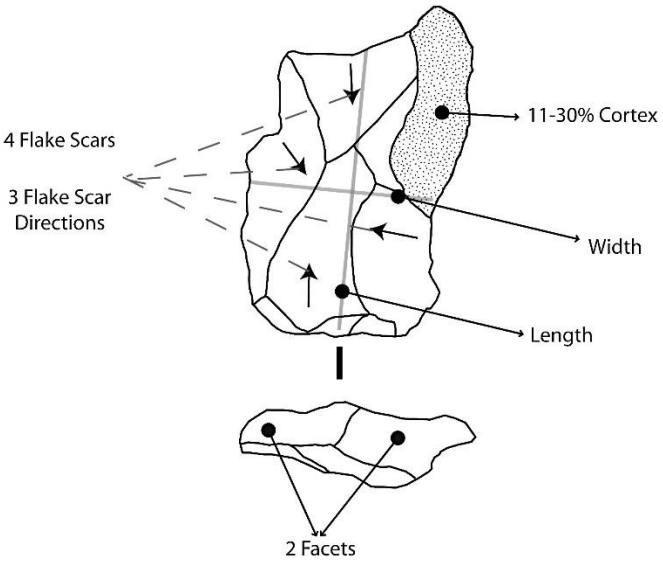


Figure 3.2. An example of basic characteristics on lithic production (Braun et al. 2008a).

Edge angle

The edge angle was estimated on the working edge of artefacts and two categories were identified: 1) <45 degrees, and 2) >45 degrees (Figure 3.3). Among cores, edge angle indicates usable platforms, as angles approach 90 degrees termination becomes difficult, and can lead to abandonment of the knapping surface (De la Torre 2011).

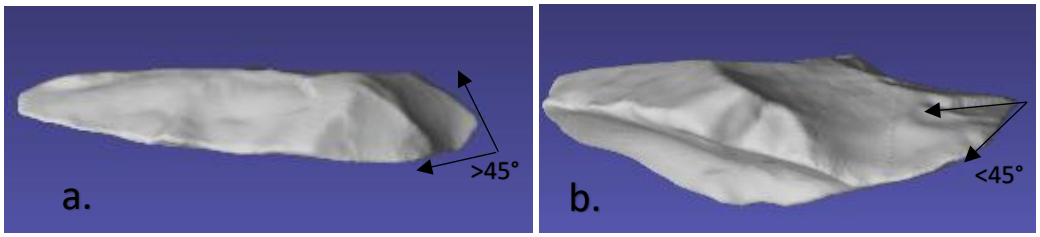


Figure 3.3. Edge angles of flaked pieces. A= angle >45°, B= angle <45°.

Cortex percentage

Cortex percentage refers to the amount of cortex left on the lithic after knapping has occurred (e.g., see Figure 3.2). The four-category cortex percentage method: 0%, <25%, <50% and > 75% (following Goren-Inbar & Saragusti 1996) was then adapted to merely show cortex percentage from 0- 100%. Percentage of cortex left indicates reduction values as more cortex is indicative of less knapping (de la Torre 2011).

Large Cutting Tools

Length, width, thickness, mass, dorsal scar numbers, edge angle and cortex percentage measurements were tabulated using the earlier mentioned methods (see Table 3.2 for an example). Picks were typologically distinguished from handaxes through their distinctly converging, heavily worked distal ends (Andrefsky 2005). Edge angles were measured along all determined bifacial working edges (Andrefsky 2005), therefore the lack of unifacial LCTs here does not introduce bias. It should be noted that edge angles within LCTs are indicative of thinning as opposed to the usable platforms, seen in cores (Andrefsky 2005).

Table 3.2. Example of LCT technological attributes.

Accession#	**Length**	**Width**	**Thick**	**Mass (g)**	**D Scars**	**Scar Dir**	**Edge Angle**	**Cortex %**
4	151	109.1	34.2	598.1	15	4	<45°	12
22	136	64.4	42.5	438.8	18	6	>45°	46

Scar directions

30 degrees was used to separate scar directions (e.g., see Figure 3.2), splitting up 360 degrees into eight possible different directions (Braun *et al.* 2008a). Scar direction is a proxy for flaking platform rotation and can reconstruct knapping processes (de la Torre *et al.* 2003; de la Torre 2011).

3.2.4 Reduction Intensity Analysis

Reduction intensity refers to the extent to which an artefact (i.e., core or LCT) was flaked relative to its overall size (Clarkson 2013; Shipton and Clarkson 2015). Scar Density Index (SDI) was used to quantify the amount of reduction in LCTs and cores from Maropeng. This SDI is calculated through the number of flake scars divided by the surface area (n/cm^2) (Clarkson 2013; Shipton and Clarkson 2015). Surface area measurements were generated by a NextEngine 3D scanner. Scan meshes were imported into MeshLab to calculate accurate surface area and volume. Scars were counted as mentioned above and SDI values were calculated. The data were then utilised to quantify reduction across core and LCT types and finally, to create SDI by distance graphs described in the section below. Reduction patterns in connection to distances to raw material sources can further indicate selectivity and transport behaviours related to the surrounding environment (Schick 1987; Braun 2005; Braun *et al.* 2008a; 2008b; Blumenschine *et al.* 2008; 2012). Reduction intensity is used in this project as an aid for characterising lithic production strategies, their landscape-scale behaviours and their mobility through comparisons with quartzite source distances. This correlation is then used to outline the raw material economy present of the landscape 1 Mya (see Chapter Five).

Previous research comparing reduction intensity and raw material source distances has found a general trend that materials located further away are typically more reduced (Braun *et al.* 2008a; 2009). Lithic production strategies of this sort were implemented to conserve resources and in turn the energy expended during transport (Braun *et al.* 2008a). The material has a complex depositional history and has undergone some movement on the landscape. Morrisey (2015) states that sediment and some artefact accumulation occurred from the eastern quartzite ridge (referred to as Quartzite Mountain Outcrop) and various high points across the landscape attributed to the assemblage formation through gradual slope-wash. However, many artefacts appear to be fresh indicating a numerous potential of artefact sources. This also indicates the use and making of lithics by hominins across the Maropeng

landscape (see section 2.5). So potential bias from artefact movement is negated as the entire Maropeng assemblage is viewed from a landscape scale.

3.2.5 Statistical Methods for Provenance

Statistical Methods for Reduction Intensity

Reduction intensity was statistically represented in two ways, and both used the Mann-Whitney U test to convey statistical significance. Linear regression plots were created using SPSS to represent SDI predictability in cores and LCTs through plotting it against volume. SDI/distance models, as mentioned before, were predicted using log transformed regression analysis. Boxplots were created in PAST to highlight SDI variance across LCT and core types. Small sample sizes remain an issue in creating datasets with little statistical significance. Linking geochemical data of artefact and raw-material sources allowed for the modelling of the raw material economy.

Statistical Methods for Provenance

Once reduction analyses had been accomplished, and geochemical profiles captured, statistical programs Microsoft Excel, PAST and SPSS were used to process and represent the data. Pie charts were created using Excel to present proportional data regarding macroscopic lithological qualities and core reduction patterns. Chemical overlap poses as a large problem for distinguishing between sources and artefacts, Pitblado *et al.* (2013) account for this chemical overlap. Here, a combination of principle component analysis (PCA) results and complete linkage cluster dendrograms were used to group quartzites by variance (Pitblado *et al.* 2013). Following the methods of Pitblado *et al.* (2013), all AD-ICPMS and P-XRF geochemical data variance (minus the contamination elements) was analysed using a PCA on artefacts and samples independently. The first five PCA scores of both tests represented ~99% of variance and were chosen for the cluster analysis. PCA's linearly transform or cluster highly correlated values together to reduce the number of variables in a dataset and predict relatedness (Drennan 2009). After, results were combined and run through a complete linkage dendrogram using Euclidian distance to determine hierarchical clustering. Hierarchical dendrograms order data by similarity, the further away they are related the more u-links they will have between them. Samples separated by a single u-link were considered to

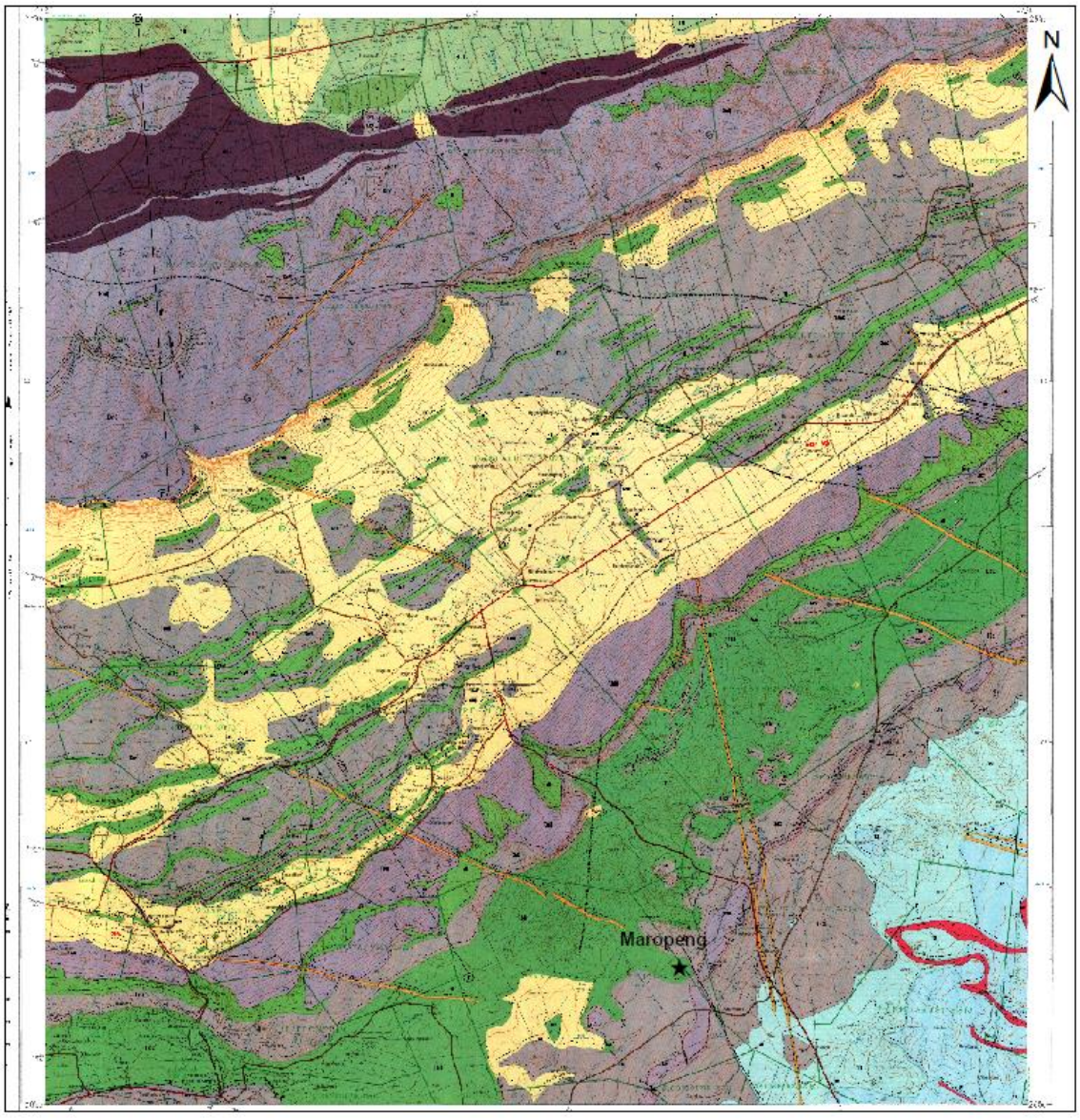
be likely related (Drennan 2009). All artefacts linked to outcrop samples by a single u-link were assigned a physical distance and plotted using SPSS line regression scatters, to determine SDI behaviours in relation to energy expenditure (see section 2.7).

3.2.6 Digital Mapping

A Global Positioning System (GPS) was utilised to capture raw material sources and characterise energy expenditure in relation to distance. Outcrop sources and source distances were visualised through ARCGIS mapping software. The GPS generated points of sample locations and outcrop outlines. Google Earth was used to create polygons of the Maropeng property and to pinpoint the Maropeng reference point. These polygons were imported into ARCGIS where they were converted into layers. Distance to raw material source was calculated by using the measure tool in ARCGIS. Distance was measured from the Maropeng reference point to the closest outcrop outline point, creating a minimum distance. The middle of the amphitheatre was chosen as the Maropeng reference point (Figure 2.1), as many excavations and most of the *ex situ* deposits come from there. Outline points of outcrops were aggregated to create outcrop shapes, using the aggregate tool. A three km radius was calculated by taking the Maropeng point and using the buffer tool. The data mentioned above created a map depicting the raw material location choices present for hominins 1 Mya (Figure 2.1).

CHAPTER 4: Results

This chapter presents the results of the geochemical and the technological analyses, the latter focused on reduction intensity of flaked pieces (cores and LCTs). These data are critical for assessing hominin raw material sourcing behaviours present on the Maropeng landscape. First, descriptions of all outcrops surveyed within the three kilometre radius of Maropeng are provided, followed by a technological analysis of the Maropeng quartzite flaked pieces, describing indicators of their reduction patterns. The chapter goes on to present data seen in a macroscopic petrological analysis of the sampled outcrop and artefactual materials. Thereafter, the geochemical data characterising outcrops and artefacts is presented. Finally, reduction strategies and intensity results and data on selection behaviours are presented, which will provide the foundation for the discussion chapter on the raw material economy of Maropeng.



0 2 4 8 Kilometers

Coordinate System: WGS 1984 World Mercator
Projection: Mercator
Datum: WGS 1984
False Easting: 0,0000
False Northing: 0,0000
Central Meridian: 0,0000
Standard Parallel 1: 0,0000
Units: Meter

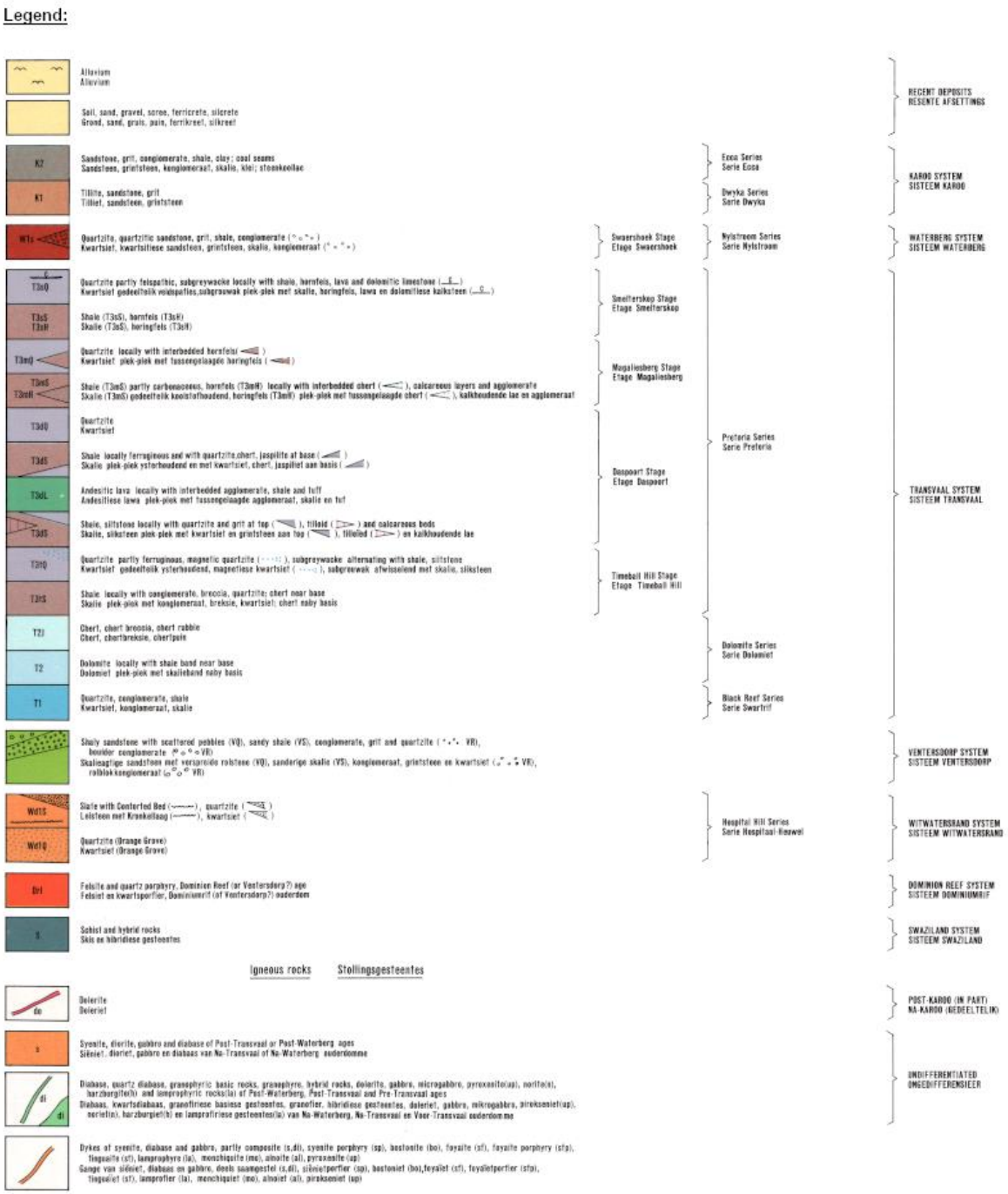


Figure 4.1. The geological map of 2527DC, with Maropeng indicated (star symbol). Accompanied by a geological legend.

All visible quartzite outcroppings were outlined through 433 GPS points (see Table 6; Appendix), and thereafter they were plotted in ARCGIS to produce digital maps of the raw material availability. Figure 4.1 is a map of 2527DC HEKPOORT and presents the geological context of Maropeng. Figure 2.1 presents the study area used in this thesis. A three kilometre buffer identified 11 different outcroppings, suggesting an abundance of potential

raw material sources. The geological units exposed in the three kilometre buffer can be described as the following: the Timeball Hill Formation which comprises of partly ferruginous quartzite and subgreywacke alternating with shale and siltstone; and secondly through, shales locally, with conglomerate, breccia, quartzite with chert near the base (Figure 2.1). The Daspoort Formation is represented by andesitic lavas, locally interbedded with agglomerate, shale and tuff. Secondly, it is defined through, shales and siltstones, locally, with quartzite and grit at the top, and thirdly through, locally, partly ferruginous shales, quartzite, chert and jaspilite at the base. The Bushy Bend Lava Member is represented by dykes of diabase (Figure 2.1). The Rooihoogte Formation is represented through chert (Figure 2.1). Recent sediments are also found and are represented through soil, sand, gravel, scree, ferricrete and silcrete (Figure 2.1).

Figure 2.1 also highlights the Skeerpoort and Hekpoort, rivers and their subsequent catchment, outlining modern waterways near Maropeng. The Skeerpoort River now appears to be ephemeral. No cobbles were seen along visible parts of the catchment, suggesting it was unlikely to be a source of raw materials. The Hekpoort River is, however, much larger and is perennial, and an abundance of gravels are now exposed. It should be noted that the Hekpoort river is calculated to be one kilometre north from Maropeng. Cobble sources were not investigated as they were thought to be too geochemically diverse to fingerprint. Inferences of cobble source locations also are limited, due to the landscape change over the past one million years, and the dominant erosional processes between six to ten metres evident in the COHWHS (Gibbon *et al.* 2014; Granger *et al.* 2015; Caruana 2017). Table 4.1, below depicts the area covered by exposed outcrops, their bearings relative to Maropeng, average GPS locations and the minimum distance needed to travel from Maropeng (further discussed in section 4.1). The point from which distances were calculated was chosen to be the centre of the modern amphitheatre built at Maropeng. This is due to many excavations being undertaken near there (e.g., M1, M2, M3 and M4), as well as the sediment dumps having provided large portions of the collected ex situ artefacts (Pollorolo *et al.* 2010; Moll 2017).

Table 4.1. Quartzite outcrops tabulated by size, GPS locations, bearing and distance from source (proximity).

Outcrop	Proximity (km)	Size (km^2)	Bearing	GPS location	Notes
MIO1	0,808902	0.003962	South	27°39'48,167"E 25°58'32,729"S	
MIO2	0,977044	0.001606	South	27°39'52,506"E 25°58'37,282"S	
MIO3	1,232274	0.00138	South	27°40'4,905"E 25°58'40,924"S	
MIO4	0,789895	0.003392	South	27°39'59,015"E 25°58'28,736"S	
MIO5	0,688327	0.004147	South	27°39'57,001"E 25°58'26,005"S	
QM	0,549196	0.176368	East	27°40'24,338"E 25°57'49,614"S	*front portion of the mountain
VMO	2,126848	0.034423	North-East	27°40'39,691"E 25°57'9,887"S	*back portion of the mountain
MGQ	0,457868	0.016414	North	27°39'32,335"E 25°57'48,387"S	
FFIO1	1,232274	0.000445	South	27°39'53,358"E 25°58'45,757"S	
FFIO2	1,424363	0.015362	South	27°40'5,447"E 25°58'54,021"S	
GO1	2,741319	0.004753	East	27°41'22,094"E 25°58'16,105"S	
GO2	2,824903	0.001553	East	27°41'24,747"E 25°58'17,42"S	

4.1 Surveyed Quartzite Outcrops

The quartzite outcrops identified within a three kilometre radius of Maropeng are described in this section. Outcrop size, lithology, distance, morphology and *in situ* exposure variability are used to detail outcrop characteristics. *In situ* exposures offer more reliability or inherent "value" when describing outcrops, as they exhibit original bedding and in situ structures. However, detached clasts are described in further detail to assess the quality of raw materials packages available on the landscape and this is relevant to the goal of characterising raw material availability. These clasts were defined through shape, size and lithology. Finally, unique observations per exposure will conclude the outcrop details presented below.

Maropeng Inland Outcrop 1 (MIO1)

MIO1 (Figure 4.2) is approximately 39 m^2 in area and is located roughly 800 m south of Maropeng. It is a flat, broad exposure of sparsely distributed, low relief, *in situ* exposures are

partially visible, flat, and often weathered. Detached clasts range in maximum dimensions measuring from 110 - 950 mm. These rocks are most commonly found in equant or tabular shapes, while several amorphic shapes are noted. Detached clasts are mostly fine-grained with fewer medium- and coarse-grained quartzites available. A variety of colours was witnessed, mainly reddish-pink and blue, while a green fine-grained variety also exists. Regular instances of banding are observed across colour and grain varieties. Certain *in situ* exposures and detached clasts are found in contact with *in situ* shale beds at MIO1.



Figure 4.2. Maropeng Inland Outcrop 1, looking north across the exposure (Photograph by D. Tasker).

Maropeng Inland Outcrop 2 (MIO2)

MIO2 (Figure 4.3) is approximately 16 m^2 in area and is located roughly 970 m south of Maropeng. It is a narrow ridge exposure orientated east-to-west, with a consistent two metre rise in elevation. *In situ* exposures are partially visible, flat (with vertically dipping bedding), and weathering into detached clasts along the top of the ridge. These clasts range in maximum dimension from 100-740 mm, the most common shapes are sub-angular, and

rounded with irregular surfaces. Clast textures are typically sandy, medium-coarse grained quartzites. Colours represented in the outcrop are mostly pink with a dark glossy rind. Large amounts of banding are also seen in the quartzites of MIO2.



Figure 4.3. Maropeng Inland Outcrop 2, looking south in front of the exposure (Photograph by Prof. D. Stratford).

Maropeng Inland Outcrop 3 (MIO3)

MIO3 (Figure 4.4) is approximately 13 m^2 in area and is located roughly 1200 m south from Maropeng. It is a narrow ridge exposure orientated north-to-south, with a three metre rise in elevation. *In situ* exposures are not visible, as they are covered by sediments and loose clasts. The clasts here range in maximum dimension from 130-1220 mm, and are mostly equant in shape, with slight edge rounding, although some clasts are amorphous and have irregular surfaces. The quartzites are mostly medium-grained rocks and some coarse-grained textures were observed, with blue, red and pink hues. Only a few cases of banding are observed at MIO3. Within this outcrop, internal flaws were abundant in pink-coloured quartzites, the blue

quartzite fractured conchoidally with fewer noticeable flaws, and red quartzites had apparent dissolution.



Figure 4.4. Maropeng Inland Outcrop 3, looking north behind the exposure (Photograph by Prof. D. Stratford).

Maropeng Inland Outcrop 4 (MIO4)

MIO4 (Figure 4.5) is approximately 33 m^2 in area and is located roughly 780 m south from Maropeng. It is a broad, ridge exposure orientated north-to-south, rising 1.5 m in elevation (more steeply on the western side than the eastern). *In situ* exposures are only partly visible, obscuring detailed descriptions. Detached clasts range in maximum dimension from 130-1360 mm, but are mostly equant shapes on the eastern side, and tubular on the western side. Fine-, medium- and course-grained detached clasts are visible throughout the outcrop, although large proportions of course grained materials were noticed. Red, blue, pink, and green hues were noted at MIO4 with few instances of banding. Detached clasts showed a

medium abundance of heavy weathering with course grained materials exhibiting the most weathering exhibited as exfoliated surfaces.



Figure 4.5. Maropeng Inland Outcrop 4, looking north across the exposure (Photograph by Prof. D. Stratford).

Maropeng Inland Outcrop 5 (MIO5)

MIO5 (Figures 4.6 and 4.7) is approximately 41 m^2 in area and is located roughly 680 m south from Maropeng. MIO5 is a broad ridge exposure orientated east-to-west and is separated into two outcrops, a northern and southern portion. This outcrop exposure was up to two metres in elevation and flattens out at the southern end. *In situ* exposures were visible, exhibiting flat surfaces with fossilized ripple marks. The detached clasts range in maximum dimension from 105-890 mm. Tabular clast shapes with slightly rounded edges were present, as well as equant shapes with irregular surfaces. Medium- and fine-grained quartzites were the only textures found at MIO5. Hues of blue, red, purple, green, and pink were present among detached clasts and only a few cases of banding were observed at MIO5. Blue

quartzites were observed to have generally undergone a greater degree of metamorphosis than pink quartzites in this outcrop.

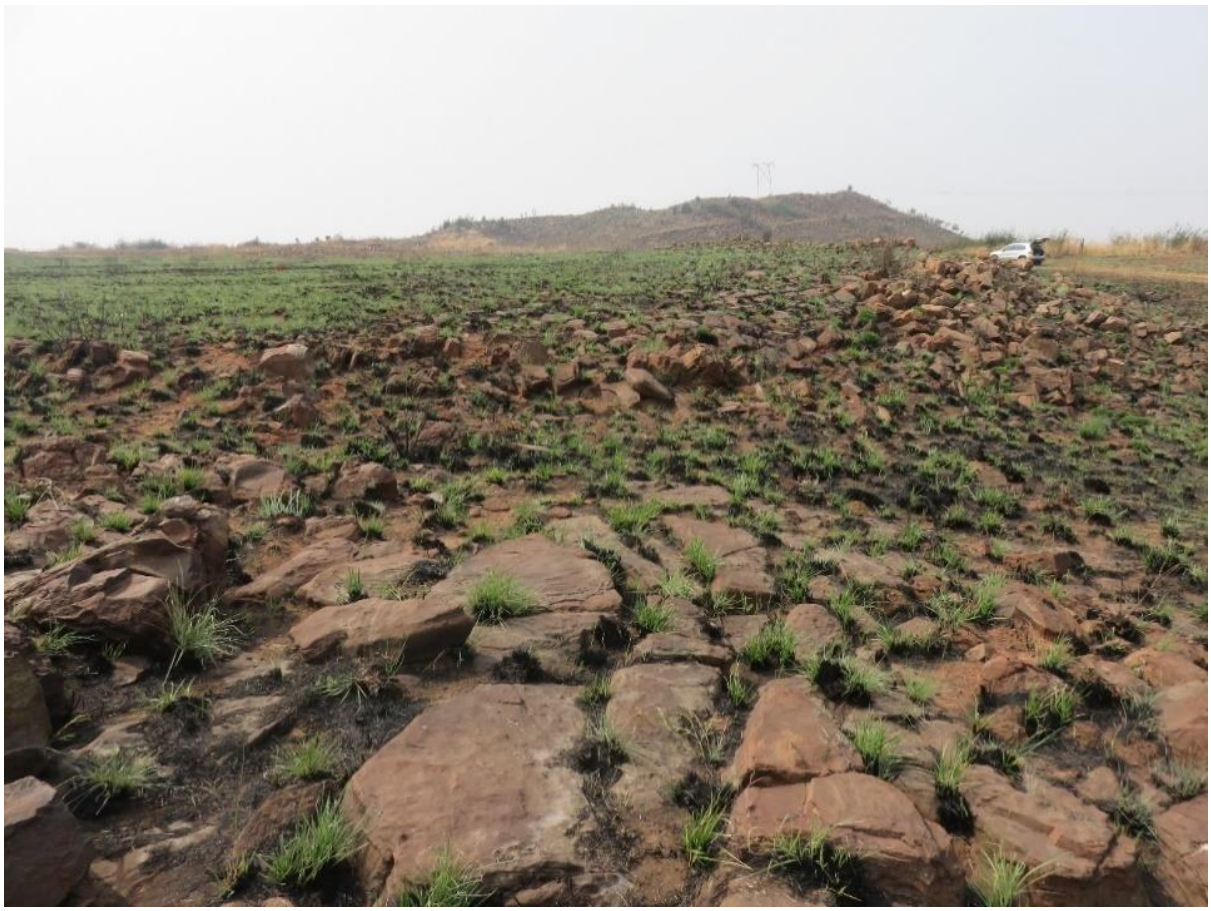


Figure 4.6. Maropeng Inland Outcrop 5, southern portion of the outcrop, looking east (Photograph by D. Tasker)



Figure 4.7. Maropeng Inland Outcrop 5, northern portion of the outcrop, looking west (Photograph by D. Tasker)

Quartzite Mountain (QM)

QM (Figure 4.8) is approximately 1763 m^2 in area and is located roughly 540 m east from Maropeng. It is a broad ridge orientated east-to-west and represents the western-most portion of this exposure. Elevation rises upwards of 50 m, although the northern slope is much gentler in gradient. *In situ* exposures were visible, conforming along the slopes, and eventually weathering into detached clasts, laterally across the top ridge. Several *in situ* exposures showed weathering along banding contacts, especially near quartz intrusions. A scree slope of loose clasts has formed, which range in maximum dimension from 120- 2200 mm. An abundance of tabular, equant, and amorphous clast shapes was present. All textures of quartzites were observed, as well as a large variety of colours (pink, red, blue, green, black, white, purple, and grey). Banding was observed at multiple locations across this outcrop. As described, QM's large exposure exhibited abundant varieties of quartzites with differing degrees of weathering. Further, Iron Age stone-walling structures made of quartzite

clasts were found. QM was also thought to be the source of sediments and clasts captured in the ABH (Pollarolo *et al.* 2010).



Figure 4.8. Quartzite Mountain shown from a far, looking north. Red arrows indicate the expanse of the outcrop (Photograph by D. Tasker)

Visagie Mountain Outcrop (VMO)

VMO (Figure 4.9) is approximately 344 m^2 in area and is located roughly 2100 m northeast of Maropeng. This is the eastern-most portion of QM orientated east-to-west. This exposure was separated to determine whether the furthest side of the mountain was distinguishable from the closer, western portion. VMO was detailed above in the QM description, therefore only differing data is presented here. Maximum dimensions of detached clasts are similar, ranging from 90- 2120 mm. Banding, clast shapes and textures were observed to be the same, however QM exhibited slightly greater colour variation due to its larger extent.



Figure 4.9. Visage Mountain Outcrop shown from a far, looking north. Red arrows indicate the expanse of the outcrop (Photograph by D. Tasker)

Mogales Gate Quartzite (MGQ)

MGQ (Figure 4.10) is approximately 164 m^2 in area and is located roughly 450 m north from Maropeng. It is a long, flat exposure seeing low elevation rises of one metre. *In situ* exposures were not visible, due to the ground and grass coverage. The detached clasts range in maximum length from 100- 1620 mm. An abundance of equant clast shapes with angular edges was noted and some had irregular surfaces due to weathering. MGQ is characterised by a dominance of blue-black quartzites with few instances of red and green hues. Fine- and medium-grain sizes characterise this outcrop and an absence of coarse-grained textures is noted, along with a very low instances of banding. Fine grained dominance was attributed to the blue-black quartzite abundance at MGQ.



Figure 4.10. Mogales Gate Quartzite outcrop, looking south towards the exposure (Photograph by Dr M. Caruana).

Fynbos Farm Outcrop 1 (FFIO1)

FFIO1 (Figure 4.11) is approximately 4.5 m^2 in area and is located roughly 1200 m south of Maropeng. FFIO1 is a flat exposure with low elevation rises. *In situ* exposures were not visible due to the grass cover. The detached clasts range in maximum length from 140-800 mm, which are mostly cubic in shape with irregular surfaces. These clasts showed a predominance of medium-grained textures, while instances of coarse-grained material were also observed. Hues only of reds and pinks were present, as well as limited abundances of banding. Quartz veins were noticed running through certain quartzites at FFIO1.



Figure 4.11. Fynbos Farm Outcrop 1, looking south across the exposure (Photograph by D. Tasker).

Fynbos Farm Outcrop 2 (FFIO2)

FFIO2 (Figure 4.12) is approximately 153 m^2 in area and is located roughly 1400 m south from Maropeng. It is a broad ridged hillock, orientated north-to-south, rising in elevation to 15 m. *In situ* exposures were flat. Detached clasts range in maximum length from 140-1200 mm, which were mostly cubic and tabular in shape with irregular surfaces and some ridge rounding present. These rocks showed a dominance of medium-grained textures, while coarse-grained material was also seen. Only red and pink hues were present, similarly to FFIO1, and small amounts of banding were noticed. Red quartzites appear to exhibit heavy dissolution features at the FFIO2 outcrop.



Figure 4.12. Fynbos Farm Outcrop 2, looking north towards the exposure (Photograph by D. Tasker).

Grazing Outcrop 1 (GO1)

GO1 (Figure 4.13) is approximately 47 m^2 in area and is located roughly 2700 m east from Maropeng. It is a flat exposure characterised by multiple clusters with low elevation rises. *In situ* exposures were not visible due to the ground cover. The detached clasts range in maximum length from 70- 1120 mm, which were mostly cubic in shape with angular edges. The quartzite showed a dominance of medium-grained textures, while instances of fine-grained material were also observed. Hues of red, blue, green, brown and pink were present, however large abundances of banding characterised the quartzite clasts of GO1.



Figure 4.13. Grazing Outcrop 1, looking north across the exposure (Photograph by H. Aberdein).

Grazing Outcrop 2 (GO2)

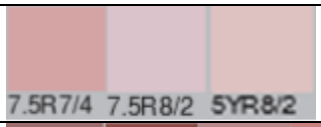
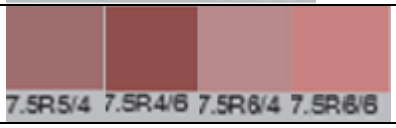
GO2 (Figure 4.14) is approximately 15 m^2 in area and is located roughly 2800 m east from Maropeng. This outcrop is a flat exposure, on the crest of a hill. GO2 experiences low elevation rises, while *in situ* exposures contoured flat with the ground and exhibited fossilized ripple marks. The detached clasts range in maximum length from 80-1090 mm, which were predominantly tabular with fewer instances of cubic shapes. Irregular surfaces due to weathering were also abundant. Fine-grained textures were most abundant with fewer instances of medium- and coarse-grained textures observed. Brown, grey, red, and pink hues were observed but banding was infrequent. Intense weathering was identified across a number of detached clasts, which correlated with an abundance of irregular surfaces. Quartz veins were noticed running through certain quartzites at FFIO1.

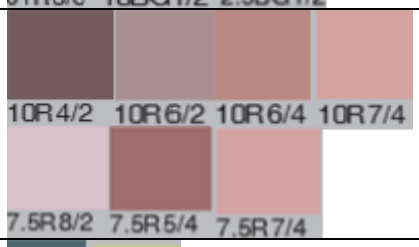
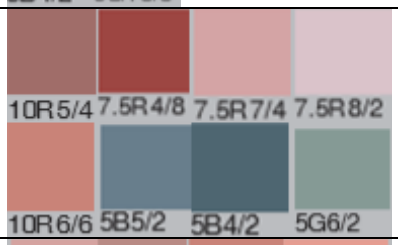
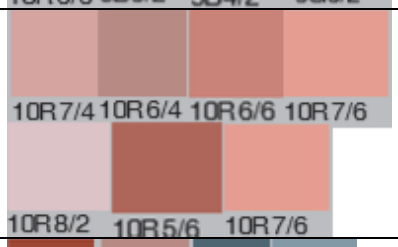
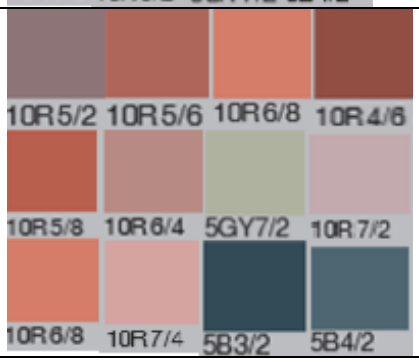


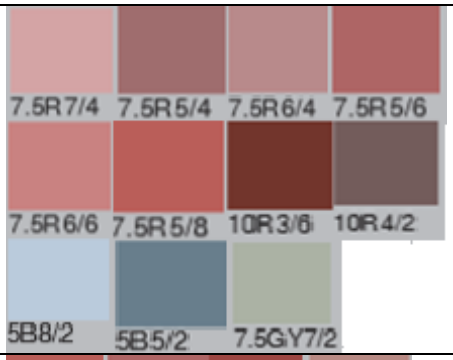
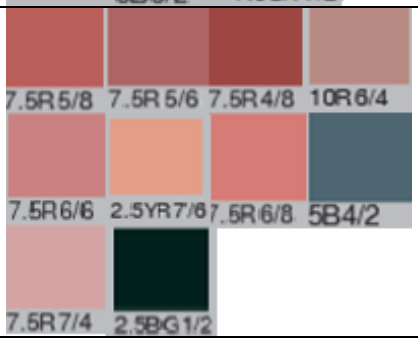
Figure 4.14. Grazing Outcrop 2 looking east across the exposure (Photograph by D. Tasker).

The descriptions of outcrops reveal that extensive intra- and inter-outcrop lithological heterogeneity was observed, throughout the three kilometre radius of the study area (see Table 7, Appendix). Statistically described in section 4.3, the variability is visually represented by the geological samples in Table 4.2. It should be noted that colours reflect only captured variance and not abundance.

Table 4.2. geological samples by macroscopic properties

Outcrop	Grain Visibility	Colour (Munsell)	Texture	Banding
FFIO1	5 Yes 0 No		0 Fine 4 Medium 1 Coarse	0 Yes 5 No
FFIO2	5 Yes 0 No		0 Fine 3 Medium 2 Coarse	0 Yes 5 No

GO1	7 Yes 3 No		2 Fine 8 Medium 0 Coarse	6 Yes 4 No
GO2	3 Yes 4 No		4 Fine 2 Medium 1 Coarse	0 Yes 7 No
MGQ1	2 Yes 3 No		3 Fine 2 Medium 0 Coarse	1 Yes 4 No
MIO1	4 Yes 5 No		6 Fine 2 Medium 1 Coarse	7 Yes 2 No
MIO2	10 Yes 0 No		0 Fine 9 Medium 1 Coarse	8 Yes 2 No
MIO3	6 Yes 0 No		0 Fine 6 Medium 0 Coarse	0 Yes 6 no
MIO4	7 Yes 0 No		1 Fine 2 Medium 4 Coarse	2 Yes 5 No
MIO5	12 Yes 3 No		7 Fine 8 Medium 0 Coarse	4 Yes 11 No

QM	9 Yes 4 No		4 Fine 5 Medium 4 Coarse	1 Yes 12 No
VMO	5 Yes 3 No		4 Fine 4 Medium 3 Coarse	2 Yes 9 No

4.2 Macroscopic lithological analysis

Macroscopic lithological properties were descriptively analysed (see Table 7, Appendix). This included 103 geological samples from 12 outcrop sources, as well as 60 cores and 22 LCTs. Results of texture, grain visibility, banding, and colour characterisations are summarised below. These characteristics follow methods highlighted in Stout *et al.* (2005) and Goldman-Neuman and Hovers (2009) and are considered the most important variables for visually classifying raw material properties (see Chapter 3).

4.2.1 Texture

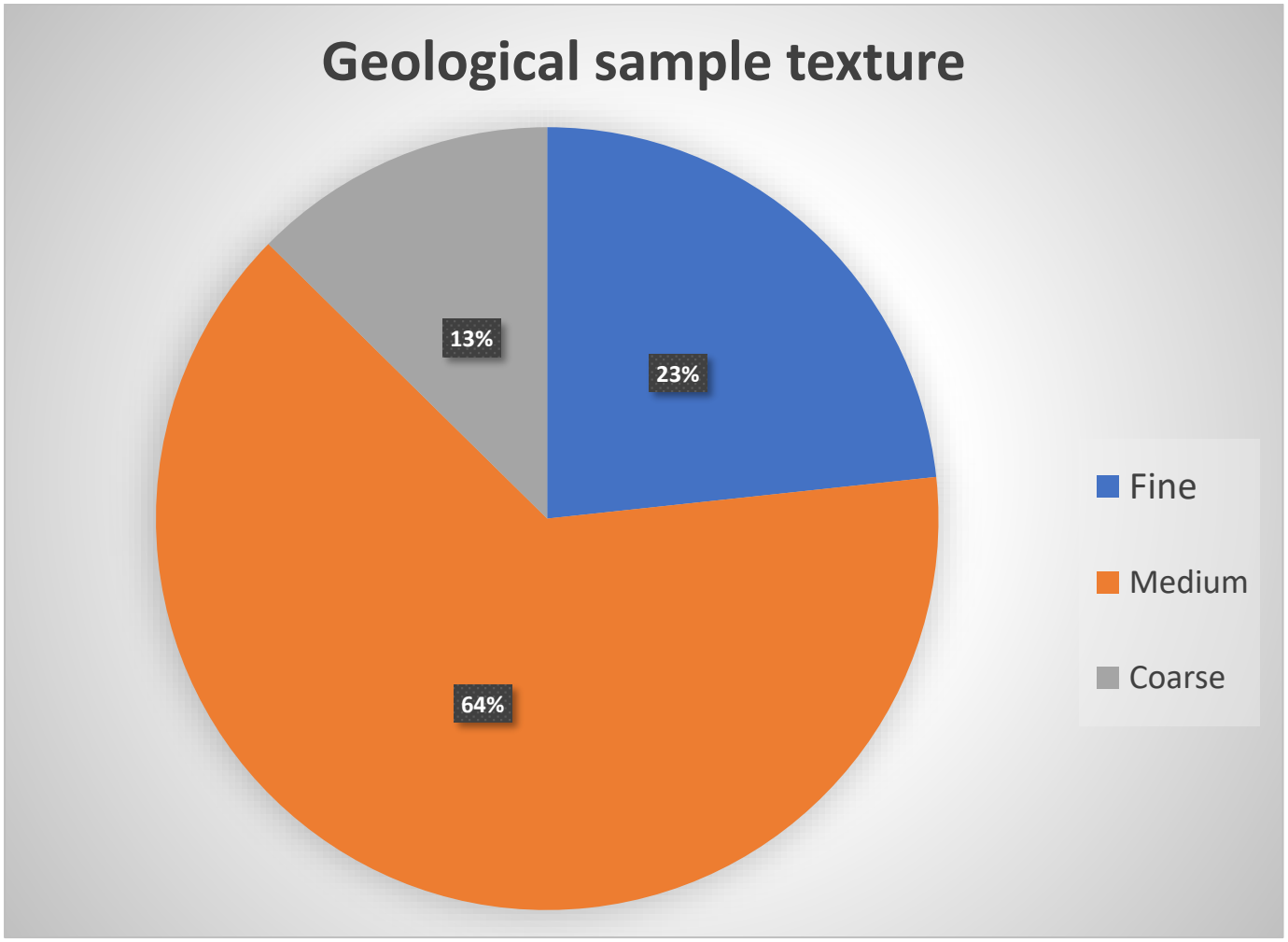


Figure 4.15. Quantification of geological sample textures (N= 103).

Figure 4.15 shows that medium grain sizes dominate the quartzite textures (66%) within the Maropeng geological sample. Fine-grained quartzites represent 23% of the sample, while 13% exhibit coarse-grained textures.

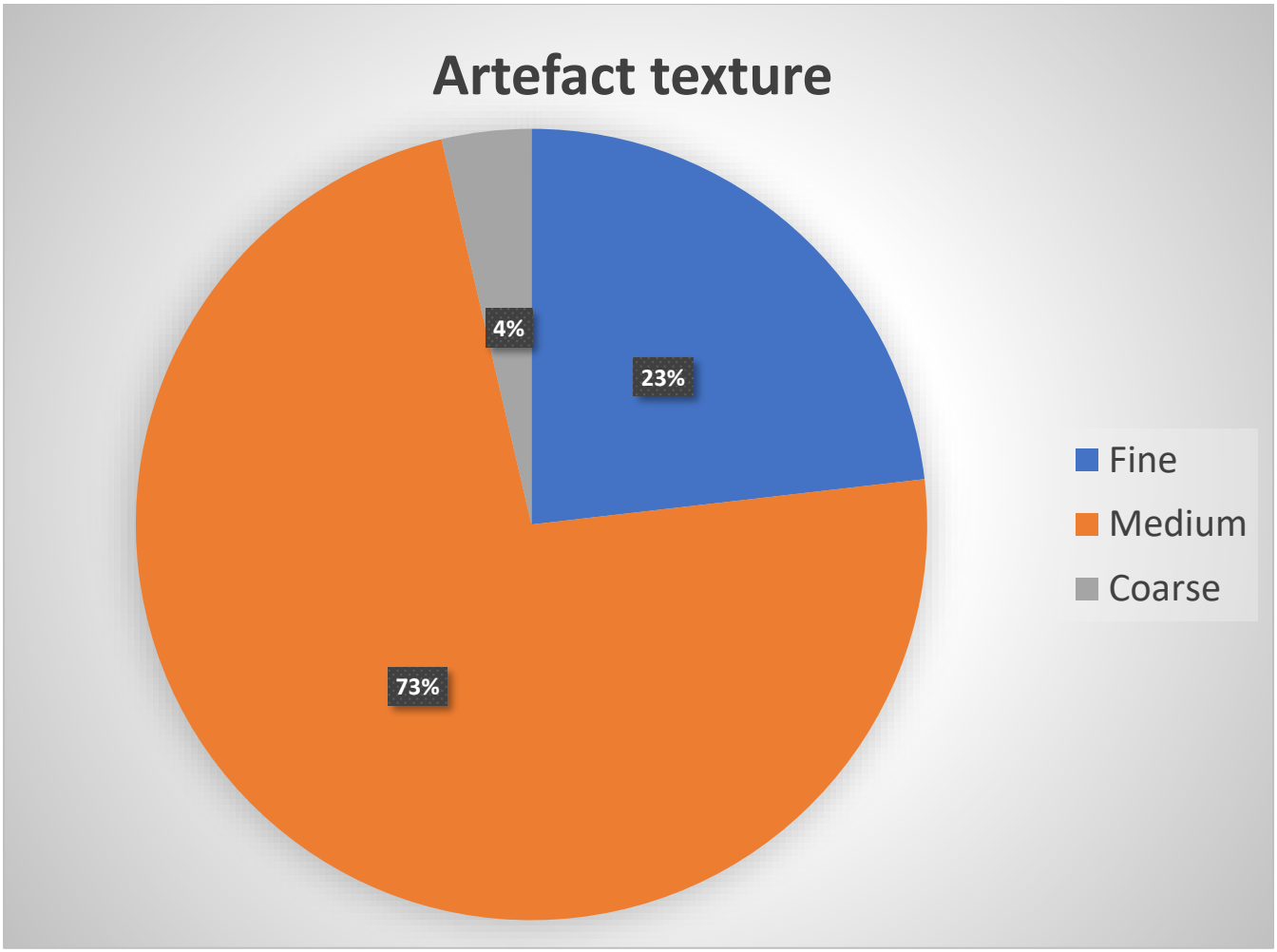


Figure 4.16. Quantification of artefact textures (N= 82)

Within the artefact sample (Figure 4.16), medium-grained textures predominate (N= 60), followed by fine-grained artefacts (N= 19), while only 3% show coarse-grained textures. This chart is reflective of the abundance of medium-grained quartzite textures seen in Figure 4.4 above.

To investigate any nuances in the selection of textures, LCT and core samples were charted separately (see Figures 4.17 and 4.18). LCTs further reflect a predominance of medium-grained (55%) textures followed by fine-grained (41%) and finally coarse-grained artefact (5%). Cores showed a pattern of medium-grained dominance (80%), then fine-grained (17%) and finally, coarse-grained (3%) textures.

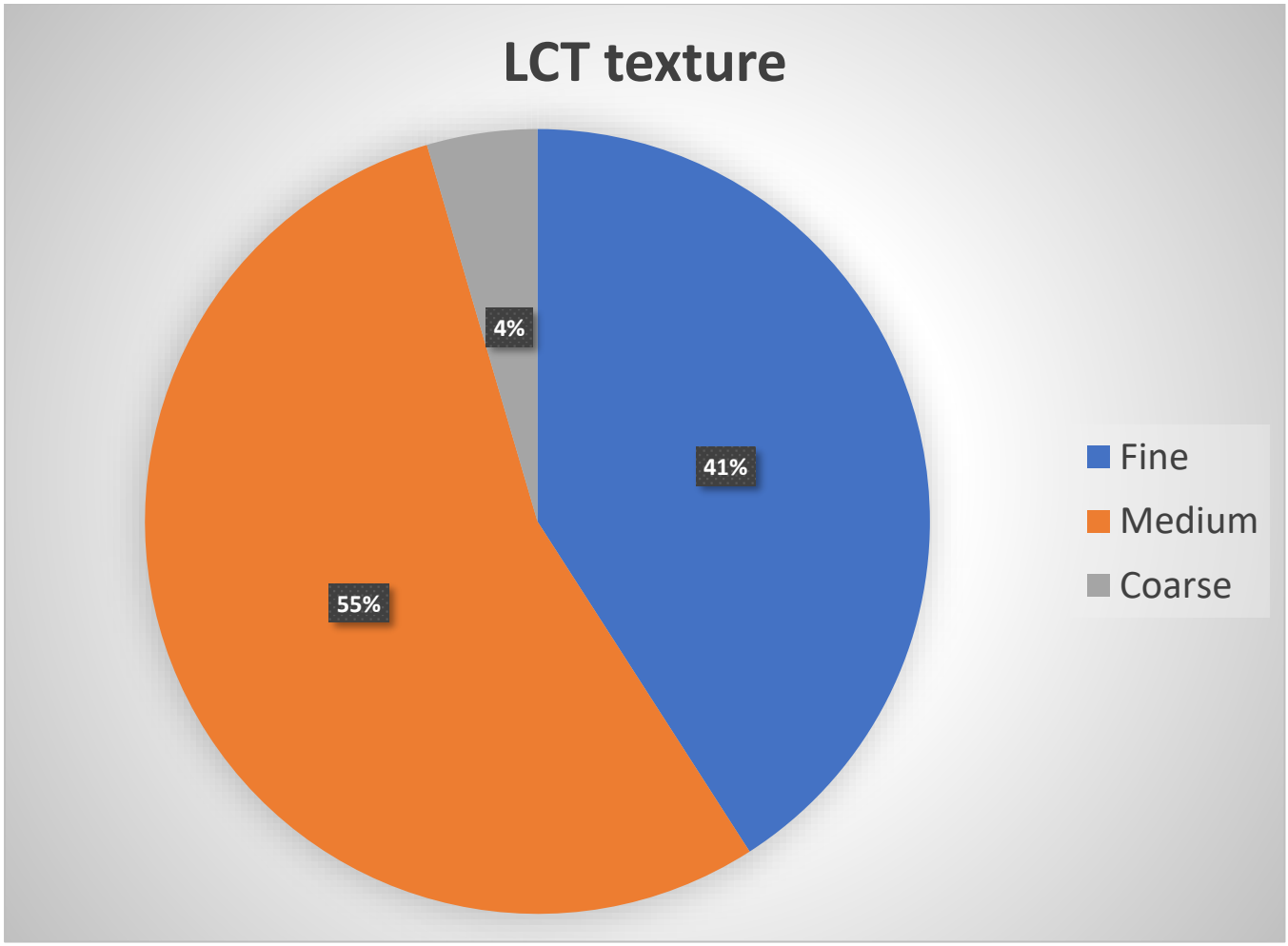


Figure 4.17. Quantification of LCT textures (N= 22)

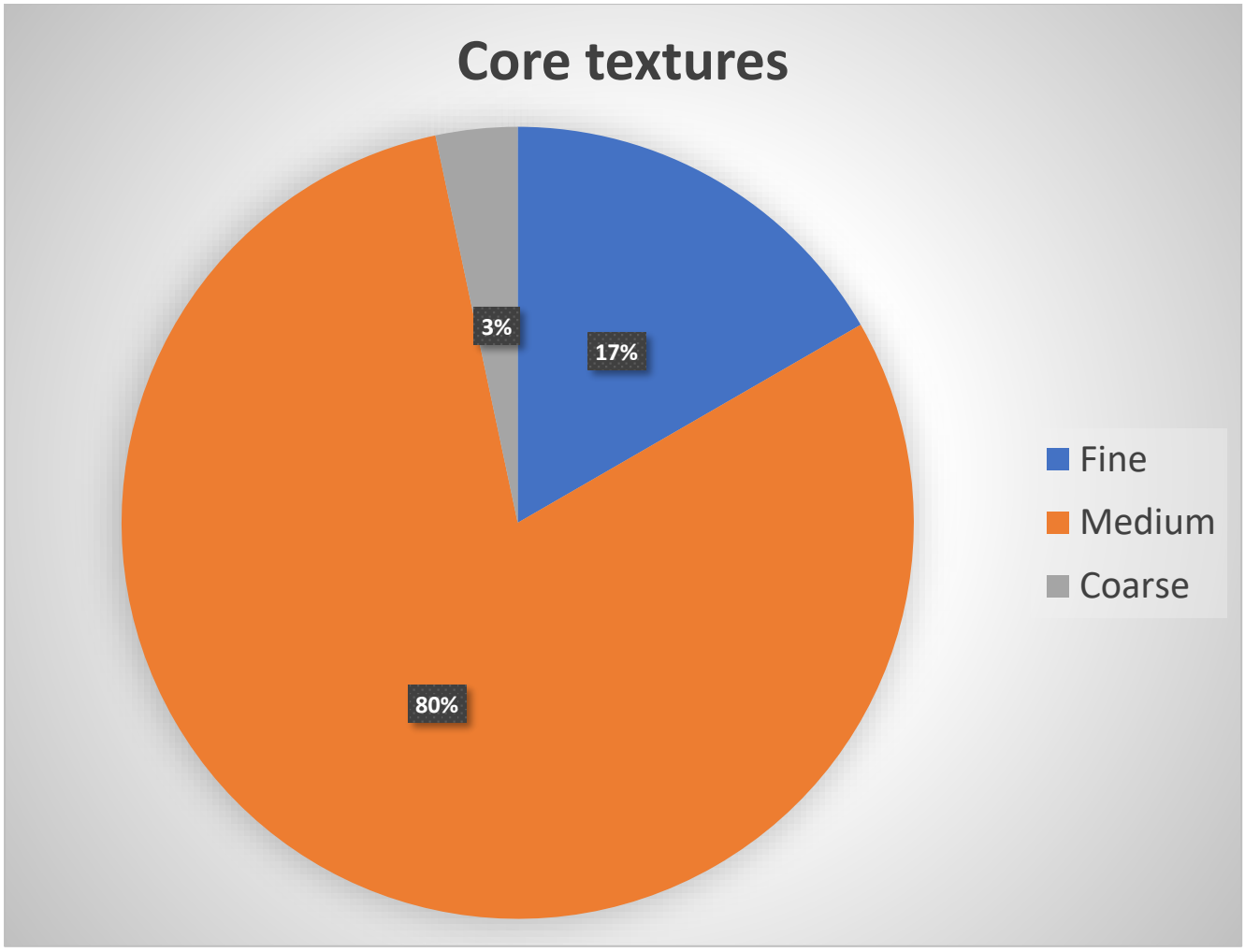


Figure 4.18. Quantification of core textures (N= 60)

4.2.2 Grain Visibility

There is a general correlation between quartzite texture and grain visibility, where grain size is not visible in fine-grained textures by definition. However, coarse quartzites had high grain-visibility with large quartz crystal inclusions, which was often paired with a sandy texture and minimal metamorphosis. Medium-grained quartzites retained smaller quartz crystal inclusions but were still visible macroscopically. The silty-sandy nature indicated a partial metamorphosis. Fine-grained examples were mostly silty in nature with quartz inclusions only visible under magnified conditions, suggesting complete fusion of interlocking quartz grains in terms of metamorphosis.

4.2.3 Banding

Figure 4.19 shows that colour banding is not common to geological outcrops, with 70% of samples lacking banding and 30% of samples showing some type of banding.

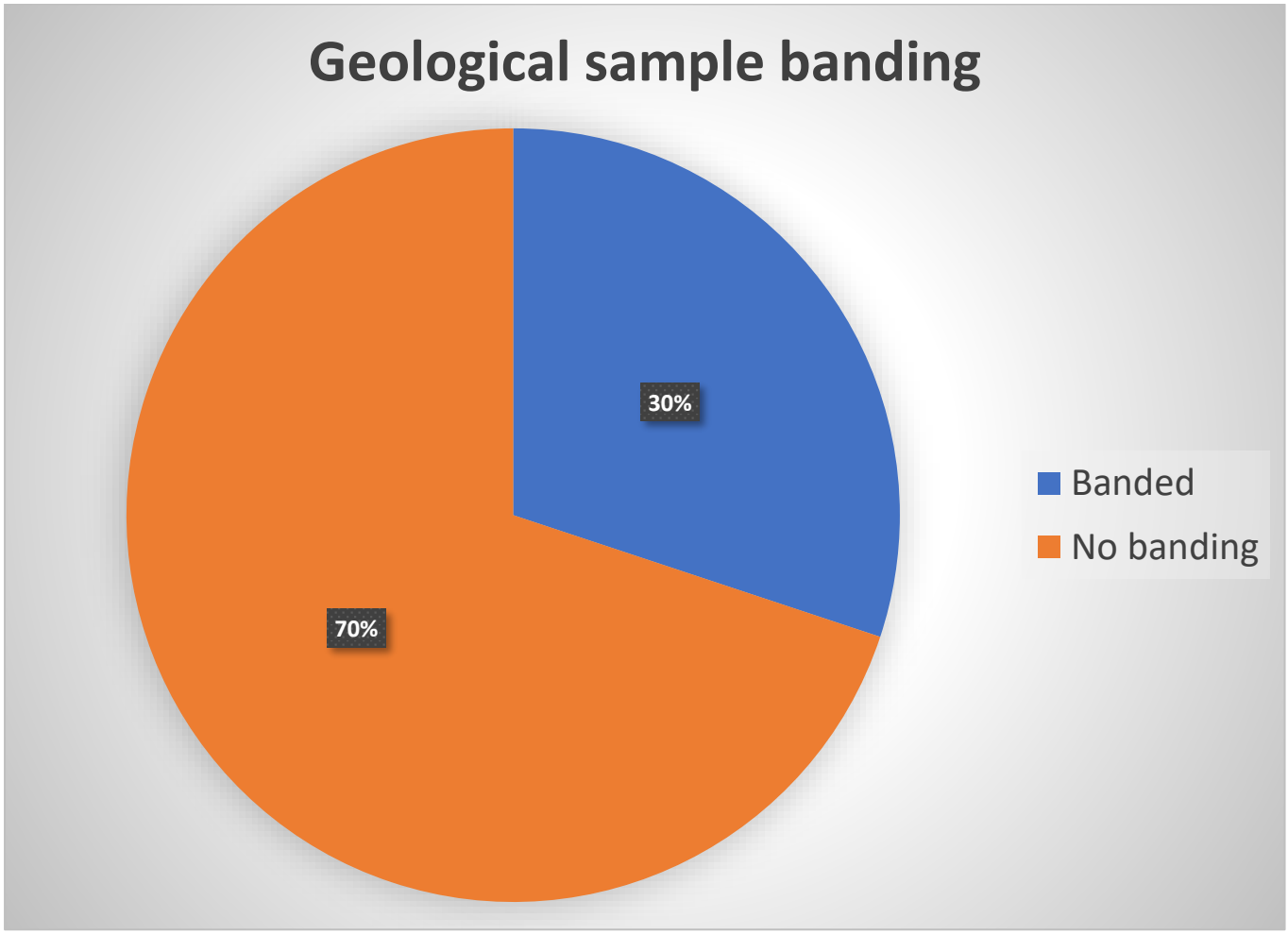


Figure 4.19. Quantification of geological sample banding (N= 103)

Figure 4.20 reflects the banding seen in artefacts, where 90% of artefacts reflect no banding, while only 10% of artefacts had banding.

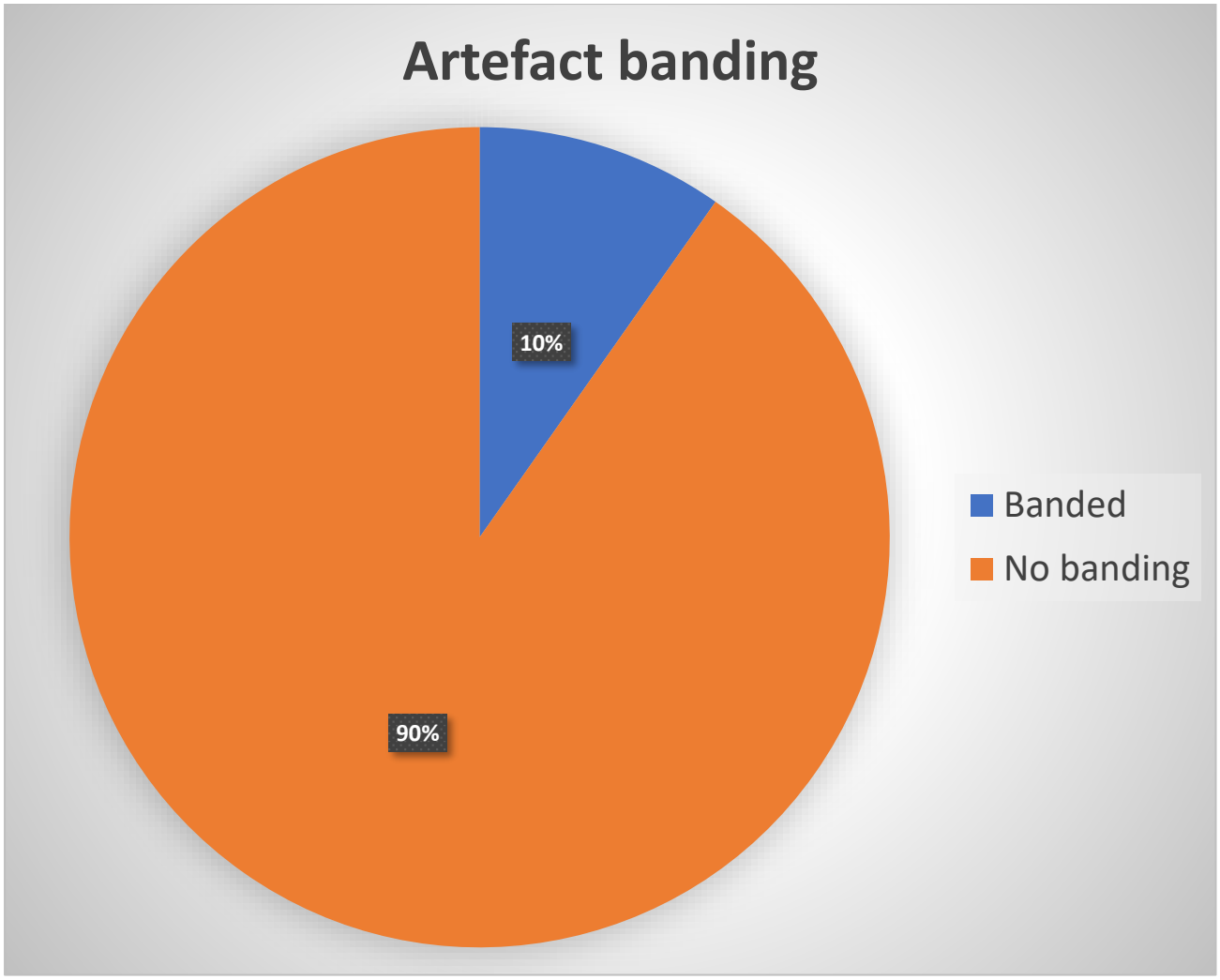


Figure 4.20. Quantification of artefact banding (N= 82)

Below in Figures 4.21 and 4.22, colour banding is divided by LCTs and cores, which show that large proportions (86% and 92%) of non-banded materials are represented in the artefact sample, while 14% of LCTs have banding along with 8% of cores.

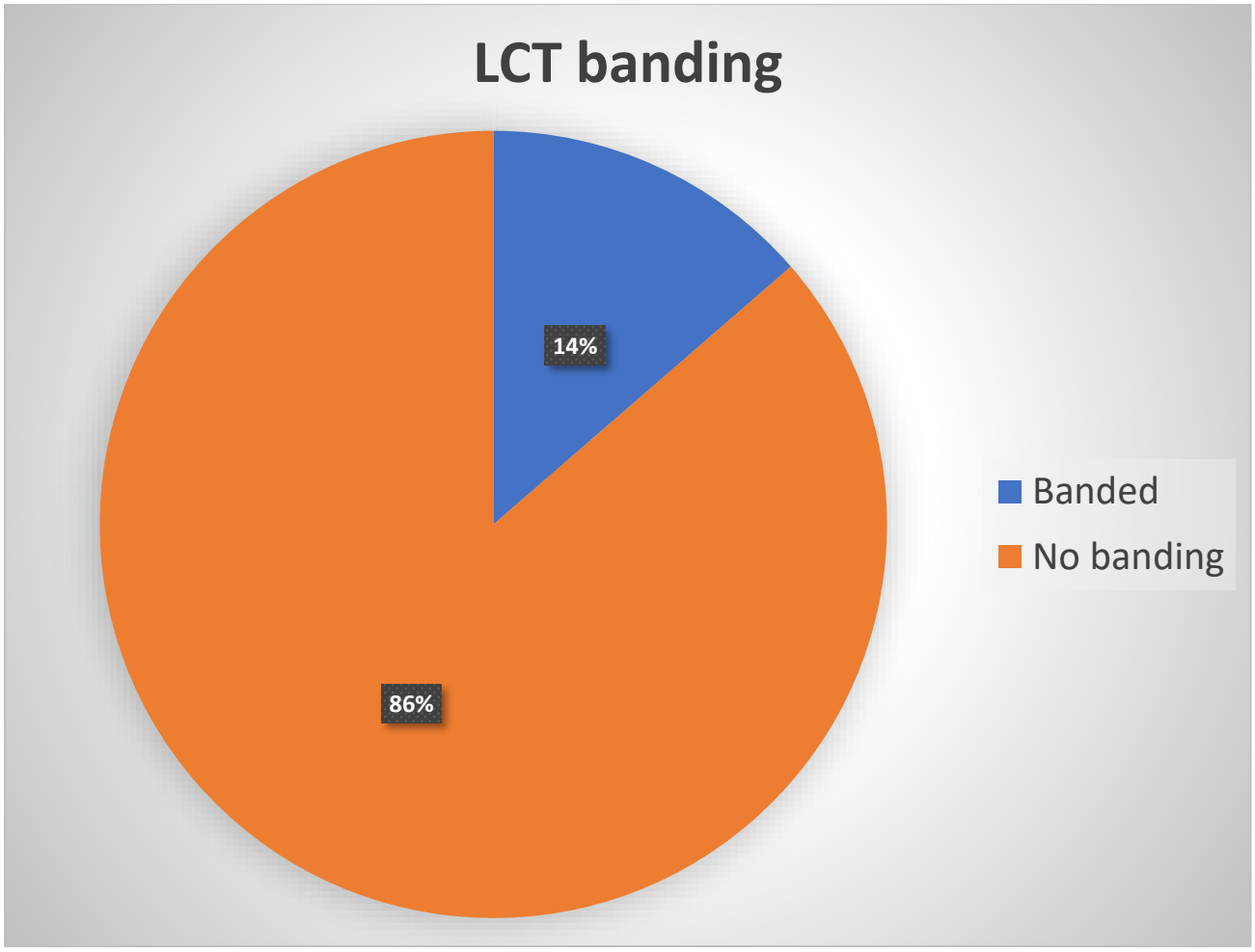


Figure 4.21. Quantification of LCT banding (N= 22)

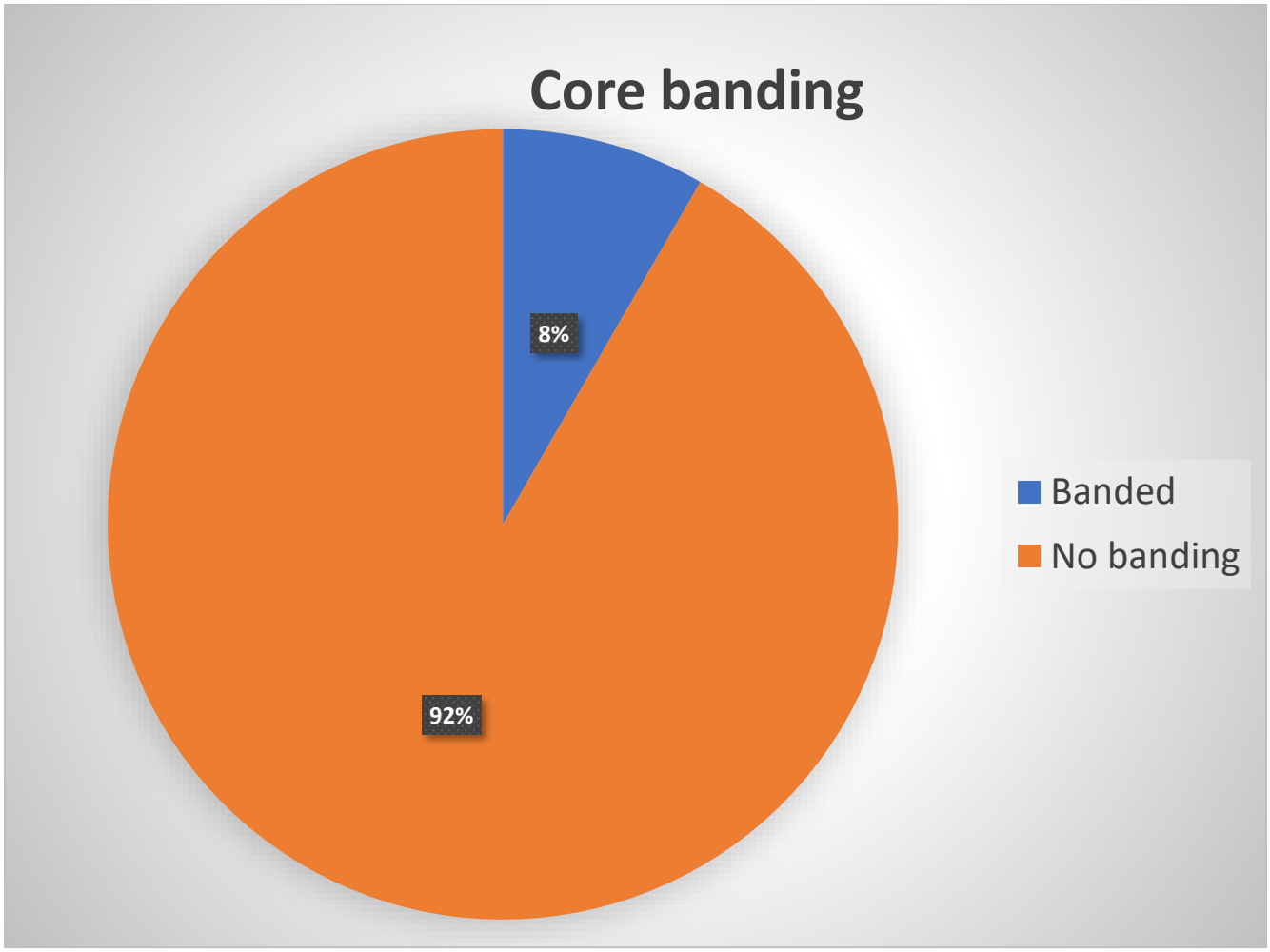


Figure 4.22. Quantification of core banding (N= 60)

4.2.4 Colour

More than 100 different colours were seen across the geological samples and artefacts, which is presented in Table 4.2 (see Table 7, Appendix). Many samples did exhibit more than one colour due to banding, however only the most dominant colour was used to summarise the results presented below (as such, complex colour variability requires further investigation through specialised petrography and can potentially reveal broader selection behaviours).

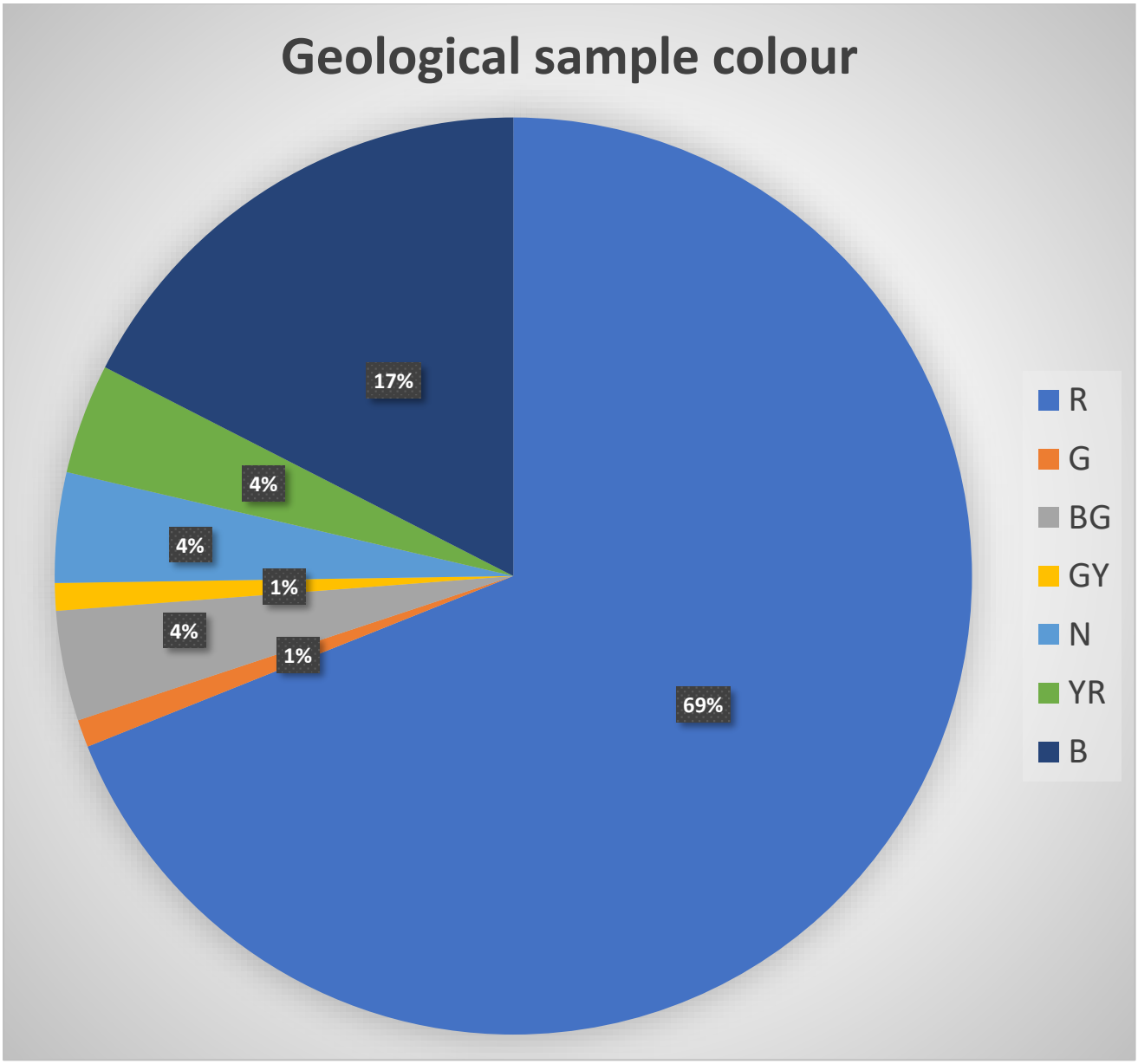


Figure 4.23. Colours present in geological samples (N= 103). Abbreviations: R= red, G=Green, N= neutral, GY= green-yellow, Y/R= yellow-red, B/G= blue-green, B=blue (corresponds to Munsell colours)

Colour was highly variable between geological samples, although the majority (69%) of quartzites were red (Fig. 4.23). This is followed by blue hues (17%) and then by yellow-red, neutral, and blue-green, each accounting for 4% of the sample, while green-yellow and green account for 1%.

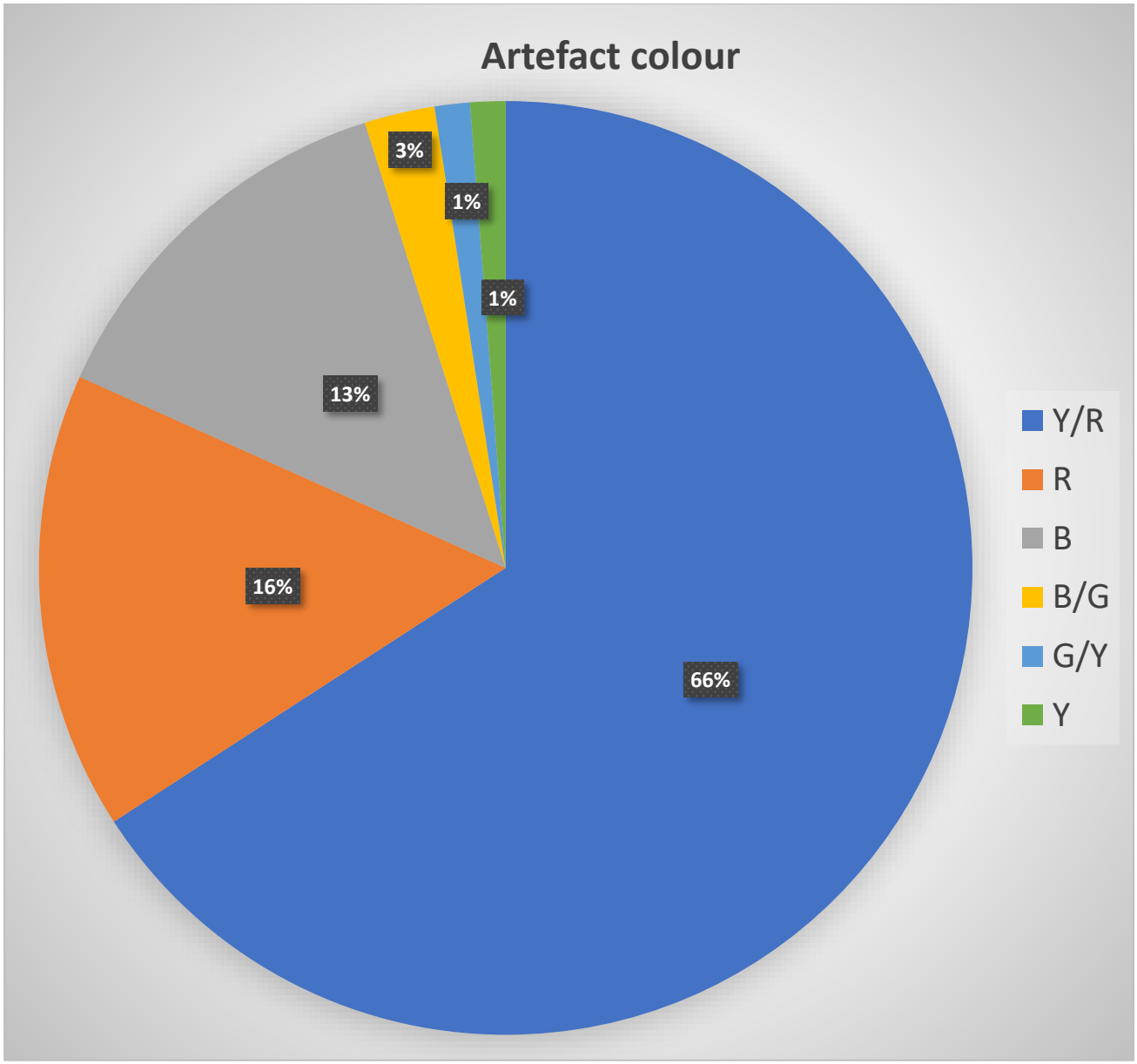


Figure 4.24. Colours present in artefacts (N= 82). Abbreviations: R= red, Y= yellow, GY= green-yellow, Y/R= yellow-red, B/G= blue-green, B=blue (corresponds to Munsell colours)

Figure 4.24 presents colour prevalence within the artefact sample, which shows a predominance of yellow-red hues (66%), followed by red (16%), blue (13%), blue-green (2%), yellow (1%) and green-yellow (1%). However, it should be noted that many artefacts are weathered, and the colour hue of quartzites seems to fade through this process, obscuring colour results to some degree (see Discussion Chapter).

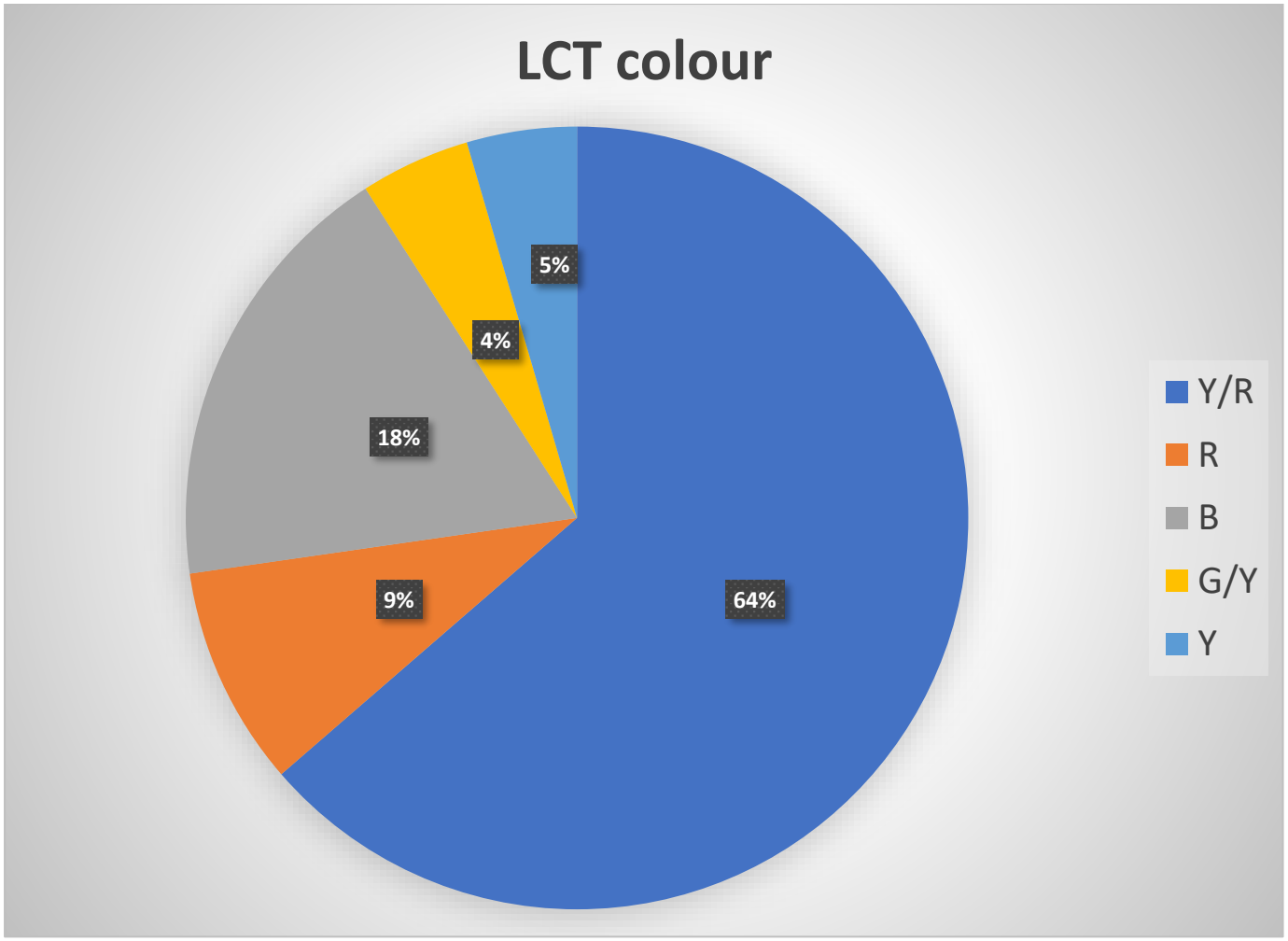


Figure 4.25. Colours present in LCT samples (N= 22). Abbreviations: R= red, Y=yellow, GY= green-yellow, Y/R= yellow-red, B=blue (corresponds to Munsell colours)

Figure 4.25 divides the LCT sample in colour groups where yellow-red hues predominate (64%), followed by blue (18%), red (9%), green-yellow (5%) and yellow (5%). Figures 4.26, 4.27 and 4.28 indicate colours prevalent within core divided by reduction strategies: bifacial, multifacial and unifacial. Yellow-red accounts for over half of the bifacial cores (60%), followed by red (27%) and blue and blue-green (7%) hues. Within the multifacial cores, yellow-red hues (77%), followed by blue (9%) and red (14%) hues. Similarly, unifacial cores are also predominated by yellow-red hued (50%), while blue (30%), red (10%), and blue-green (10%) hues comprise the rest of the sample.

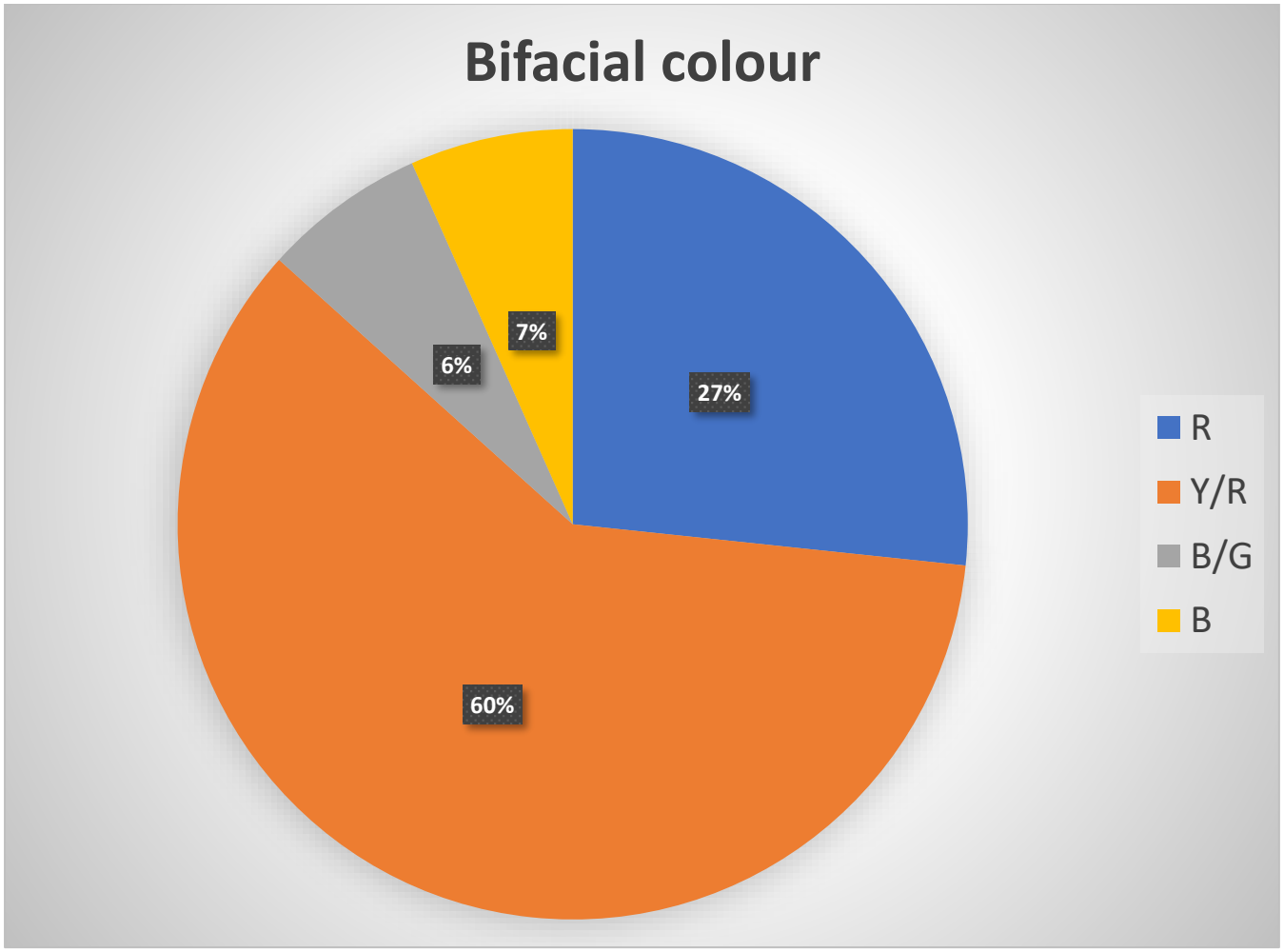


Figure 4.26. Colours present for bifacial core flaking strategies (N= 15). Abbreviations: R= red, Y/R= yellow-red, B/G= blue-green, B=blue (corresponds to Munsell colours)

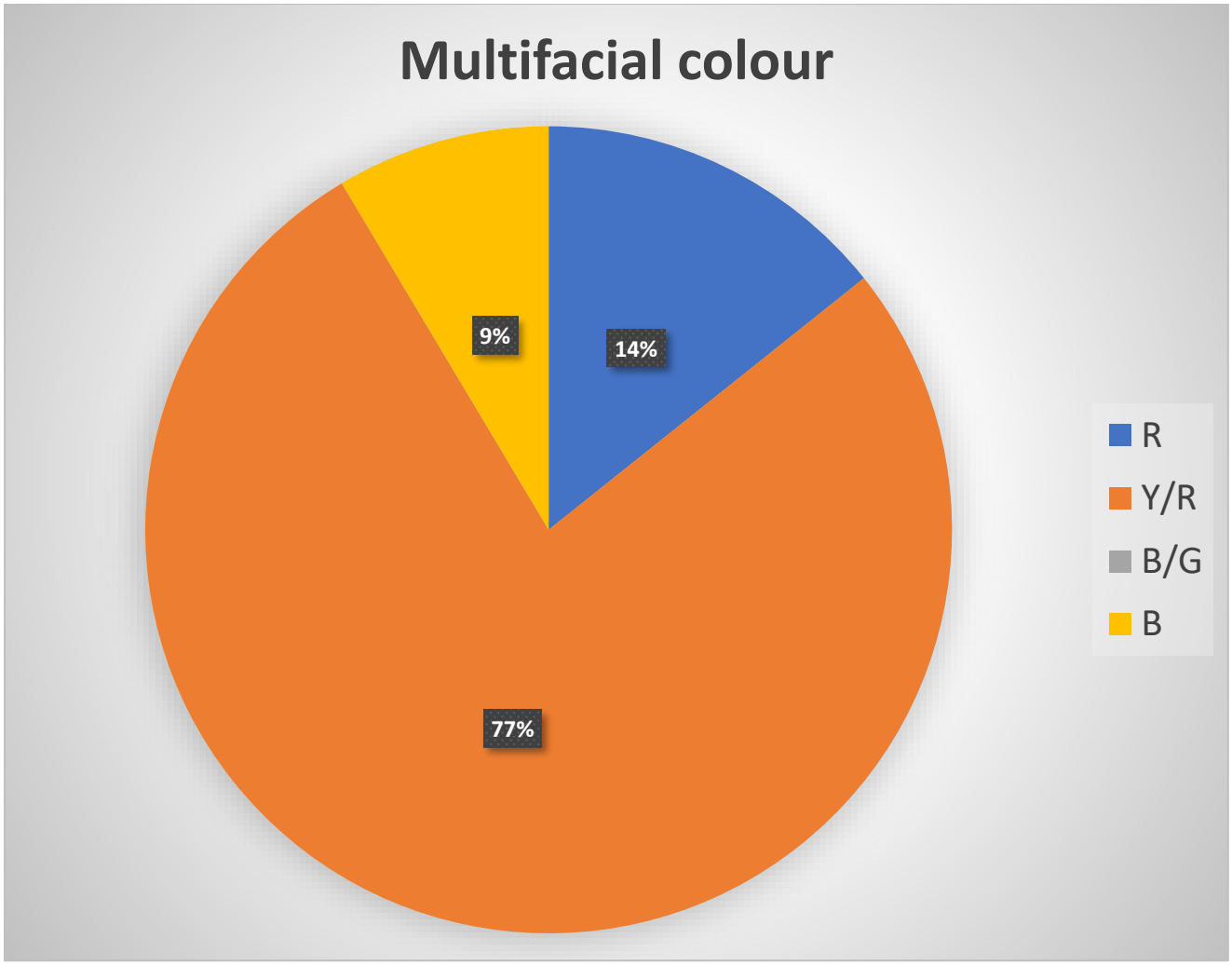


Figure 4.27. Colours present in multifacial core flaking strategies (N= 35) Abbreviations: R= red, Y/R= yellow-red, B/G= blue-green, B=blue (corresponds to Munsell colours)

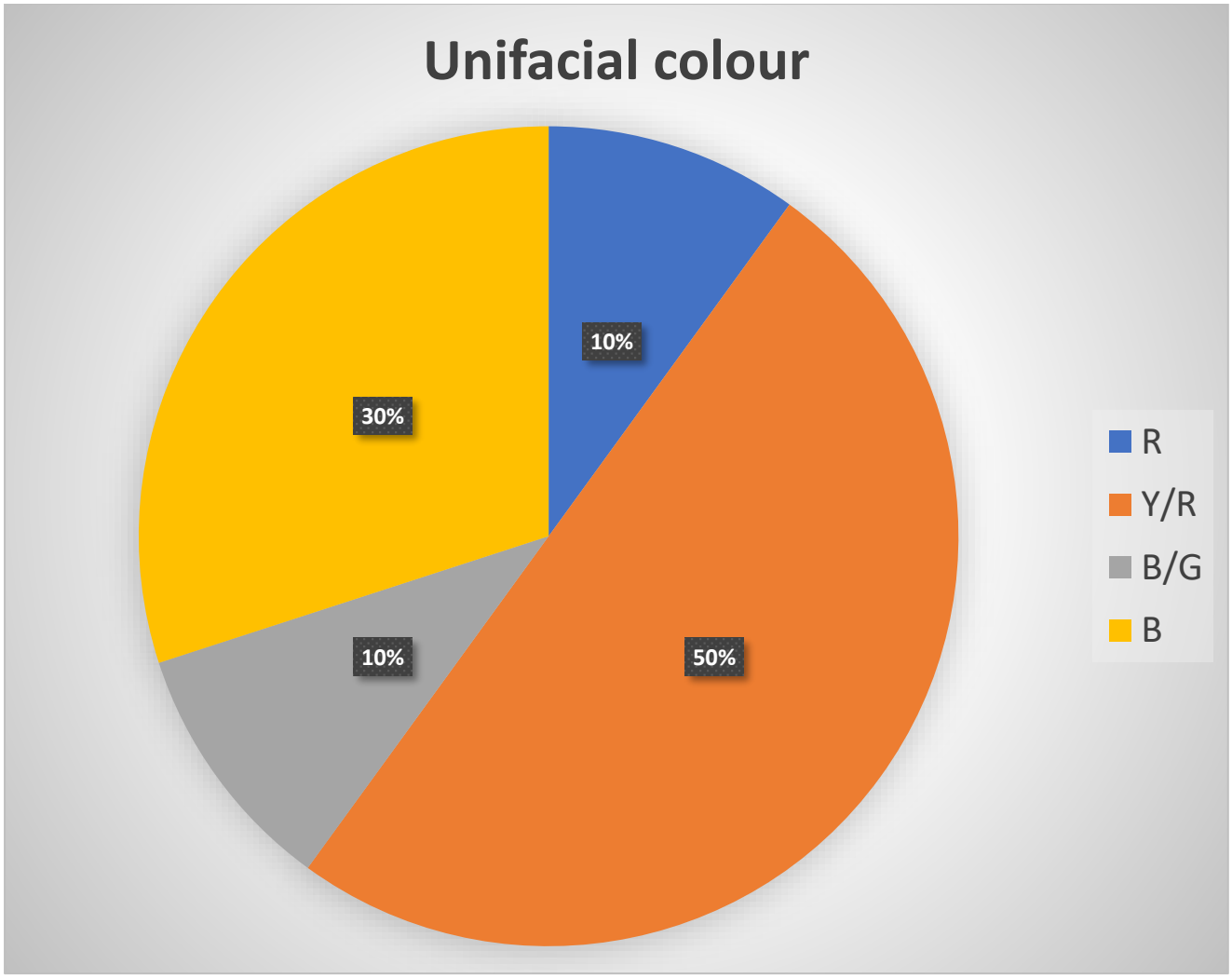


Figure 4.28. Colours present in unifacial core flaking strategies (N= 10) Abbreviations: R= red, Y/R= yellow-red, B/G= blue-green, B=blue (corresponds to Munsell colours)

4.3 Technological analysis

Tables 4.3 and 4.4 present results of descriptive statistics broken down by core and LCT types. For a detailed breakdown, Tables 1 and 2 (Appendix) depict the raw data concerning the technological analysis of the 60 Maropeng cores and 22 LCTs.

4.3.1 Cores

Bifacial cores

For bifacial cores, mean length is 101.1 mm, mean width is 75.6 mm and mean thickness is 47.4 mm, with average mass at 456 g. Flake scar numbers average 10.5 and range from two

to 20 in total, reflecting differences in reduction intensities, which is further reflected in cortex percentages that average 48% but vary from 0 to 90%. >45° angles (N= 9) are most prevalent when compared to <45° angles (N= 6). The mean area is 180.9 mm^2 and the mean volume is 170.5 mm^2. When divided by reduction strategy following the schemes of de la Torre (2011), bifacial reduction schemes are largely comprised of simple partial exploitation (BSP) (N= 11), followed by one abrupt partial exploitation (BAP), two peripheral (BP) and two alternating partial (BALP) exploitation techniques (see Table 2, Appendix).

Multifacial cores

Multifacial cores (Table 4.3) have a mean length 100.1 mm, a mean width of 72.6 mm and a thickness mean of 63.3 mm with an average mass of 481.63. Mass measurements also exhibit a large range in variance 1144.9 g. Scar counts are the highest in mean value at 14, which range from 3- 33 scars and cortex percentages are lowest within the core sample with a mean of 34%. >45° angles (N= 32) are more prevalent than <45° angles (N= 3), which is similar to bifacial cores, and mean area and volume are 183.2 mm and 184 mm, respectively. According to exploitation strategies, only multifacial reductions were seen with no clear signs of organization in flaking (see Table 2, Appendix).

Unifacial cores

Unifacial cores (Table 4.3) have a mean length of 94.2 mm, a mean width of 64.8 mm and a mean thickness of 47.1 mm. Interestingly, width showed little variation in unifacial cores when compared with other types. The mean mass for unifacial cores is 335.2 g suggesting they are comparatively smaller in size. An average of eight flake scars characterise unifacial cores but show a large variance ranging from 1- 24 scars. Cortex percentages vary from 0 to 90% and have the highest mean value among core strategies, at 59%. >45° angles (N= 8) are more prevalent in the assemblage than <45° angles (N= 2) and the mean area is 147.2 mm and the mean volume is 126.9 mm. Unifacial reduction strategies are predominated by unidirectional abrupt (UAU1) exploitation (N= 5), followed by two simple partial (USP), two unifacial centripetal (UC) and one abrupt unidirectional total exploitation (UAUT) exploitation scheme (see Table 2, Appendix) (de la Torre 2011). Total exploitative techniques

(unifacial centripetal exploitations and unifacial abrupt unidirectional total exploitation) are not as apparent at just three of the ten unifacial cores.

Table 4.3. Descriptive analysis of core technological attribute

Bifacial cores (N= 15)	**Length**	**Width**	**Thickness**	**Mass (g)**	**Scars**	**Cortex %**	**Area**	**Volume**
Mean	101.14	75.60	47.41	456.01	10.46	48.26	180.86	170.51
Median	105.2	73.1	46.1	447.34	10	40	192.67	164.2
Standard Dev.	20.43	19.19	7.79	236.88	5.16	27.1	66.67	87.01
Range	64.1	56	25.8	910.44	20	90	239.16	330.24
Minimum	70.3	50.5	35.3	143.82	2	0	87.44	57.58
Maximum	134.4	106.5	61.1	1054.26	22	90	326.6	387.82
Multifacial cores (N= 35)	**Length**	**Width**	**Thickness**	**Mass (g)**	**Scars**	**Cortex %**	**Area**	**Volume**
Mean	100.08	72.61	51.45	481.63	14.6	34	183.16	184.65
Median	95.5	72.5	50.8	401.31	13	28	171.81	150.02
Standard Dev.	28.44	17.22	13.65	315.43	8.79	26.69	81.65	122.21
Range	113.2	71.7	63.3	1144.9	31	85	283.76	444.92
Minimum	59.6	45.3	21.6	86.71	2	0	65.35	33.08
Maximum	172.8	117	84.9	1231.61	33	85	349.11	478
Unifacial cores (N= 10)	**Length**	**Width**	**Thickness**	**Mass (g)**	**Scars**	**Cortex %**	**Area**	**Volume**
Mean	94.18	64.78	47.1	335.15	8	59	147.218	126.98
Median	88.95	65	46.5	254.19	4	72.5	125.93	98.95
Standard Dev.	20.47	6.88	12.7	179.87	8.15	33.86	50.27	65.58
Range	70.3	24.1	34.7	497.91	24	90	147.24	187.91
Minimum	60.3	50	31	115.7	1	0	85.05	46.3
Maximum	130.6	74.1	65.7	613.61	25	90	232.29	234.21

Table 4.4. Descriptive analysis of LCT technological attributes

Cleavers (N= 4)	**Length**	**Width**	**Thickness**	**Mass (g)**	**Scars**	**Scar Directions**	**Cortex (%)**	**Area**	**Volume**
Mean	133.32	84.2	40.125	545.67	11.25	4.25	21.5	230.01	211.41
Median	126.15	81.05	37	378.1	11.5	4	20	192.48	148.16
Standard Deviation	21.29	15.69	13.77	369.52	3.5	0.5	16.19	86.31	144.99
Range	46.6	35.7	32.5	770.83	8	1	34	182.83	306.81
Minimum	117.2	69.5	27	327.83	7	4	6	176.14	121.26

Maximum	163.8	105.2	59.5	1098.66	15	5	40	358.97	428.07
Handaxes (N= 14)	**Length**	**Width**	**Thickness**	**Mass (g)**	**Scars**	**Scar Directions**	**Cortex (%)**	**Area**	**Volume**
Mean	135.12	80.49	42.25	492.46	17.71	4.5	23.35	213.01	184.93
Median	121.9	76.25	41.95	374.175	18.5	4.5	20	178.605	141.94
Standard Deviation	28.30	13.30	8.64	240.60	5.53	1.16	15.06	66.06	86.75
Range	78	40.8	30.8	788.42	19	4	43	189.53	264.22
Minimum	108.8	68.3	28.3	300	8	3	4	150.45	110.89
Maximum	186.8	109.1	59.1	1088.42	27	7	47	339.98	375.11
Picks (N= 4)	**Length**	**Width**	**Thickness**	**Mass (g)**	**Scars**	**Scar Directions**	**Cortex (%)**	**Area**	**Volume**
Mean	155.12	77.47	47.6	553.22	25	5	27.75	231.2	210.00
Median	154.4	79.1	45.8	572.045	20	5	27	234.855	218.16
Standard Deviation	17.46	22.46	6.07	209.74	12.19	1.82	15.12	60.68	78.98
Range	39.7	46.3	13.8	436	26	4	35	123.33	163.89
Minimum	136	52.7	42.5	316.41	17	3	11	165.88	119.9
Maximum	175.7	99	56.3	752.41	43	7	46	289.21	283.79

4.3.2 Large Cutting Tools

Cleavers

Cleavers have a length mean of 133.3 mm, a mean width of 84.2 mm, a mean thickness of 40.1 mm and an average mass of 545.67 g (Table 4.4). Scar counts average at 11.25 and scar directions average 4.25, albeit the maximum amount of rotational directions is five, suggesting that rotation was common during cleaver production. Cortex percentage has a mean of 21.5% and the maximum is 40% and cleavers only exhibit >45° angles (N= 4), with no <45° angles recorded. The mean area is 230 mm^2 and the mean volume is 211.4 mm^2.

Handaxes

Handaxes have a mean length of 135.1 mm, a mean width of 80.5 mm, a mean thickness of 42.3 mm and an average mass of 492.5 g, which is lowest within the LCT sample (Table 4.4). Scar counts are higher than cleavers with a mean of 17.7 while scar directions similarly average at 4.5. Cortex percentage is low, at a mean of 23.4% but retained cortex values of up to 47%. Seven handaxes retained <45° edge angles and the remaining seven displayed >45° angles and mean area is 213 mm^2 and the mean volume is 184 mm^2. Areas and volumes are noticeably smaller on handaxes when compared to cleavers and picks.

Picks

Picks exhibit a mean length of 155.1 mm, a mean width of 77.5 mm, a mean thickness of 47.6 mm, with an average mass of 553.2 g (Table 4.4). Length and thicknesses are observably larger on average compared with the overall LCT sample. Picks also exhibited the highest average scar count (25) and scar directions. Cortex percentage held an average value of 27.8% varying between 11% and 46%. Half of the picks (N= 2) exhibited <45° angles while, the remaining two held >45° angles. The mean area is 231.2 mm^2 and the mean volume is 210 mm^2 showing similar measurements to cleavers. One pick was trihedral-like while the others depicted bifacial working and a large focus on the creation of a pick-like tip.

4.4 Reduction intensity

The measurement of reduction intensity was calculated through the Scar Density Index (SDI) (Clarkson 2013; Shipton & Clarkson 2015). This calculation assumes that flaked pieces (i.e., cores and LCTs) with ratios of less surface area (mm^2) to higher flake scar counts are comparatively more reduced than artefacts demonstrating the opposite trend. Statistical Mann-Whitney U tests were used to indicate statistical significance on the boxplots below. P-values of 0.05 or lower indicate statistical significance (Drennan 2009). R^2 and p-values are used to show the correlation of the data and their significance respectively, and regression graphs were used to model these relationships. R^2-values approach either negative (-1) or positive (1) relationship values and are ranked, being weak (0-0.3) moderate (0.3-0.7) or strong (0.7-1) relationships The results (see Tables 8 and 9, Appendix) of these methods are presented below on the Maropeng assemblage.

4.4.1 Scar Density Index

Cores

Figure 4.29 depicts the SDI values across core types in a boxplot. The Mann-Whitney U tests between bifacial and unifacial cores showed no statistical significance (U=206, z=1.19 and p=0.24). No statistical significance was also shown when comparing bifacial to multifacial cores (U=51, z=1.3, and p=0.192). Results indicated that near statistical significance (approaching 0.05) was achieved when comparing unifacial to multifacial cores (U= 107, z= 1.84 and p= 0.065). The range indicated through the whiskers demonstrates that multifacial cores display the highest range of SDI scores as well as the highest reduction intensity measures across core types. Unifacial reduction strategies capture the second highest variability in core SDI scores. The low observable mean may link to limited knapping platforms, while the large variability can be attributed to one of the cores utilising total exploitation techniques (see Table 2, Appendix). Bifacial cores show the smallest variance with outliers of two total exploitational techniques, potentially skewing the data. Low variance may link to core abandonment of bifacial strategies early in the reduction sequence, due to loss of workable platforms.

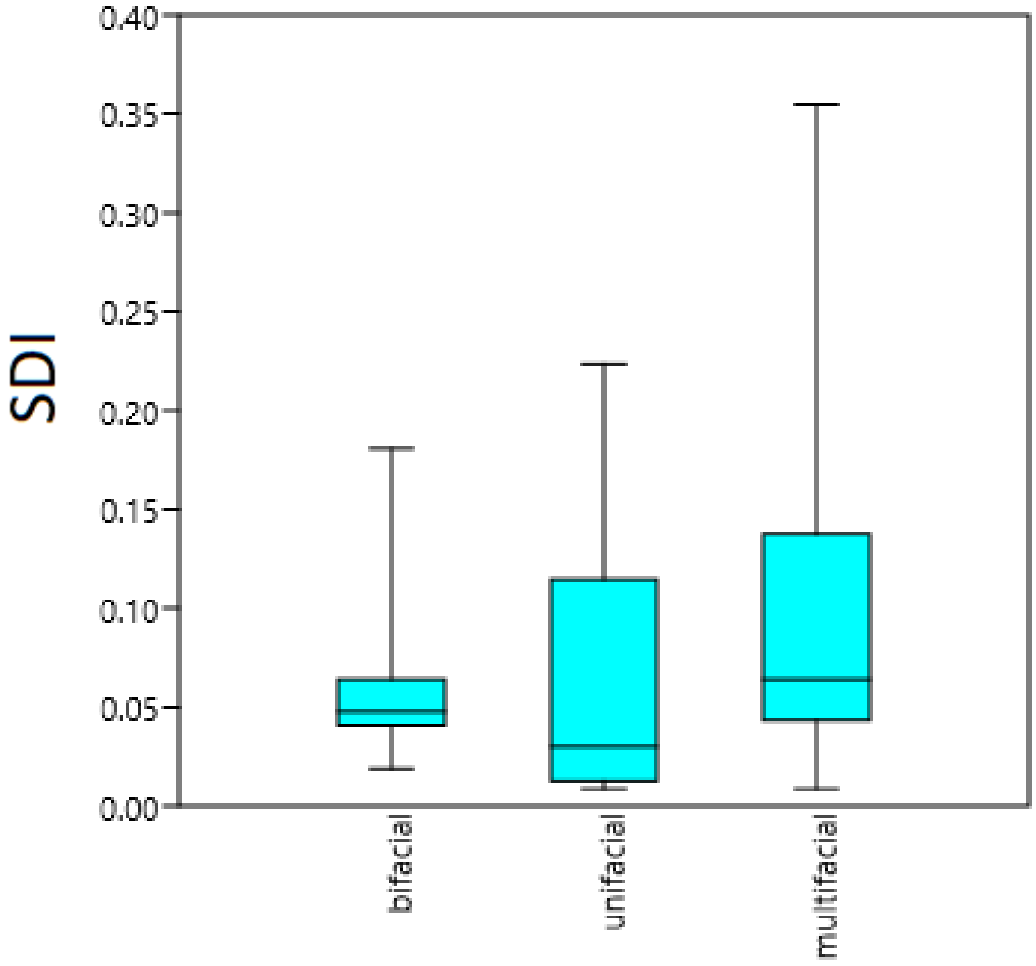


Figure 4.29. SDI values calculated across reduction strategies (bifacial: N=15, unifacial: N=10 and multifacial: N= 35).

Large Cutting Tools

Figure 4.30 depicts SDI scores of LCT types through a boxplot. Mann-Whitney U tests revealed that the relationship between handaxes and picks was not statistically significant (U= 17, z= 1.12, and p= 0.265). On the other hand, the relationship was minimally statistically significant when comparing handaxes to cleavers (U= 9, z= 1.97, and p= 0.049). While the relationship between cleavers and picks nearly approached significant difference (U= 4, z= 1.88, p= 0.065). The whiskers shown in this boxplot detail handaxes to capture the highest SDI variance and the largest amount of reduction. Cleavers see the smallest variance

in SDI values, potentially due to their focus on the cleaving edge, seen in the lower scar direction counts (Table 4.4). Picks hold the highest mean SDI values potentially due to the reduction needed to produce an elongated pick-like tip seen in high scar direction counts (Table 4.4). Small sample sizes may have affected the statistical significance scores.

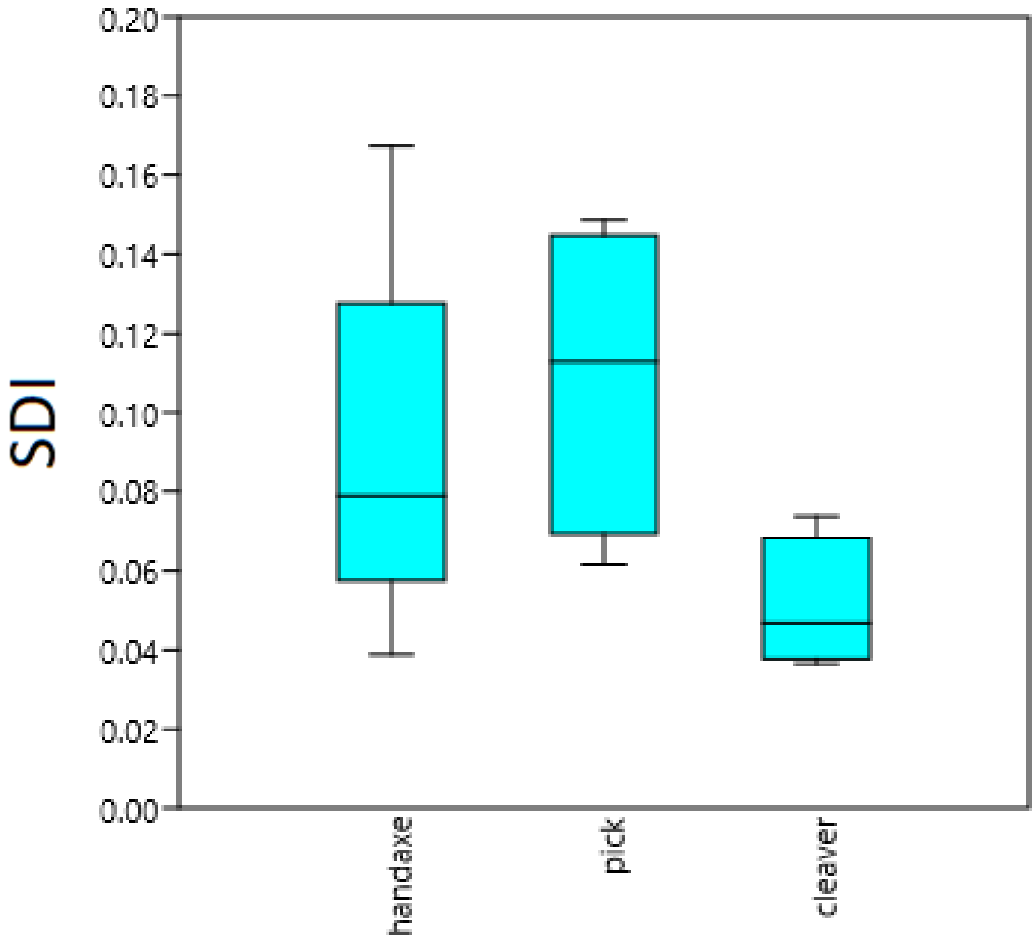


Figure 4.30. SDI values across LCT types (handaxes: N= 14, cleavers N= 4 and picks: N=4).

Comparing cores and Large Cutting Tools

Figure 4.31 indicates the variability of SDI within cores and LCTs. Results between types were not statistically significant (U= 524, z= 1.42p= 0.156). Cores and LCTs both show generally low SDI scores and therefore both reflect low reduction intensities. Cores depict a larger variance, but a smaller mean compared to LCTs. Looking to Figure 4.29, the large variability, observed here in the core whiskers is explained due to the variance in multifacial core reduction patterns.

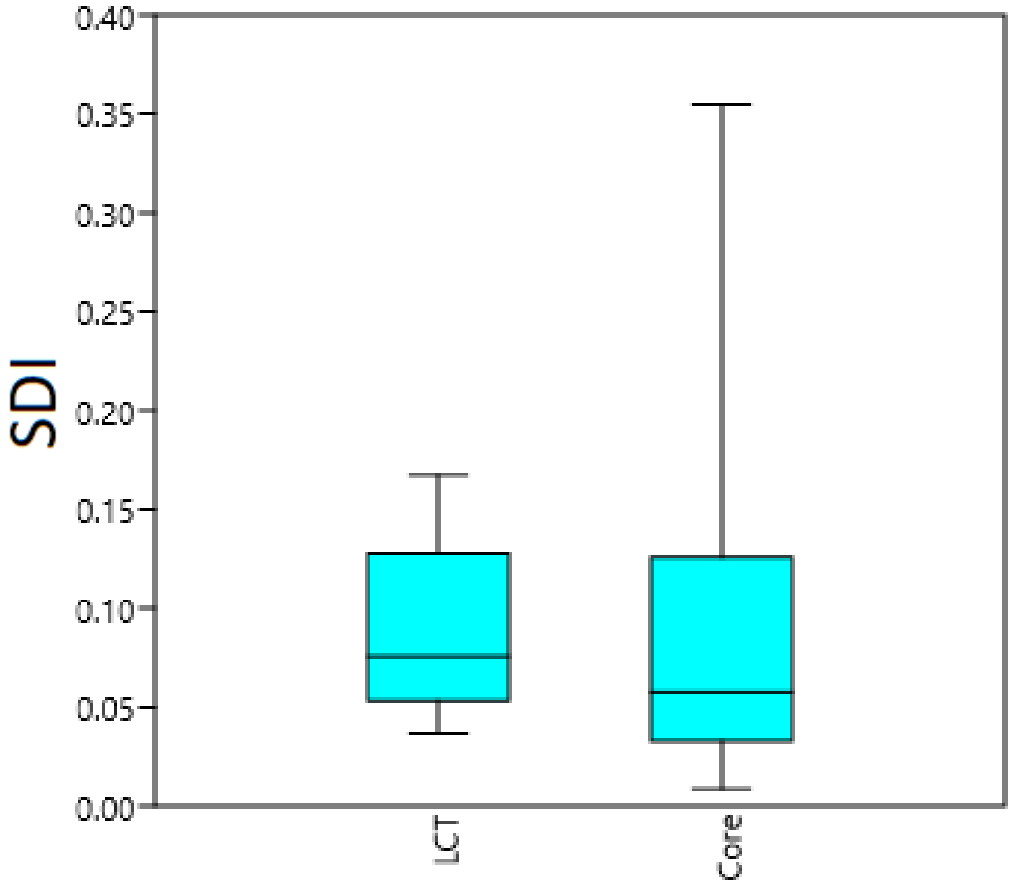


Figure 4.31. LCT and core SDI variability within the Maropeng assemblage (LCTs: N= 22 and cores: N= 60).

Scar Density Index by Volume

This thesis calculated the reduction intensity of Maropeng LCT and core types through SDI values. To verify the use of this index, SDI values of the flaked pieces samples analysed here are regressed against volume. This test assesses the hypothesis that higher SDI values will correlate significantly with flaked pieces with less volume, 'verifying' the use of the SDI as an indicator of reduction intensity (Clarkson 2013). Figure 4.32 shows that the r^2 correlation value is relatively weak (r^2= 0.197), although the best fit line visually indicates a negative correlation, which reflects that as flaking increases, so does volumetric loss. These variables are significantly correlated (p= 0.001), which demonstrates that the SDI measurement predicts volumetric loss in flaked pieces and is an accurate representation of reduction intensity.

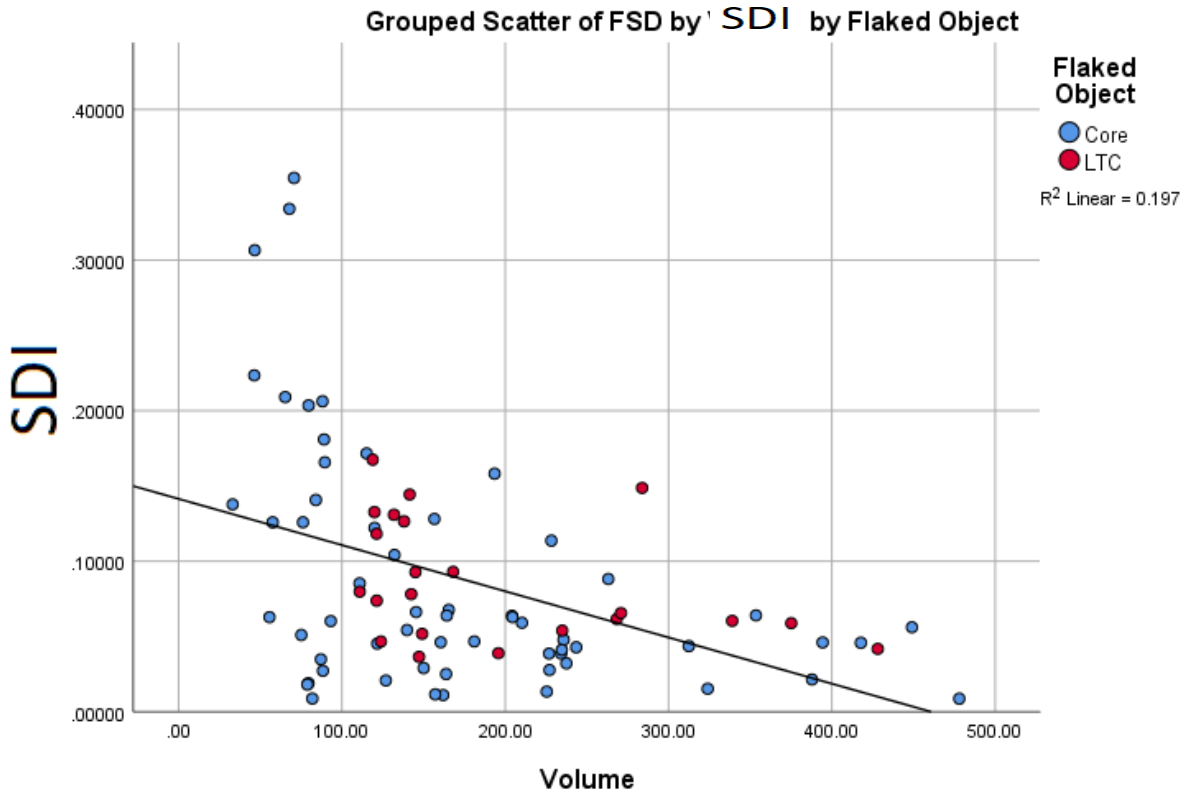


Figure 4.32. A linear regression plotting SDI by volume in flaked objects

4.5 Geochemistry

AD-ICPMS and P-XRF results were both employed to geochemically distinguish outcrops on the Maropeng landscape. AD-ICPMS measured 41 trace elements, mostly immobile rare

earth elements, while P-XRF methods captured the composition of 38 major elements. Utilising two methods allowed for a larger range of elements to be quantified, which provided the best chances of chemically characterizing quartzite outcrops.

Within the AD-ICPMS results, phosphorus, copper, chromium and barium show the highest concentrations, while vanadium, zinc and zirconium show the lowest (Figure 4.33). Within the P-XRF results, iron and silica show the highest concentrations within quartzite samples, while phosphorus, potassium, calcium and aluminium show the smallest (Figure 4.34).

In general, overall elemental homogeneity characterizes the quartzite outcrops (see Tables 8 and 9, Appendix), which possibly relates to similarities in the formation processes, despite differences in petrographic properties (Dalpra & Pitblado 2015; Pitblado *et al.* 2008; 2013; Soto *et al.* 2020). However, variation in the proportions of elements between quartzite outcrop samples distinguish them when statistically compared (Pitblado *et al.* 2013).

Pearson correlation matrix tests were run to examine the extent of geochemical homogeneity of quartzite outcrop within AD-ICPMS and P-XRF results. Results in Tables 8 and 9 (Appendix) showed high correlations across all samples in both the AD-ICPMS and P-XRF datasets. While this confirmed expected homogeneity, hierarchical clustering analysis based on PCA factoral scores, were used to distinguish outcrops. This was based on the variance of geochemical element concentrations following Pitblado *et al.* (2013).

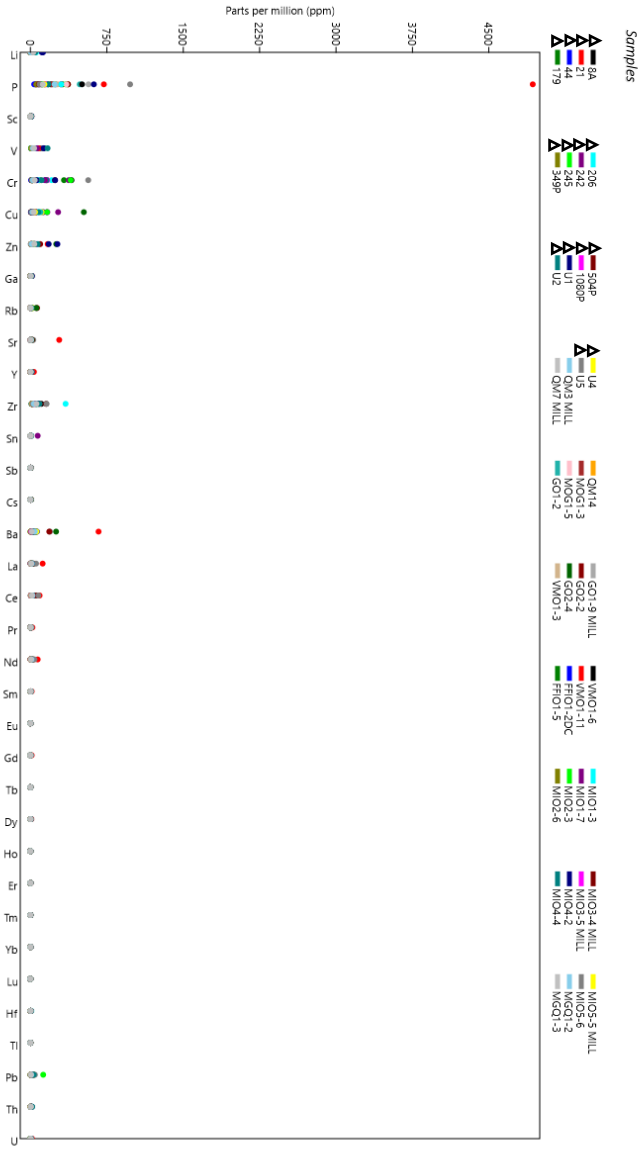


Figure 4.33. Parts per million values of elements across geological and archaeological samples, detected though AD-ICPMS. Artefact samples are distinguished through the use of triangles.

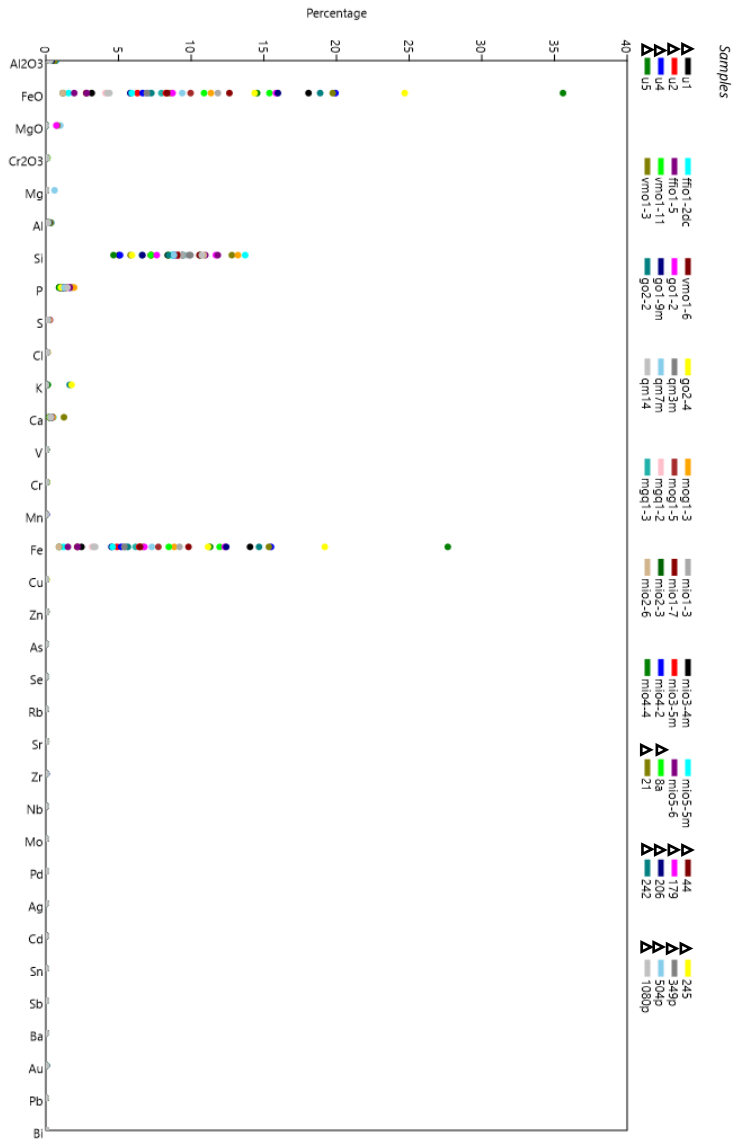


Figure 4.34. Percentage values of elements across geological and archaeological samples, detected though P-XRF. Artefact samples are distinguished through the use of triangles.

4.5.1 Calculating variance

Principle component analyses (PCA) were applied to both geochemical datasets to attain factoral (PC) scores that grouped chemical elements by their percentage of variance. The first five PC scores accounted for 98.59% of the geochemical variance within the AD-ICPMS sample and 99.97% of the P-XRF sample (see Table's 10 and 11, Appendix). Following Pitblado *et al.* (2013), these PC scores were then used in a heirarchical cluster analysis to assess their similarities in element variance through a dendrogram graph. Samples with a

single u-link demonstrate a high likelyhood of being related by a specific measure (Drennan 2009).

AD-ICPMS PCA linkage of outcrop samples

Figure 4.35 portrays a dendrogram results for AD-ICPMS tests cluster, which shows few natural pairings between outcrops in u-links.

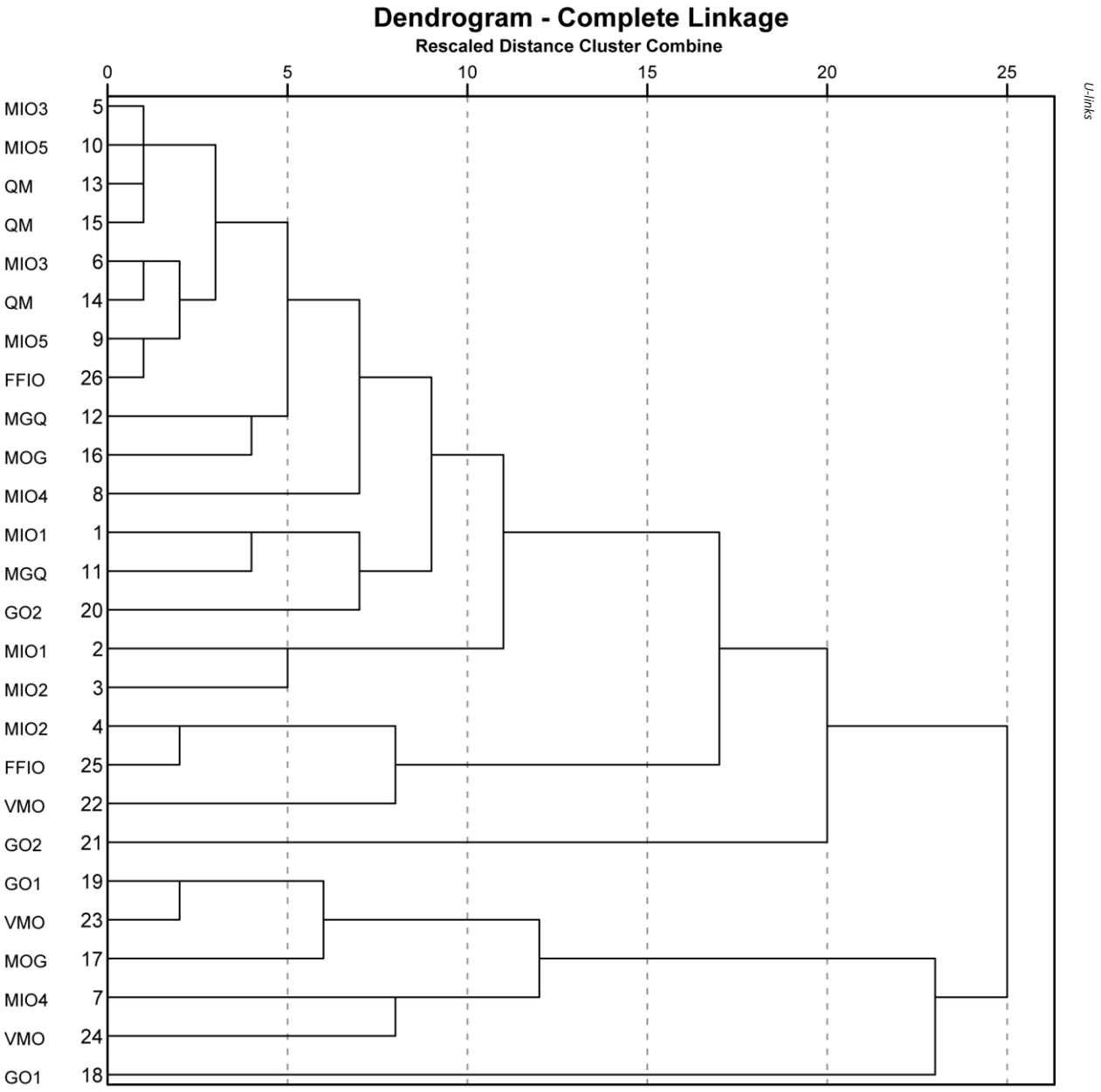


Figure 4.35. Geological AD-ICPMS samples displayed in a hierarchical cluster dendrogram

P-XRF PCA linkage of outcrop samples

Figure 4.36 displays the dendrograph graph for P-XRF results, which comparatively shows more u-links between common outcrop samples. When analyzing the quartzite outcrops, there are few u-links between samples from related sources. This attests to the high percentage of geochemical homogeneity and has been found in other studies using similar types of data and methods (Pitblado *et al.* 2013). It is further possible that small sample sizes (i.e. the number of physical samples taken and tested) have impacted geochemical sorting. Nonetheless, the P-XRF results do display single u-links between samples from a common outcrop, which suggests better geochemical distinguishing.

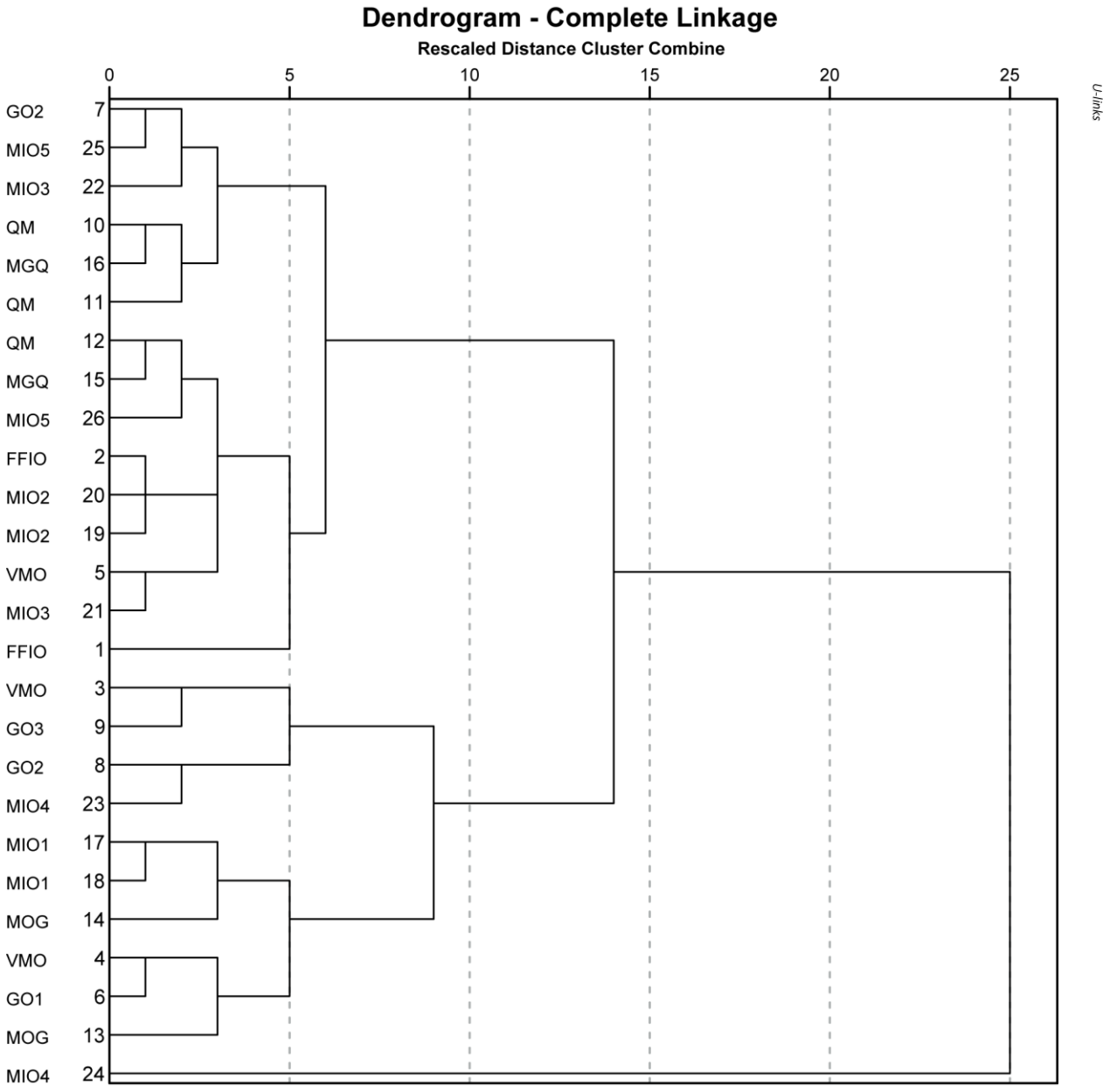


Figure 4.36. Geological P-XRF samples displayed in a hierarchical cluster dendrogram

AD-ICPMS PCA linkage across outcrop and archaeological samples

Figure 4.37 depicts the dendrogram linkage between quartzite outcrop and Maropeng artefact samples acccording to AD-ICPMS data. This further confirms that geological samples from common outcrops do not cluster well, and moreover the Maropeng artefacts form a distinct branch, unrelated to outcrops samples. This suggests that the Marpeng artefacts are more related to each other geochemically than to the sampled quartzite outcrops, when traced

through trace elements. These results do not support chemical relationships between artefacts and outcrops that can be used for sourcing studies.

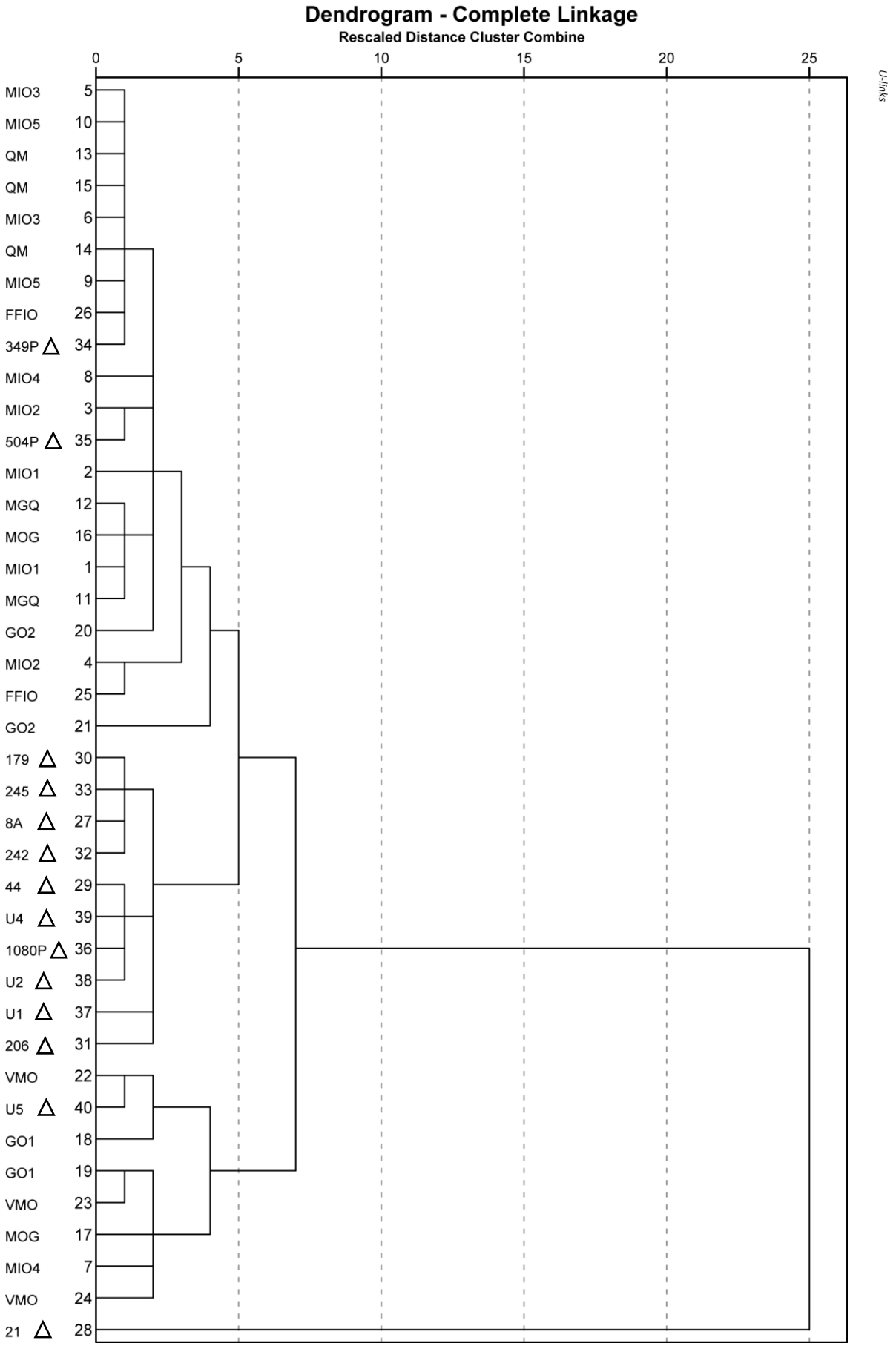


Figure 4.37. Archaeological and geological AD-ICPMS samples displayed in a hierarchical cluster

dendrogram. Artefact samples are distinguished through the use of triangles.

P-XRF PCA linkage across outcrop and archaeological samples

Figure 4.38 displays the dendrogram linkages between quartzite outcrops and Maropeng artefact samples according to the P-XRF results. Twelve of the 14 archaeological samples correlated to specific outcrop samples within this dendrogram. This likely relates to the greater variance traced in PC scores detected between major elements, which better distinguish quartzite outcrops. The two remianing un-linked artefacts potentially come from a source not identified within this study. Some artefacts were directly related by u-links to two different outcrops, such as 1080p, 349, U2 and U4. To rectify this complication, petrographic properties of artefacts and outcrops were cross referenced. Colour and texture linked 1080P to MIO2, 349 to MQG, U2 to QM, and finally U4 to QM as well.

It is noted that artefact 504p was made on a river cobble that subsequently linked to QM, while U5, also a river cobble, linked to MIO1. This may suggest that cobble conglomerates along local river systems may be highly variable in chemical composition (Pitblado *et al.* 2013) but also may be developed from the erosion of similarly composed quartzite sources upstream. These discrepancies can potentially be solved by larger sample sizes.

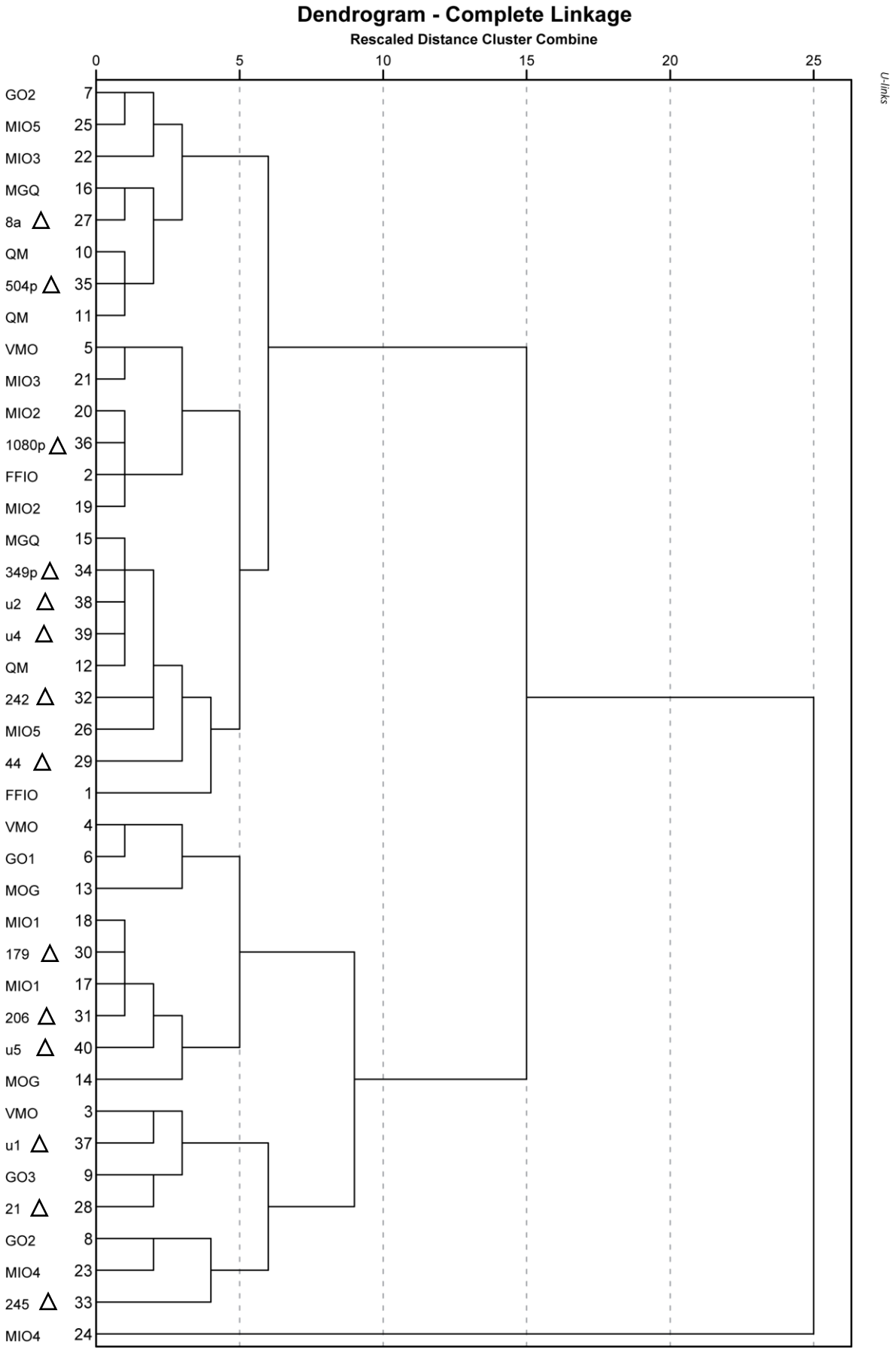

Dendrogram - Complete Linkage
Rescaled Distance Cluster Combine
0
5
10
15
20
25
U-links
GO2 7
MIO5 25
MIO3 22
MGQ 16
8a 27
QM 10
504p 35
QM 11
VMO 5
MIO3 21
MIO2 20
1080p 36
FFIO 2
MIO2 19
MGQ 15
349p 34
u2 38
u4 39
QM 12
242 32
MIO5 26
44 29
FFIO 1
VMO 4
GO1 6
MOG 13
MIO1 18
179 30
MIO1 17
206 31
u5 40
MOG 14
VMO 3
u1 37
GO3 9
21 28
GO2 8
MIO4 23
245 33
MIO4 24

Figure 4.38. Archaeological and geological P-XRF samples displayed in a hierarchical cluster dendrogram. Artefact samples are distinguished through the use of triangles.

4.6 Quartzite provenance predictions

Following Clarkson's (2013) and Shipton & Clarkson's (2015) methods discussed in Chapters Two and Three, SDI was plotted against distance to quartzite outcrops identified in the P-XRF dendrogram graph, as linking to Maropeng artefacts. Minimum distances from quartzite outcrops to the Maropeng archaeological site were used in the regression analysis. Figure 4.39 demonstrates an insignificant relationship between SDI values (reduction intensity) and quartz outcrop distances (p= 0.122). It also produced a very weak correlation (r^2= 0.04), likely due to small sample sizes. The graph does not demonstrate the typical linear relationship with distance, i.e., materials located further away were reduced to a greater extent (higher SDI value). Instead source distance correlated weakly with reduction intensity. Larger sample sizes producing more geochemical data may reveal stronger relationships between lithic procurement and eventual discard.

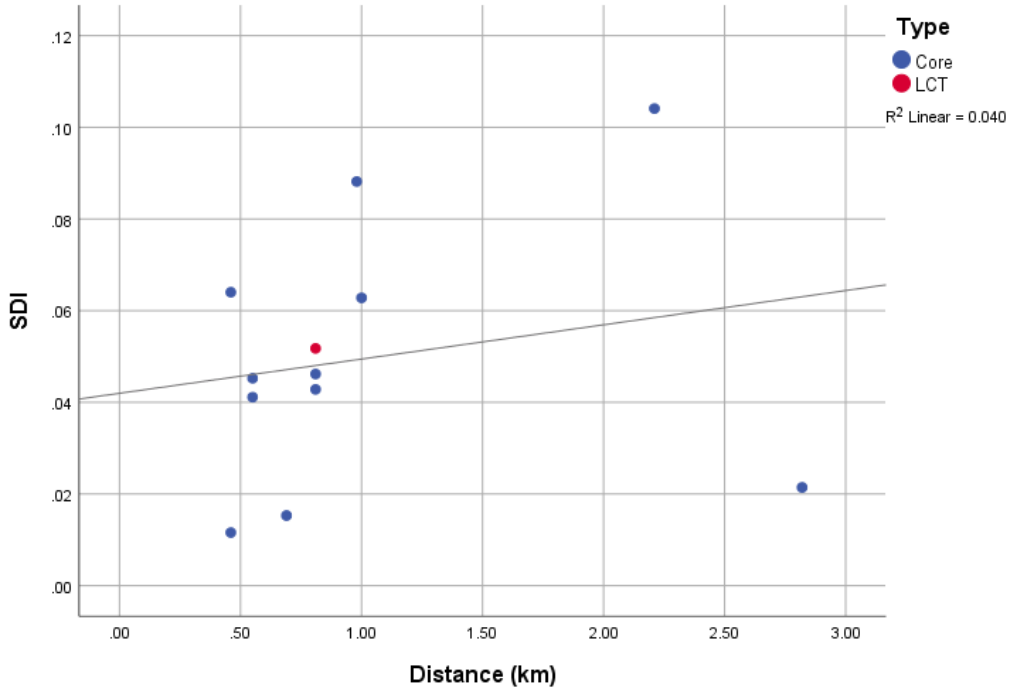


Figure 4.39. Line regression scatter plotting SDI by distance of geochemically sourced artefacts.

CHAPTER 5: Discussion

Utilizing the methodologies outlined in Chapter Three geochemical and technological aspects of the Maropeng lithic assemblage, were investigated to highlight potential patterns in raw material procurement strategies. Assessing Maropeng from a landscape-scale approach is a vital aspect for understanding economic trends in raw material selection and reduction behaviours. The first aim of this research was to ascertain whether artefacts and outcrops could be geochemically characterized or 'fingerprinted.' This is discussed below through general overviews of the landscape, outcrops and macroscopic lithological traits, which tie into the geochemical characterisation of quartzites (section 5.1). The second aim was to identify patterns in the reduction of flaked pieces, i.e., cores and LCTs, that might correlate with the selection of raw materials from specific outcrops. Lastly, the geochemical and technological datasets are brought together in the search for correlations between: the specific outcrops on the Maropeng landscape, the reduction intensity of flaked pieces, and the relationship between raw material source distances and reduction intensity. This is used to discuss aspects of landscape use and the raw material economy present at Maropeng >1 Mya.

5.1 Geochemical characterisation of the landscape

In order to provide a geochemically based discussion of the quartzite characterisation, descriptions of the landscape (based on outcrops and macroscopic traits thereof) are needed to apply the landscape-scale approach detailed in previous chapters.

5.1.1 The landscape

Through the survey of the three kilometre buffer zone, 12 different outcrops were identified. All sourced quartzites come from the Timeball Hill Formation, which include partly ferruginous quartzites or shale bedded locally with conglomerate, breccia, quartzite and chert (Figure 2.1). General observations across outcrops indicated almost all quartzites have a red to brown outer weathered layer, which is due to the geology of the area being high in iron during its formation (Schweigart 1965; Erikson 1973; Dorland 1999; Catuneanu & Erikson 2002; Yamaguchi *et al.* 2005). High iron content of the quartzite is also seen in the XRF results which are discussed below.

In Figure 2.1, we observe two rivers in close proximity to Maropeng (within two kilometres). Certain aspects of hominin needs are integrally tied to water bodies (Reynolds *et al.* 2011), and the utilisation of blank types from river cobble sources is well documented in the ESA (Potts 1991; Field 1999; Kuman 2003, 2007; Braun *et al*, 2008a; Harmand 2009; de la Torre 2011; Goldman-Neuman & Hovers 2012; Caruana 2017; McHenry & de la Torre 2018). This is important, as quartzite cobbles were utilized in knapping toolkits at Maropeng (Pollarolo *et al.* 2010; Moll 2017). The subsequent transport of these cobbles into Maropeng, where areas are rich in potential manuports from primary sources, leads to discussions of blank choice (see below). Further investigation into the cobble sources may reveal raw material selection behaviours and will be explored in future publications on Maropeng.

In general, the vast number of quartzite outcroppings within a three kilometre radius could be a determining factor for why Acheulean hominin occupied the Maropeng landscape. Previous studies in the COHWHS, have spoken to the increased need for quartzite during the Acheulean LCT production (Kuman 2003; 2007; Kuman & Field 2009; Sherwood 2013). Chronologically, the need for quartzite in LCT production, coincides with the recorded timeframe (~1 Mya and potentially even older) of Earlier Acheulean lithic production at Maropeng. With this in mind, the potential for future discoveries of other open-air Acheulean sites around Maropeng seems high, considering that water and quartzite sources were possibly widely available. By increasing the number of open-air sites, broadscale landscape behaviours may be inferred and compared to other Acheulean regions.

5.1.2 Outcrops

Outcrops ranged in size considerably (see Table 4.1) with QM being the largest. Quartzite outcroppings mainly morphologically conformed to narrow ridges, while some were broad and flat. As previously mentioned, most outcrops were confined to a one kilometre proximity. GO1 and GO2 were amongst the furthest, requiring increased potential energy expenditure and presumptively, knappers would have to either scale the large hill (QM) or walk around it. The validity of this statement lessens as the cradle's morphology has not been stable over the past two million years (Dirks *et al.* 2016), potentially skewing the outcrop observations. *In situ* exposures were mostly obscured by the landscape and did not provide enough detail to consider within the scope of this discussion.

Analysing the available raw material packages through detached clast (i.e., loose clasts) descriptions, provided distinctions of potential knapping choices. Detached clasts were variable is size (70-2200 mm), but a large abundance of transportable size clasts was observed. The detached clasts mainly conform to an equant or tabular shape, with angular or rounded edges, but often exhibited irregular surfaces. As such, The Maropeng landscape may have been an environment where 'knap-able' clasts were abundant, although toolmakers had to adapt reduction strategies to specific blank shapes (see section 5.2.3). Weathering has potentially played a large role in the shape categories present on the landscape, but further investigation is needed. Lithologically speaking, banding is present across almost all outcrops with a lot of the banding appearing to be quartz veins (see section 5.1.3 below). There is a variety of grain sizes and grain visibility across and within outcrops, which potentially related to the local quartzite recrystallisation apparent within the Timeball Hill Formation (Lenhardt *et al.* 2012).

The variety of colours (see Table 4.2) is too variable to characterise certain outcrops and only petrographic studies can potentially provide enough detail to confidently group the quartzites. Preliminary observations do suggest that red quartzites appear to be coarser grained and more susceptible to weathering, with dissolution appearing frequently. Blue quartzite, while variable, was mostly medium to fine grained and were more resistant to weathering. Pink quartzite was the most frequent recurring colour witnessed on the landscape, often in times being linked to medium-grain sizes.

5.1.3 Macroscopic lithological traits in artefacts and geological samples

In correlating the lithological properties of artefacts and outcrops examined in this study, a general trend of raw material selection mirroring the available quartzite types on the landscape was observed. Colour and grain visibility of artefacts mimicked the geological sample trends in being medium-grained, yellow-red hued, with quartz crystal inclusions being visible. Considering many artefacts have a similar weathering rind, the possibility of yellow diabase weathering stains and iron staining skewing results into the yellow-red category is likely. Adequate colour assertions remain out of reach as methods to note the internal colour, are destructive to the artefact. Therefore, grain size inferences from this study are more reliable than any colour deductions as of right now. Further work into

petrographical studies is needed, to shed light onto distinctions in raw material procurement and quality thereof.

Patterns of banding and texture within the artefact sample did suggest some selective factors for lithic production. Quartz intrusions, a type of banding, were noted within almost all outcrops surveyed, although selection practices, within the artefactual sample, demonstrate that clasts with quartz intrusions were avoided by toolmakers. This may reflect a preference for homogenous materials in general, indicating the ability to recognise clasts with less favourable fracture mechanics introduced through banding (Brantingham *et al.* 2000). Medium-grained textures dominate the quartzite artefacts, as well as the landscape, but may indicate specific selection of these quartzite varieties. Sherwood (2013) noted an abundance of medium-grained quartzites from Swartkrans Members 2 and 3 and demonstrated that their fracture mechanics and flaking predictability were similar to fine-grained samples. Logically, fine-grained textures are more conducive to conchoidal fracture and would thus be more preferable (Brantingham *et al.* 2000). However, due to the variability of textures within quartzite outcrops, fine-grained clasts are not as common as medium-grained clasts. Nonetheless, there seems to be a clear preference for both medium- and fine-grained raw materials within the Maropeng lithic assemblage, with few examples of coarse-grained quartzites being utilized for toolmaking.

5.1.4 Geochemical characterisations

The results of the geochemical data echo the issues of homogeneity similar to Pitblado *et al.* (2013). In general, the chemical composition of quartzite outcrops tested on the Maropeng landscape are similar and thus difficult to 'fingerprint' or differentiate through both AD-ICP-MS and P-XRF methods. Pearson correlation tests confirmed this result, suggesting a high degree of chemical overlap, which has been recorded in previous studies (see Chapter 3) (Pitblado *et al.* 2008, 2013; Dalpra & Pitblado 2015; Soto *et al.* 2020). Further, the dendrogram produced from PC scores of the AD-ICP-MS data did not perform well through lesser visible natural links between geological samples and artefacts (Figure 4.37. On the other hand, P-XRF data did perform well, which linked 12 artefacts to geological samples (Figure 4.38). This suggests that, despite the high homogeneity of chemical signatures, variance can be detected through major element analysis. Also, increasing sample size and subsequent re-testing of the data will strengthen this hypothesis.

Multi-scalar approaches through physical and chemical compositions has been stressed to produce the most accurate results for quartzite provenancing (Pitblado *et al.* 2008, 2013; Soto *et al.* 2020). Section 5.1.3 points to the inability of using macroscopic lithological traits to determine sources, although they prove useful in addressing the mentioned chemical overlap. Where artefacts were linked to two differing samples, macroscopic trait observations provided the means to link samples.

Quartzites appear to have formed all along a similar timeline geologically (Proterozoic), which has made chemical overlap a considerable problem. Therefore, this issue remains problematic when characterising outcrops by a single geochemical fingerprint. Another issue arises in the fact that there is variability, both chemically and lithologically within a single outcrop, which is highlighted in the dendrogram showing few u-links between samples from related sources. To resolve these issues, a concerted effort to collect larger samples of chemical data per outcrop should be done to replicate and further results. Utilising the cost and time efficiency of P-XRF will lend to the testing of large-scale outcrop geochemical characterisation.

5.2 Landscape-use and raw material economy characterisation

5.2.1 Reduction intensity at Maropeng

The SDI values (reduction intensity) of Maropeng artefacts correlates with volumetric loss (see Figure 4.32), although the correlation coefficient was relatively weak, these variables were significantly related and thus dependent. Furthermore, the SDI boxplots for cores and LCTs (Figures 4.29, 4.30, and 4.31) were generally low in value, suggesting that reduction sequences of flaked pieces was relatively short, which indicates limited exploitation, easy access to materials and expedient knapping.

5.2.2 Comparison to Moll (2017)

Quartzite technological summary from the current study

Core reduction within the Maropeng assemblage is dominated by multifacial (n=35) strategies, followed by bifacial (n=15) and unifacial (n=10) strategies. Core length ranges from 59.6 – 172.8 mm, width from 45.3 – 117 mm and thickness from 21.6 – 84.9 mm, while

core mass varies from 86.71 – 1231.61 g. Flake scars also show large variance ranging from 1 – 33 scars, and >45° angles (n=49) are more prevalent than <45° angles (n=11). Cortex percentages vary from 0 to 90%. Large variations in scar counts, mass and metrical measurements lend to the conclusion that multiple behaviours regarding expedient and energy conservative methods were employed on the landscape. A dominance of multifacial cores with large amounts of >45° angles speaks to the influence of the original blank type and available platforms.

LCT length is unstandardized with a range of 78 mm and data being on the larger side with a mean length of 138.43 mm. LCT width range is 56.4 mm and thickness is 32.5 mm. LCT length, width and thickness show large variance, which may be due to the blank shape influencing the form. Mass has high variance as its range is 798.66 g, a probable cause for the discrepancy may be due to LCTs having been made on both cobbles and flakes. Flake scars present high variance ranging from 7 - 43 scars, indicating various flaking intensities. Scar directions range from 3-7 with the mean being just 4.54, indicating minimal rotation. Edge angles are distributed fairly between >45° (n=13) and <45° (n=9). Cortex percentage on the LCTs range from 4 - 46% and can be used as a proxy of poor mass management or LCT production strategies (i.e., cobble vs large flake production).

Comparison between studies

Cores across both this and Moll's (2017) studies retained a dominance of multifacial strategies. The apparent dominance of multifacial cores (58,3%) is reflective of the dominant blocky blank types. Limited exploitation of cores is evident in cores sometime retaining up to 90% of their original cortex and low flake scar counts (N=1) being seen. However, the simple reduction seen in Moll (2017) does not fully characterise the varieties of reduction systematics in this assemblage. Quartzite cores retain the widest variety of SDI values, leading to the conclusion that both expedient and resource conservative behaviours are apparent. Moll (2017) records little organised core reduction strategies and suggests that limited technological progress may account for this. Bifacial and unifacial strategies are low in frequency (n=3) and do not indicate complex organization of knapping sequences, which may rather reflect a lesser need to conserve raw material resources. Raw materials were found as far as 2.8 km away, therefore the lack of platform rejuvenation seen in Moll (2017) may point towards deficient cognitive capacities in combination with blank type.

When comparing both studies simple and limited shaping is evident in Maropeng LCTs. Evidence for such is seen in the low counts for mean scar directions, indicating limited rotation. Inefficient central blank mass reduction is also seen, as thickness and maximum cortex percentage is high in both studies. However, this study, found quartzite LCTs to carry a slightly wider variety of shaping behaviours. This is seen in large ranges between maximum and minimum metric measurements, flake scars counts and SDI values. The slow, time-averaged accumulation of the ABH may, however, represent multiple LCT cultural behaviours, across time.

5.2.3 Raw material economy of Maropeng

Previous interpretations of raw material procurement patterns suggested that QM was a primary source of the artefact accumulations within the ABH at Maropeng (Pollarolo et al. 2010). The results of the geochemical analyses outlined in this study suggest that patterns of procurement were more complex and extended beyond QM. In fact, raw material collection ranged up to 2.8 km from the Maropeng site indicating mobility patterns across the landscape by hominins that extended far beyond QM. This is further supported through the findings of Morrisey (2015), which indicated that certain artefacts were locally discarded and lacked slope-movement abrasion. As such, this conclusion demonstrates a degree of mobility within the Maropeng Acheulean lithic assemblage that was previously undetected.

Higher reduction intensities have been linked to the general increase in distance to source, in an effort to constrain the energetic costs of transporting raw materials (Kuhn 1991, 2004; Wallace & Shea 2006; Caruana *et al.* 2019). The results presented here suggest that there is no significant correlation between the reduction intensity of raw materials and distances to their sources. This suggests a lack of ‘economic efficiency’ in the transport and reduction of collected materials. While conclusions remain preliminary, as small sample sizes may have contributed bias, distinct behaviours are exhibited. However, Blumenschine et al. (2008) criticize the linear relationship between distances to raw material sources and their reduction, arguing that mobility cannot be defined as straight-lines, attributing factors such as task-specific utility, butchery and scavenging and ecological setting, resulting in complex mobility behaviours (cf. Blumenschine & Peters 1998). Moreover, Maropeng offers a unique

perspective in understanding landscape use and lithic production strategies, which provides insight into the economy of raw material procurement and use.

The distinct lack of a raw material economy potentially points to other factors driving the selection and reduction of raw materials at Maropeng, such as texture quality and banding. Furthermore, clast package size and shape may have potentially played a significant role in reduction strategies. The irregular, blocky shape of clasts available on the Maropeng landscape suggests that blank morphology, including the number of suitable platforms for knapping, promoted multifacial reduction strategies and high rotation patterns. Similar adaptations are seen at Swartkrans in the Oldowan assemblage (Caruana 2017). Caruana (2017) argues for cubic (blocky) manuports incentivising multifacial strategies to exploit core mass in the COHWHS Oldowan. Cubic clasts approach 90 degrees far more quickly as they become rounded during reduction sequences, hence the need to exploit multiple working edges through extensive core rotation. Although, a lack of organization occurs as the exploitation of cubic clasts for suitable platforms, creates high instances of core rotation patterns (Caruana 2017). Furthermore, without the careful maintenance of exterior platform angles on cores, this manner of multifacial knapping is more likely to result in shorter knapping sequences as platform edges reach steep angles sooner. Nonetheless, I argue that multifacial strategies were an adaptation to knapping irregular cubic blank types at Maropeng, albeit with limited evidence of managing core surface and edge angles. Around eighty percent (49 out of 60) of cores exhibit >45° angles, which suggest a lack of management throughout knapping sequences. The simple reduction strategies and lack of core management point to previous deductions attributing Maropeng to the Earlier Acheulean.

CHAPTER 6: Conclusion

Research into accurate provenancing of quartzite, remains in its infancy (Pitblado *et al.* 2008). Chemical characterization such as ICPMS, XRF and hyperspectral techniques, and physical characterisation such as petrography and scanning electron microscopy have all produced varying results. The handful of studies point to diverse techniques, having produced different results based on regionality, as quartzite elemental make-up is not universal. Therefore, a blanket approach for all quartzite provenance has yet to be established. Pitblado *et al.* (2013) discuss the challenges of chemical overlap in provenancing quartzite, often requiring the linkage of both physical and chemical distinctions. Similar problems are encountered within the Maropeng region, as neither trace elements nor broad lithological descriptions have aided substantially in quartzite distinction, so far. Preliminary results of major element testing through P-XRF remain a promising avenue for Timeball Hill ferruginous quartzite fingerprinting. However, this does not represent a stand-alone method (i.e., the secondary requirement of macroscopic lithological properties to increase accuracy) and to justify this claim, further multi-scalar replicative studies, are required. The ultimate goal is to eventually identify a general approach that limits or avoids the destruction of artefacts, upon which entire quartzite assemblages may be provenanced. New techniques into fast, non-destructive hyperspectral imaging (Sciuto *et al.* 2019) present an alternative to destructive petrographical methods and shall be the focus of further analyses.

Geochemical linking can only ever be described as tentative rather than exact (Elburg & van der Kroft 2006; Barrientos *et al.* 2018). The results from the preliminary data presented in this thesis suggest that quartzite sources require more geochemical results and possibly petrography, to adequately be separated from each other. Nonetheless, 12 quartzites were linked tentatively to their respective sources on the Maropeng landscape. Through the subsequent reduction intensity analysis, source provenance, and the comparison to technological results, the raw material economy of Maropeng was encapsulated.

Maropeng offers an insight into the cognitive approaches to the raw material economy in the Earlier Acheulean. The relationship between distance and SDI values indicates the lack of an apparent raw material economy, meaning reduction intensities were not dependent on source proximities, and are possibly related to other potential factors. The conservative raw material collections mostly within a one kilometre radius and the lack of core surface management

throughout reduction sequences further point to the lack of a quartzite raw material economy. Broader geochemical results across more quartzites and other raw materials could refine these interpretations. Manuport reduction decisions appear to be landscape based only selecting for grain and banding properties. Through the characterization of Maropeng's raw material economy, broader aspects of cognition and behavioral patterns are able to be addressed, as well as the characterization of inter- and intra-site variability during the Acheulean. Another Acheulean site within the COHWHS, Swartkrans, has also exhibited lesser cognitive approaches to selection, through lower raw material quality choices (Sherwood 2013). Maropeng remains an irreplaceable lithic site in regards to large-scale landscape approaches of understanding hominin cognition, in the COHWHS. As such, the stone tools of this open-air site hold information unattainable in karstic assemblages and initiate discussion, in linking open-air Acheulean behaviours across Africa. However, only through the continued investigation of Acheulean sites within the COHWHS, may the overarching cognitive aspects with respect to mobility and landscape use be defined. Hence, the call for new research into the discovery of open-air sites of the COHWHS (Caruana & Stratford 2018; Caruana *et al.* 2019) is echoed in this thesis.

6.1 Further research

There is a multitude of avenues in which this research may be furthered. Building on this study, petrographical analysis (purely geological) and a larger sample area may divulge even more information relating to raw material sourcing behaviors of Maropeng hominins, 1 Mya and older. A study detailing a hyperspectral look into the quartzites of Maropeng, and whether new and fast hyperspectral methods are able to distinguish the outcrops to circumvent the "outcrop overlap," is of particular interest to this research. Geochemically characterizing quartzites and other raw materials within the COHWHS will allow for research within this region to utilize this database, therefore expediating research processes. Ultimately encouraging the focus upon discovering and research of open-air sites in the COHWHS, in order to provide future research of landscape-scale characterisations.

References

Amati, D. and Shallice, T. 2007. On the emergence of modern humans. *Cognition* 103(3): 358-385.

Ambrose, S.H. 2001. Paleolithic technology and human evolution. *Science* 291(5509): 1748-1753.

Ambrose, S.H. 2006. Howiesons Poort lithic raw material procurement patterns and the evolution of modern human behavior: a response to Minichillo (2006). *Journal of Human Evolution* 50(3): 365-369.

Andrefsky, W.Jr. 2005. *Lithics: Macroscopic Approaches to Analysis*. Cambridge: Cambridge University Press.

Archer, W., Aldeias, V. and McPherron, S.P. 2020. What is 'in situ'? A reply to Harmand et al. (2015). *Journal of Human Evolution* 142: 102740. DOI: 10.1016/j.jhevol.2020.102740

Arrizabalaga, A., Rios-Garaizar, J. and Alvarez-Alonso, D. 2015. The past is out there: Open-air Palaeolithic sites and new research strategies in the Cantabrian region (northern Iberia). *Quaternary International* 364: 181-187.

Attas, M., Fossey, J.M. and Yaffe, L. 1984. Corrections for drill bit contamination in sampling ancient pottery for neutron activation analysis. *Archaeometry* 26(1): 104-107.

Aubry, T., Barbosa, A.F., Luís, L., Santos, A.T. and Silvestre, M. 2016. Quartz use in the absence of flint: Middle and Upper Palaeolithic raw material economy in the Côa Valley (North-eastern Portugal). *Quaternary International* 424: 113-129.

Bailey, G. 2007. Time perspectives, palimpsests and the archaeology of time. *Journal of Anthropological Archaeology* 26(2): 198-223.

Balter, V., Blichert-Toft, J., Braga, J., Telouk, P., Thackeray, F. and Albarède, F. 2008. U–Pb dating of fossil enamel from the Swartkrans Pleistocene hominid site, South Africa. *Earth and Planetary Science Letters* 267(1-2): 236-246.

Barca, D., De Francesco, A.M., Crisci, G.M. and Tozzi, C. 2008. Provenance of obsidian artifacts from site of Colle Cera, Italy, by LA-ICP-MS method. *An International Journal of Period*. 77: 41-52.

Barrientos, G., Belardi, J.B., Catella, L., Marina, F.C. and Oliva, F. 2018. Continuous spatial models as an aid for sourcing lithic raw materials: examples from the Argentine Pampas and Patagonia. *Journal of Archaeological Science: Reports* 22: 330-343.

Barton, C.M., Bernabeu, J., Aura, J.E. and Garcia, O. 1999. Land-use dynamics and socioeconomic change: an example from the Polop Alto Valley. *American Antiquity* 64(4): 609-634.

Barton, C.M., Bernabeu, J., Aura, J.E., Garcia, O., Schmich, S. and Molina, L. 2004. Long-term socioecology and contingent landscapes. *Journal of Archaeological Method and Theory* 11(3): 253-295.

Bar-Yosef, O., Gilead, I. and Goren-Inbar, N. 1993. *The Lithic Assemblages of Ubeidiya, a Lower Palaeolithic Site in the Jordan Valley*. Jerusalem: Institute of Archaeology, Hebrew University of Jerusalem.

Bar-Yosef, O. and Belfer-Cohen, A. 2001. From Africa to Eurasia—early dispersals. *Quaternary International* 75(1): 19-28.

Beaumont, P.B. 1990. Canteen Kopje (Klipdrif). *Guide to Archaeological Sites in the Northern Cape. Kimberley: McGregor Museum*: 14-16.

Beaumont, P.B. and McNabb, J. 2000. Canteen Kopje: the recent excavations. *The Digging Stick* 17(3): 3-7.

Becker, J.S. 2002. Applications of inductively coupled plasma mass spectrometry and laser ablation inductively coupled plasma mass spectrometry in materials science. *Spectrochimica Acta Part B: Atomic Spectroscopy* 57(12): 1805-1820.

Belmaker, M., Tchernov, E., Condemi, S. and Bar-Yosef, O. 2002. New evidence for hominid presence in the Lower Pleistocene of the Southern Levant. *Journal of Human Evolution* 43(1): 43-56.

Beyene, Y. 2003. The emergence and development of the Acheulean at Konso. *Anthropological Science* 111: 58.

Beyene, Y., Katoh, S., WoldeGabriel, G., Hart, W.K., Uto, K., Sudo, M., Kondo, M., Hyodo, M., Renne, P.R., Suwa, G. and Asfaw, B. 2013. The characteristics and chronology of the earliest Acheulean at Konso, Ethiopia. *Proceedings of the National Academy of Sciences* 110(5): 1584-1591.

Bienenfeld, P. and Andrefsky, W. 1984. Projected Point Life Cycles and Use-Resharpening Analysis, paper presented at the 49th Annual Meeting of the Society for American Archaeology, Portland.

Blatt, H., Tracy, R. and Owens, B. 2006. *Petrology: Igneous, Sedimentary, and Metamorphic*. New York: Macmillan.

Blomme, A., Degryse, P., Van Peer, P. and Elsen, J. 2012. The characterization of sedimentary quartzite artefacts from Mesolithic sites. *Geologica Belgica* 15(3): 193-199.

Blumenschine, R.J. and Masao, F.T. 1991. Living sites at Olduvai Gorge, Tanzania? Preliminary landscape archaeology results in the basal Bed II lake margin zone. *Journal of Human Evolution* 21(6): 451-462.

Blumenschine, R.J. and Peters, C.R. 1998. Archaeological predictions for hominid land use in the paleo-Olduvai Basin, Tanzania, during lowermost Bed II times. *Journal of Human Evolution* 34(6): 565-608.

Blumenschine, R.J., Masao, F.T., Tactikos, J.C. and Ebert, J.I. 2008. Effects of distance from stone source on landscape-scale variation in Oldowan artifact assemblages in the Paleo-Olduvai Basin, Tanzania. *Journal of Archaeological Science* 35(1): 76-86.

Blumenschine, R.J., Stanistreet, I.G., Njau, J.K., Bamford, M.K., Masao, F.T., Albert, R.M., Stollhofen, H., Andrews, P., Prassack, K.A., McHenry, L.J. and Fernández-Jalvo, Y. 2012. Environments and hominin activities across the FLK Peninsula during Zinjanthropus times (1.84 Ma), Olduvai Gorge, Tanzania. *Journal of Human Evolution* 63(2): 364-383.

Brain, C.K. 1983. *The hunters or the hunted?: an introduction to African cave taphonomy*. Chicago: University of Chicago Press.

Brain, C.K. ed. 1993. *Swartkrans: A cave's chronicle of early man*. Pretoria: Transvaal Museum Monograph No. 8.

Brantingham, P.J., Olsen, J.W., Rech, J.A. and Krivoshapkin, A.I. 2000. Raw material quality and prepared core technologies in Northeast Asia. *Journal of Archaeological Science* 27(3): 255-271.

Brantingham, P.J. 2003. A neutral model of stone raw material procurement. *American Antiquity* 68(3): 487-509.

Braun, D.R. and Harris, J.W. 2003. Technological developments in the oldowan of koobi fora: innovatives techniques of artifact analysis. *Treballs d'Arqueologia* 9: 117-144.

Braun, D.R. 2005. Examining flake production strategies: examples from the Middle Paleolithic of Southwest Asia. *Lithic Technology* 30(2): 107-125.

Braun, D.R. Tactikos, J.C. Ferraro, J.V. Arnow, S.L. and Harris, J.W. 2008a. Oldowan reduction sequences: methodological considerations. *Journal of Archaeological Science* 35: 2153-2163.

Braun, D.R. Plummer, T. Ditchfield, P. Ferraro, J.V. Maina, D. Bishop, L.C. and Potts, R. 2008b. Oldowan behavior and raw material transport: perspectives from the Kanjera Formation. *Journal of Archaeological Science* 35(8): 2329-2345.

Braun, D.R., Plummer, T.W., Ditchfield, P.W., Bishop, L.C. and Ferraro, J.V. 2009. Oldowan technology and raw material variability at Kanjera South. In: Hovers, E. & Braun, D.R. (eds) *Interdisciplinary Approaches to the Oldowan*: 99-110. New York: Springer.

Braun, D.R., Levin, N.E., Stynder, D., Herries, A.I., Archer, W., Forrest, F., Roberts, D.L., Bishop, L.C., Matthews, T., Lehmann, S.B. and Pickering, R. 2013. Mid-pleistocene hominin occupation at Elandsfontein, western Cape, South Africa. *Quaternary Science Reviews* 82: 145-166.

Braun, D.R., Aldeias, V., Archer, W., Arrowsmith, J.R., Baraki, N., Campisano, C.J., Deino, A.L., DiMaggio, E.N., Dupont-Nivet, G., Engda, B. and Feary, D.A. 2019. Earliest known Oldowan artifacts at> 2.58 Ma from Ledi-Geraru, Ethiopia, highlight early technological diversity. *Proceedings of the National Academy of Sciences* 116(24): 11712-11717. DOI: 10.1073/pnas.1820177116

Button, A. 1986. The Transvaal sub-basin of the Transvaal Sequence. In: Anhaeusser, C.R. & Maske, S. (eds) *Mineral Deposits of Southern Africa v 1*: 811-817. Johannesburg: Geological Society of South Africa.

Caruana, M.V., Tasker, D. and Stratford, D.J. 2019. Identifying Raw Material Transportation and Reduction Strategies from the Lithic Scatters at Elandsdrift Farm (Cradle of Humankind World Heritage Site), South Africa. *African Archaeological Review* 36(2): 271-289. DOI: 10.1007/s10437-019-09331-3

Catuneanu, O. and Eriksson, P.G. 2002. Sequence stratigraphy of the Precambrian Rooihoogte–Timeball Hill rift succession, Transvaal Basin, South Africa. *Sedimentary Geology* 147(1-2): 71-88.

Chazan, M., Ron, H., Matmon, A., Porat, N., Goldberg, P., Yates, R., Avery, M., Sumner, A. and Horwitz, L.K. 2008. Radiometric dating of the Earlier Stone Age sequence in excavation I at Wonderwerk Cave, South Africa: preliminary results. *Journal of Human Evolution* 55(1): 1-11.

Chazan, M., Porat, N., Sumner, T.A. and Horwitz, L.K. 2013. The use of OSL dating in unstructured sands: The archaeology and chronology of the Hutton Sands at Canteen Kopje (Northern Cape Province, South Africa). *Archaeological and Anthropological Sciences* 5(4): 351-363.

Chazan, M. 2015. Technological trends in the Acheulean of Wonderwerk cave, South Africa. *African Archaeological Review* 32(4): 701-728. DOI: 10.1007/s10437-015-9205-8

Clark, J.D. 1999 Cultural Continuity and Change in Hominid Behaviour in Africa During the Middle to Upper Pleistocene Transition. *Hominid Evolution: Lifestyles and Survival Strategies*: 277-292.

Clark, J.D., Beyene, Y., WoldeGabriel, G., Hart, W.K., Renne, P.R., Gilbert, H., Defleur, A., Suwa, G., Katoh, S., Ludwig, K.R. and Boisserie, J.R. 2003. Stratigraphic, chronological and behavioural contexts of Pleistocene Homo sapiens from Middle Awash, Ethiopia. *Nature* 423(6941): 747-752.

Clarkson, C. 2013. Measuring core reduction using 3D flake scar density: a test case of changing core reduction at Klasies River Mouth, South Africa. *Journal of Archaeological Science* 40(12): 4348-4357.

Cnudde, V., Dewanckele, J., De Kock, T., Boone, M., Baele, J.M., Crombe, P. and Robinson, E. 2013. Preliminary structural and chemical study of two quartzite varieties from the same geological formation: a first step in the sourcing of quartzites utilized during the Mesolithic in northwest Europe. *Geologica Belgica* 16(1-2): 27-34.

Coolidge, F.L. and Wynn, T. 2005. Working memory, its executive functions, and the emergence of modern thinking. *Cambridge Archaeological Journal* 15(1): 5-26.

Cowan, F.L. 1999. Making sense of flake scatters: lithic technological strategies and mobility. *American Antiquity* 64(4): 593-607.

Dalpra, C.L. and Pitblado, B.L. 2016. Discriminating quartzite sources petrographically in the Upper Gunnison Basin, Colorado: implications for Paleoamerican lithic-procurement studies. *PaleoAmerica* 2(1): 22-31.

de la Torre, I. Mora, R. Domínguez-Rodrigo, M. de Luque, L. and Alcalá, L. 2003. The Oldowan industry of Peninj and its bearing on the reconstruction of the technological skills of Lower Pleistocene hominids. *Journal of Human Evolution* 44(2): 203-224.

de la Torre, I. and Mora, R. 2005. Technological strategies in the lower Pleistocene at Olduvai Beds I & II. *Eraul* 112: 1-255.

de la Torre, I., Mora, R. and Martínez-Moreno, J. 2008. The early Acheulean in Peninj (Lake Natron, Tanzania). *Journal of Anthropological Archaeology* 27(2): 244-264.

de la Torre, I. 2009. Technological Strategies in the Lower Pleistocene at Peninj (west of Lake Natron, Tanzania). *The Cutting Edge: New Approaches to the Archaeology of Human Origins*: 93-113.

de la Torre, I. and Mora, R. 2009. Remarks on the current theoretical and methodological approaches to the study of early technological strategies in Eastern Africa. *Interdisciplinary Approaches to the Oldowan*: 15-24.

de la Torre, I. 2011. The early Stone age lithic assemblages of Gadeb (Ethiopia) and the Developed Oldowan/early Acheulean in east Africa. *Journal of Human Evolution* 60(6): 768-812.

de la Torre, I. and Mora, R. 2014. The transition to the Acheulean in East Africa: an assessment of paradigms and evidence from Olduvai Gorge (Tanzania). *Journal of Archaeological Method and Theory* 21(4): 781-823.

de Pablo, J.F.L. and Barton, C.M. 2015. Bayesian estimation dating of lithic surface collections. *Journal of Archaeological Method and Theory* 22(2): 559-583.

de la Torre, I. and Mora, R. 2018. Technological behaviour in the early Acheulean of EF-HR (Olduvai Gorge, Tanzania). *Journal of Human Evolution* 120: 329-377.

De Wit, M.C.J. 2008. Canteen Koppie at Barkly West: South Africa's first diamond mine. *South African Journal of Geology* 111(1): 53-66.

Deacon, T.W. 1997. *The symbolic species: The co-evolution of language and the brain* (No. 202). New York: WW Norton & Company.

Deino, A.L. and McBrearty, S. 2002. 40Ar/39Ar dating of the Kapthurin formation, Baringo, Kenya. *Journal of Human Evolution* 42(1-2): 185-210.

Díez-Martin, F., Sánchez-Yustos, P., Gómez-González, J.A. and de la Rúa, D.G. 2008. Earlier Palaeolithic settlement patterns: landscape archaeology on the river Duero Basin Plateaus (Castilla y León, Spain). *Journal of World Prehistory* 21(2): 103-137.

Díez-Martín, F., Yustos, P.S., Uribelarrea, D., Baquedano, E., Mark, D.F., Mabulla, A., Fraile, C., Duque, J., Díaz, I., Pérez-González, A. and Yravedra, J. 2015. The origin of the Acheulean: the 1.7 million-year-old site of FLK West, Olduvai Gorge (Tanzania). *Scientific Reports* 5(1): 1-9.

Dirks, P.H.G.M., Placzek, C., Fink, D., Dosseto, A. and Roberts, E.M. 2016. Using 10be dating to reconstruct the evolving landscape in the Cradle of Humankind, South Africa. *Journal of Human Evolution* 96: 19-34.

Doelman, T., Webb, J. and Domanski, M. 2001. Source to discard: Patterns of lithic raw material procurement and use in Sturt National Park, northwestern New South Wales. *Archaeology in Oceania* 36(1): 15-33.

Dorland, H.C. 1999. Paleoproterozoic laterites, red beds and ironstones of the Pretoria Group with reference to the history of atmospheric oxygen. Unpublished PhD dissertation. Johannesburg: University of Johannesburg.

Drennan, R.D. 2009. *Statistics for archaeologists: A commonsense approach*. New York: Plenum Press.

Ebright, C.A. 1987. Quartzite petrography and its implications for prehistoric use and archeological analysis. *Archaeology of Eastern North America*: 29-45.

Egeland, C.P., Fadem, C.M., Byerly, R.M., Henderson, C., Fitzgerald, C., Mabulla, A.Z., Baquedano, E. and Gidna, A. 2019. Geochemical and physical characterization of lithic raw materials in the Olduvai Basin, Tanzania. *Quaternary International* 526: 99-115.

Eriksson, K.A. 1973. The Timeball Hill Formation- a fossil delta. *Journal of Sedimentary Research* 43(4).

Eriksson, P.G., Schweitzer, J.K., Bosch, P.J.A., Schereiber, U.M., Van Deventer, J.L. and Hatton, C.J. 1993. The Transvaal sequence: an overview. *Journal of African Earth Sciences (and the Middle East)* 16(1-2): 25-51.

Eriksson, O., Cousins, S.A. and Bruun, H.H. 2002. Land-use history and fragmentation of traditionally managed grasslands in Scandinavia. *Journal of Vegetation Science* 13(5): 743-748.

Field, A.S. 1999. An analytical and comparative study of the Earlier Stone Age archaeology of the Sterkfontein Valley. Unpublished PhD dissertation. Johannesburg: University of the Witwatersrand.

Foley, R. 1981. Off-site archaeology: an alternative approach for the short-sited. *Pattern of the Past: Studies in Honour of David Clarke*: 157-183.

Forssman, T.R., Kuman, K., Leader, G.M. and Gibbon, R.J. 2010. A Later Stone Age assemblage from Canteen Kopje, Northern Cape. *The South African Archaeological Bulletin* 65(192): 204-214.

Gallotti, R. 2013. An older origin for the Acheulean at Melka Kunture (Upper Awash, Ethiopia): techno-economic behaviours at Garba IVD. *Journal of Human Evolution*. 65(5): 594-620.

Gallotti, R. and Mussi, M. 2018. Before, During, and After the Early Acheulean at Melka Kunture (Upper Awash, Ethiopia): A Techno-economic Comparative Analysis.*The Emergence of the Acheulean in East Africa and Beyond*: 53–92.

Gauthier, G. and Burke, A.L. 2011. The effects of surface weathering on the geochemical analysis of archaeological lithic samples using non-destructive polarized energy dispersive XRF. *Geoarchaeology* 26(2): 269-291.

Gibbon, R.J., Granger, D.E., Kuman, K. and Partridge, T.C. 2009. Early Acheulean technology in the Rietputs Formation, South Africa, dated with cosmogenic nuclides. *Journal of Human Evolution* 56(2): 152-160.

Gibbon, R.J., Granger, D.E., Kuman, K., Leader, G.M.L., Lotter, M.G. and Forssman, T. 2013. Isochron burial dating of the earlier stone age deposits at canteen Kopje, South Africa. *Association of Southern African Professional Archaeologists Biennial Conference, Gaborone, Botswana*: 3-7.

Gibbon, R.J., Pickering, T.R., Sutton, M.B., Heaton, J.L., Kuman, K., Clarke, R.J., Brain, C.K. and Granger, D.E. 2014. Cosmogenic nuclide burial dating of hominin-bearing Pleistocene cave deposits at Swartkrans, South Africa. *Quaternary Geochronology* 24: 10-15.

Goldman-Neuman, T. and Hovers, E. 2009. Methodological Considerations in the Study of Oldowan Raw Material Selectivity: Insights from A. L. 894 (Hadar, Ethiopia). In: Hovers, E., Braun, D.R. (eds) *Interdisciplinary Approaches to the Oldowan. Vertebrate Paleobiology and Paleoanthropology:* 71-84. Dordrecht: Springer.

Goldman-Neuman, T. and Hovers, E. 2012. Raw material selectivity in late Pliocene Oldowan sites in the Makaamitalu Basin, Hadar, Ethiopia. *Journal of Human Evolution* 62(3): 353-366.

Goodwin, A.J.H. 1929. *The Stone Age Cultures of South Africa*, Cape Town: Annals of the South African Museum, 27.

Goren-Inbar, N. and Saragusti, I. 1996. An Acheulian biface assemblage from Gesher Benot Ya'aqov, Israel: indications of African affinities. *Journal of Field Archaeology*. 23(1): 15-30.

Gowlett, J.A.J. 1986. Culture and conceptualisation: the Oldowan-Acheulian gradient. *Stone Age Prehistory: Studies in Memory of Charles McBurney*: 243-260.

Granger, D.E., Gibbon, R.J., Kuman, K., Lotter, M.G. and Erlanger, E. 2013. Isochron burial dating method and application to an Earlier Stone Age chronosequence on the Sundays River, South Africa. *Poster presented at the Association of Southern African Professional Archaeologists Biennial Conference, Gaborone, Botswana***.**

Granger, D.E., Gibbon, R.J., Kuman, K., Clarke, R.J., Bruxelles, L. and Caffee, M.W. 2015. New cosmogenic burial ages for Sterkfontein Member 2 Australopithecus and Member 5 oldowan. *Nature* 522(7554): 85-88.

Gratuze, B. 1999. Obsidian characterization by laser ablation ICP-MS and its application to prehistoric trade in the Mediterranean and the Near East: sources and distribution of obsidian within the Aegean and Anatolia. *Journal of Archaeological Science* 26(8): 869-881.

Hall, G., Pickering, R., Lacruz, R., Hancox, J., Berger, L.R. and Schmid, P. 2006. An Acheulean hand axe from Gladysvale cave site, Gauteng. *South African Journal of Science* 102: 1030-105.

Hannah, J.L., Bekker, A., Stein, H.J., Markey, R.J. and Holland, H.D. 2004. Primitive Os and 2316 Ma age for marine shale: implications for Paleoproterozoic glacial events and the rise of atmospheric oxygen. *Earth and Planetary Science Letters* 225(1-2): 43-52.

Harmand, S. 2009. Variability in raw material selectivity at the late Pliocene sites of Lokalalei, West Turkana, Kenya. In: Hovers, E. & Braun, D.R. (eds) *Interdisciplinary approaches to the Oldowan*: 85-97. Dordrecht: Springer.

Harmand, S. Lewis, J.E. Feibel, C.S. Lepre, C.J. Prat, S. Lenoble, A. Boës, X. Quinn, R.L. Brenet, M. Arroyo, A. and Taylor, N. 2015. 3.3-million-year-old stone tools from Lomekwi 3, West Turkana, Kenya. *Nature* 521(7552): 310-315.

Hay, R.L. 1976. *Geology of the Olduvai Gorge*. Berkeley: University of California Press.

Herries, A.I. and Shaw, J. 2011. Palaeomagnetic analysis of the Sterkfontein palaeocave deposits: Implications for the age of the hominin fossils and stone tool industries. *Journal of Human Evolution* 60(5): 523-539.

Hodgson, D. 2015. The symmetry of Acheulean handaxes and cognitive evolution. *Journal of Archaeological Science: Reports* 2: 204-208.

Holdaway, S., McPherron, S. and Roth, B. 1996. Notched tool reuse and raw material availability in French Middle Paleolithic sites. *American Antiquity* 61(2): 377-387.

Holdaway, S., Witter, D., Fanning, P., Musgrave, R., Cochrane, G., Doelman, T., Greenwood, S., Pigdon, D. and Reeves, J. 1998. New approaches to open site spatial archaeology in Sturt National Park, New South Wales, Australia. *Archaeology in Oceania* 33(1): 1-19.

Horwitz, L.K. and Chazan, M. 2015. Past and present at Wonderwerk Cave (Northern Cape Province, South Africa). *African Archeological Review 32(4):* 595-612.

Howard, J.L. 2005. The quartzite problem revisited. *The Journal of Geology* 113(6): 707-713.

Isaac, G. 1981 *Stone Age Visiting Cards: Approaches to the Study of Early Land-Use Patterns*. Cambridge: Cambridge University Press.

Jercher, M., Pring, A., Jones, P.G. and Raven, M.D. 1998. Rietveld X-ray diffraction and X-ray fluorescence analysis of Australian aboriginal ochres. *Archaeometry* 40(2): 383-401.

Keeley, L.H. and Toth, N. 1981. Microwear polishes on early stone tools from Koobi Fora, Kenya. *Nature* 293(5832): 464-465.

Klein, R.G. 2009. *The human career: human biological and cultural origins*. Chicago: University of Chicago Press.

Kleindienst, M.R. 1962. Components of the East African Acheulian assemblage: an analytic approach. *Actes du IVeme Congres Panafricain de Préhistoire et de L'étude du Quaternaire* 40: 81-105.

Kristmanson, H. 2004. The application of X-ray fluorescence analysis to archaeological samples: a case study from Newfoundland and Cape Breton Island. *Canadian Journal of Archaeology/Journal Canadien D'Archéologie* 28: 342-352.

Kuhn, S.L. 1991. "Unpacking" reduction: lithic raw material economy in the Mousterian of west-central Italy. *Journal of Anthropological Archaeology* 10(1): 76-106.

Kuhn, S.L. 2004. Upper Paleolithic raw material economies at Üçağızlı cave, Turkey. *Journal of Anthropological Archaeology* 23(4): 431-448.

Kuman, K. 1994. The archaeology of Sterkfontein: preliminary findings on site formation and cultural change. *South African Journal of Science* 90(4): 215-219.

Kuman, K. 1998. The earliest South African industries. *Early Human Behaviour in Global Context: The Rise and Diversity of the Lower Palaeolithic Record*: 151-186.

Kuman, K. and Clarke, R.J. 2000. Stratigraphy, artefact industries and hominid associations for Sterkfontein, Member 5. *Journal of Human Evolution* 38(6): 827-847.

Kuman, K. 2003. Site formation in the early South African Stone Age sites and its influence on the archaeological record. *South African Journal of Science* 99: 251-254.

Kuman, K. 2007. *The Earlier Stone Age in South Africa: Site Context and the Influence of Cave Studies*. Indiana: Stone Age Institute Press.

Kuman, K. and Field, A.S. 2009. The Oldowan industry from Sterkfontein caves, South Africa. *The Cutting Edge: New Approaches to the Archaeology of Human Origins*: 151-170.

Kuman, K., Li, C. and Li, H. 2014. Large cutting tools in the Danjiangkou Reservoir Region, central China. *Journal of Human Evolution* 76: 129-153.

Kuman, K. and Gibbon, R.J. 2018. The Rietputs 15 site and Early Acheulean in South Africa. *Quaternary International* 480: 4-15.

Leader, G.M. 2009. Early Acheulean in the Vaal River basin, Rietputs Formation, Northern Cape Province, South Africa. Unpublished MSc Dissertation. Johannesburg: University of the Witwatersrand.

Leader, G.M. 2014. New Excavations at Canteen Kopje, Northern Cape Province, South Africa: A Technological Comparison of Three Earlier Acheulean Assemblages with New Interpretations on the Victoria West Phenomenon. Unpublished PhD dissertation. Johannesburg: University of the Witwatersrand.

Leader, G.M., Kuman, K., Gibbon, R.J. and Granger, D.E. 2018. Early Acheulean organised core knapping strategies ca. 1.3 Ma at Rietputs 15, Northern Cape Province, South Africa. *Quaternary International* 480: 16-28.

Leakey, M.D. (1971). *Olduvai Gorge. Vol 3. Excavations in Beds I and II, 1960–1963*. Cambridge: Cambridge University Press.

Lenhardt, N., Eriksson, P.G., Catuneanu, O. and Bumby, A.J. 2012. Nature of and controls on volcanism in the ca. 2.32–2.06 Ga Pretoria Group, Transvaal Supergroup, Kaapvaal craton, South Africa. *Precambrian Research* 214: 106-123.

Lepre, C.J., Roche, H., Kent, D.V., Harmand, S., Quinn, R.L., Brugal, J.P., Texier, P.J., Lenoble, A. and Feibel, C.S. 2011. An earlier origin for the Acheulian. *Nature* 477(7362): 82-85.

Li, H., Li, C.R. and Kuman, K. 2014. Rethinking the "Acheulean" in East Asia: evidence from recent investigations in the Danjiangkou Reservoir Region, central China. *Quaternary International* 347: 163-175.

Li, H., Kuman, K. and Li, C. 2016. Quantifying the reduction intensity of handaxes with 3D technology: A pilot study on handaxes in the Danjiangkou Reservoir region, central China. *PloS One* 10(9): 1-7. e0135613. DOI: 10.1371/journal.pone.0135613

Li, H., Kuman, K., Lotter, M.G., Leader, G.M. and Gibbon, R.J. 2017. The Victoria West: earliest prepared core technology in the Acheulean at Canteen Kopje and implications for the cognitive evolution of early hominids. *Royal Society Open Science* 4(6): 170-288.

Lotter, M.G. 2016. The archaeology of the lower Sundays River Valley, Eastern Cape province, South Africa: an assessment of Earlier Stone Age alluvial terrace sites. Unpublished PhD dissertation. Johannesburg: University of the Witwatersrand.

Lotter, M.G., Gibbon, R.J., Kuman, K., Leader, G.M., Forssman, T. and Granger, D.E. 2016. A geoarchaeological study of the middle and upper Pleistocene levels at Canteen Kopje, Northern Cape Province, South Africa. *Geoarchaeology* 31(4): 304-323.

Lotter, M.G. and Kuman, K. 2018. The Acheulean in South Africa, with announcement of a new site (Penhill Farm) in the lower Sundays River Valley, Eastern Cape Province, South Africa. *Quaternary International* 480: 43-65.

Lycett, S.J. 2008. Acheulean variation and selection: does handaxe symmetry fit neutral expectations?. *Journal of Archaeological Science* 35(9): 2640-2648.

Lycett, S.J. and von Cramon-Taubadel, N. 2008. Acheulean variability and hominin dispersals: a model-bound approach. *Journal of Archaeological Science* 35(3): 553-562.

Ma, J., Bolhar, R., Weisler, M.I., Feng, Y. and Zhao, J. 2011. Reproducibility of elemental analyses of basaltic stone artefacts by quadruple ICP-MS using different sample sizes and digestion methods, with implications for archaeological research. *Archaeometry* 53(5): 890-899.

Mantler, M. and Schreiner, M. 2000. X-ray fluorescence spectrometry in art and archaeology. *X-Ray Spectrometry: An International Journal* 29(1): 3-17

Marks, A., Shokler, J. and Zilhlo, J. 1991. Raw material usage in the Paleolithic. *Raw Material Economies Among Prehistoric Hunter-Gatherers, University of Kansas Publications in Anthropology* 19: 127-140.

Martinez, M.M. 1998. Differential raw material use in the Middle Pleistocene of Spain: evidence from Sierra de Atapuerca, Torralba, Ambrona and Aridos. *Cambridge Archaeological Journal* 8(1): 15-28.

Martini, J.E., Wipplinger, P.E., Moen, H.F. and Keyser, A. 2003. Contribution to the speleology of sterkfontein cave, Gauteng Province, South Africa. *International Journal of Speleology* 32(1): 4.

Marwick, B. 2008. What attributes are important for the measurement of assemblage reduction intensity? Results from an experimental stone artefact assemblage with relevance to the Hoabinhian of mainland Southeast Asia. *Journal of Archaeological Science* 35(5): 1189-1200.

Mason, R.J. 1957. Preliminary note on an earlier Stone Age site at Wonderboom South, Pretoria. *South African Journal of Science* 53(17): 431-434.

Mason, R.J. 1958. An Earlier Stone Age Site at Wonderboom South, Pretoria: Archaeological Survey of the Union of South Africa. *The South African Archaeological Bulletin* 13(49): 36-37.

Mason, R.J. 1962. Australopithecus and the beginning of the Stone Age in South Africa. *South African Archaeological Bulletin* 16:8–14.

Matmon, A., Ron, H., Chazan, M., Porat, N. and Horwitz, L.K. 2012. Reconstructing the history of sediment deposition in caves: A case study from Wonderwerk Cave, South Africa. *Bulletin* 124(3-4): 611-625.

McHenry, L.J. and de la Torre, I. 2018. Hominin raw material procurement in the Oldowan-Acheulean transition at Olduvai Gorge. *Journal of Human Evolution* 120: 378-401.

McNabb, J., Binyon, F. and Hazelwood, L. 2004. The large cutting tools from the South African Acheulean and the question of social traditions. *Current Anthropology* 45(5): 653-677.

McNabb, J. and Beaumont, P. 2011. *A report on the archaeological assemblages from excavations by Peter Beaumont at Canteen Koppie, Northern Cape, South Africa*. Oxford: Archaeopress.

McNabb, J. and Cole, J. 2015. The mirror cracked: Symmetry and refinement in the Acheulean handaxe. *Journal of Archaeological Science: Reports* 3: 100-111.

Meierhoff, J., Golitko, M. and Morris, J. 2010. Sourcing of obsidian from the ancient Maya farming community of Chan, Belize using portable-XRF. *Vibrational Spectroscopy* 43(2): 420-426.

Moll, R. 2017. A technological study of the lithic artefacts from the Earlier Stone Age Site of Maropeng, Cradle of Humankind, South Africa. Unpublished MSc thesis. Johannesburg: University of the Witwatersrand.

Moncel, M.H., Despriee, J., Voinchet, P., Tissoux, H., Moreno, D., Bahain, J.J., Courcimault, G. and Falgueres, C. 2013. Early evidence of Acheulean settlement in northwestern

Europe-La Noira Site, a 700 000-year-old occupation in the center of France. *PloS One* 8(11). e103634. DOI: 10.1371/journal.pone.0103634

Morrissey, P. 2015. A geoarchaeological investigation of the Earlier Stone Age site at Maropeng in the Cradle of Humankind. Unpublished Honours dissertation. Johannesburg: University of the Witwatersrand.

Nash, D.J., Coulson, S., Staurset, S., Ullyott, J.S., Babutsi, M., Hopkinson, L. and Smith, M.P. 2013a. Provenancing of silcrete raw materials indicates long-distance transport to Tsodilo Hills, Botswana, during the Middle Stone Age. *Journal of Human Evolution* 64(4): 280-288.

Nash, D., Coulson, S., Staurset, S., Smith, M. and Ullyott, J. 2013b. Provenancing silcrete in the Cape coastal zone: implications for Middle Stone Age research in South Africa. *Journal of Human Evolution* 65(5): 682-688.

Nash, D.J., De Cort, G., Chase, B.M., Verschuren, D., Nicholson, S.E., Shanahan, T.M., Asrat, A., Lézine, A.M. and Grab, S.W. 2016. African hydroclimatic variability during the last 2000 years. *Quaternary Science Reviews* 154: 1-22.

Neff, H. 2003. Analysis of Mesoamerican plumbate pottery surfaces by laser ablation-inductively coupled plasma-mass spectrometry (LA-ICP-MS). *Journal of Archaeological Science* 30(1): 21-35.

Negash, A., Shackley, M.S. and Alene, M. 2005. Source provenance of obsidian artifacts from the Early Stone Age (ESA) site of Melka Konture, Ethiopia. *Journal of Archaeological Science* 33(12): 1647-1650.

Obbes, A.M. 2000. *The structure, stratigraphy and sedimentology of the Black Reef-Malmani-Rooihoogte succession of the Transvaal Supergroup southwest of Pretoria* (Vol. 127). Pretoria: Council for Geoscience.

Pappu, S., Gunnell, Y., Akhilesh, K., Braucher, R., Taieb, M., Demory, F. and Thouveny, N. 2011. Early Pleistocene presence of Acheulian hominins in south India. *Science* 331(6024): 1596-1599.

Pickering, R. and Kramers, J.D. 2010. Re-appraisal of the stratigraphy and determination of new U-Pb dates for the Sterkfontein hominin site, South Africa. *Journal of Human Evolution* 59(1): 70-86.

Pitblado, B.L., Dehler, C., Neff, H. and Nelson, S.T. 2008. Pilot study experiments sourcing quartzite, Gunnison Basin, Colorado. *Geoarchaeology: An International Journal* 23(6): 742-778.

Pitblado, B.L., Cannon, M.B., Neff, H., Dehler, C.M. and Nelson, S.T. 2013. LA-ICP-MS analysis of quartzite from the Upper Gunnison Basin, Colorado. *Journal of Archaeological Science* 40(4): 2196-2216.

Plummer, T. 2004. Flaked stones and old bones: biological and cultural evolution at the dawn of technology. *American Journal of Physical Anthropology* 125(S39): 18-164.

Pollarolo, L., Susino, G., Kuman, K. and Bruxelles, L. 2010. Acheulean artefacts at Maropeng in the Cradle of Humankind world heritage site, Gauteng province, South Africa. *The South African Archaeological Bulletin*: 65(191): 3-12.

Potts, R. 1991. Why the Oldowan? Plio-Pleistocene toolmaking and the transport of resources. *Journal of Anthropological Research* 47(2): 153-176.

Potts, R. 1994. Variables versus models of early Pleistocene hominid land use. *Journal of Human Evolution* 27(1-3): 7-24.

Potts, R., Behrensmeyer, A.K. and Ditchfield, P. 1999. Paleolandscape variation and Early Pleistocene hominid activities: members 1 and 7, Olorgesailie Formation, Kenya. *Journal of Human Evolution* 37(5): 747-788.

Presnyakova, D., Braun, D.R., Conard, N.J., Feibel, C., Harris, J.W., Pop, C.M., Schlager, S. and Archer, W. 2018. Site fragmentation, hominin mobility and LCT variability reflected in the early Acheulean record of the Okote Member, at Koobi Fora, Kenya. *Journal of Human Evolution* 125: 159-180.

Prieto, A., Yusta, I. and Arrizabalaga, A. 2018. Defining and characterizing archaeological quartzite: sedimentary and metamorphic processes in the lithic assemblages of El Habario and El Arteu (Cantabrian Mountains, northern Spain). *Archaeometry* 61(1): 14-30.

Prieto, A., Yusta, I. and Arrizabalaga, A. 2020. From petrographic analysis to stereomicroscopic characterisation: a geoarchaeological approach to identify quartzite artefacts in the Cantabrian Region. *Archaeological and Anthropological Sciences* 12(1): 32.

Reynolds, S.C., Bailey, G.N. and King, G.C. 2011. Landscapes and their relation to hominin habitats: case studies from Australopithecus sites in eastern and southern Africa. *Journal of Human Evolution* 60(3): 281-298.

Rightmire, G.P. 2004. Brain size and encephalization in early to mid-Pleistocene Homo. *American Journal of Physical Anthropology: The Official Publication of the American Association of Physical Anthropologists* 124(2): 109-123.

Roe, D.A. 1994. A metrical analysis of selected sets of handaxes and cleavers from Olduvai Gorge. In: Leakey, M.D., Roe, D.A. (eds.), *Olduvai Gorge, vol. 5.*: 146-234. Cambridge: Cambridge University Press.

Rollinson, H.R. 1993. A terrane interpretation of the Archaean Limpopo Belt. *Geological Magazine* 130: 755-765.

Sahle, Y., Morgan, L.E., Braun, D.R., Atnafu, B. and Hutchings, W.K. 2014. Chronological and behavioral contexts of the earliest Middle Stone Age in the Gademotta formation, main Ethiopian rift. *Quaternary International* 331: 6-19.

Schick, K.D. 1987. Experimentally- derived criteria for assessing hydrologic disturbance of archaeological sites. *Natural Formation Processes and the Archaeological Record* 352: 86-107.

Schick, K.D. and Toth, N.P. 1993. *Making silent stones speak: Human evolution and the dawn of technology*. New York: Simon and Schuster.

Sciuto, C., Geladi, P., La Rosa, L., Linderholm, J. and Thyrel, M. 2019. Hyperspectral imaging for characterization of lithic raw materials: the case of a Mesolithic dwelling in northern Sweden. *Lithic Technology* 44(1): 22-35.

Semaw, S. 2000. The world's oldest stone artifacts from Gona, Ethiopia: their implications for understanding stone technology and patterns of human evolution between 2.6-1.5 million years ago. *Journal of Archaeological Science* 27: 1197-1214.

Shackley, M.S. 2005. *Obsidian: geology and archaeology in the North American Southwest*. Arizona: University of Arizona Press.

Shackley, M.S. 1998. Geochemical differentiation and prehistoric procurement of obsidian in the Mount Taylor volcanic field, northwest New Mexico. *Journal of Archaeological Science* 25(11): 1073-1082.

Shackley, M.S. 2011. An introduction to X-ray fluorescence (XRF) analysis in archaeology. In: Shackley, M. S. (eds.) *X-ray Fluorescence Spectrometry (XRF) in Geoarchaeology*: 7–44. New York: Springer.

Shackley, M.S. 2012. Portable X-ray fluorescence spectrometry (pXRF): the good, the bad, and the ugly. *Archaeology Southwest Magazine* 26(2): 1-8.

Sharon, G. 2010. Large flake Acheulian. *Quaternary International* 223: 226-233.

Sherwood, N.L. 2013. Lithic raw material procurement through time at Swartkrans: Earlier to Middle Stone Age. Unpublished MSc thesis. Johannesburg: University of the Witwatersrand.

Shick, K.D. 1987. Modeling the formation of Early Stone Age artifact concentrations. *Journal of Human Evolution* 16(7-8): 789-807.

Shipman, P. and Walker, A. 1989. The costs of becoming a predator. *Journal of Human Evolution* 18(4): 373-392.

Shipton, C. 2011. Taphonomy and behaviour at the Acheulean site of Kariandusi, Kenya. *African Archaeological Review* 28(2): 141. DOI: 10.1007/s10437-011-9089-1

Shipton, C. and Clarkson, C. 2015. Flake scar density and handaxe reduction intensity. *Journal of Archaeological Science: Reports* 2: 169-175.

Shipton, C., Clarkson, C. and Cobden, R. 2019. Were Acheulean bifaces deliberately made symmetrical? Archaeological and experimental evidence. *Cambridge Archaeological Journal* 29(1): 65-79.

Shoval, S. 2018. The application of LA-ICP-MS, EPMA and Raman micro-spectroscopy methods in the study of Iron Age Phoenician Bichrome pottery at Tel Dor. *Journal of Archaeological Science: Reports* 21: 938-951.

Solodenko, N., Zupancich, A., Cesaro, S.N., Marder, O., Lemorini, C. and Barkai, R. 2015. Fat residue and use-wear found on Acheulian biface and scraper associated with

butchered elephant remains at the site of Revadim, Israel. *PloS One* 10(3): 1-17. e0118572. DOI: 10.1371/journal.pone.0118572

Soto, M., Favreau, J., Campeau, K., Carter, T., Abtosway, M., Bushozi, P.M., Clarke, S., Durkin, P.R., Hubbard, S.M., Inwood, J. and Itambu, M. 2020. Fingerprinting of quartzitic outcrops at Oldupai Gorge, Tanzania. *Journal of Archaeological Science: Reports* 29: 102010.

Stanford, C.B. 1996. The hunting ecology of wild chimpanzees: implications for the evolutionary ecology of Pliocene hominids. *American Anthropologist*: 96-113.

Stern, N. 1991. The scatters-between-the-patches: a study of early hominid land use patterns in the Turkana Basin, Kenya. Unpublished PhD dissertation. Cambridge: Harvard University.

Stern, N. 1994. The implications of time-averaging for reconstructing the land-use patterns of early tool-using hominids. *Journal of Human Evolution* 27(1-3): 89-105.

Stetzenbach, K.J., Amano, M., Kreamer, D.K. and Hodge, V.F. 1994. Testing the Limits of ICP-MS: Determination of Trace Elements in Ground Water at the Part-Per-Trillion Level. *Groundwater* 32(6): 976-985.

Stout, D. 2010. The evolution of cognitive control. *Topics in Cognitive Science* 2(4): 614-630.

Stout, D. 2011. Stone toolmaking and the evolution of human culture and cognition. *Philosophical Transactions of the Royal Society B: Biological Sciences* 366(1567): 1050-1059.

Stout, D., Quade, J., Semaw, S., Rogers, M.J. and Levin, N.E. 2005. Raw material selectivity of the earliest stone toolmakers at Gona, Afar, Ethiopia. *Journal of Human Evolution*, *48*(4): 365-380.

Stout, D., Quade, J., Semaw, S., Rogers, M.J. and Levin, N.E. 2006. Raw material selectivity of the earliest stone toolmakers at Gona, Afar, Ethiopia. *Journal of Human Evolution* 48(4): 365-380.

Stratford, D.J. 2011. The underground central deposits of the Sterkfontein Caves, South Africa. Unpublished PhD dissertation. Johannesburg: University of the Witwatersrand.

Sunyer, M.R., Torcal, R.M., Figueroa, F.J.P., Martínez-Moreno, J. and Benito-Calvo, A. 2017. Quartzite selection in fluvial deposits: The N12 level of Roca dels Bous (Middle Palaeolithic, southeastern Pyrenees). *Quaternary International* 435: 49-60.

Sutton, M. 2012. The archaeology of Swartkrans cave, Gauteng, South Africa: new excavations of members 1 and 4. Unpublished PhD dissertation. Johannesburg: University of the Witwatersrand.

Sutton, M.B., Kuman, K. and Steininger, C. 2017. Early Pleistocene stone artefacts from Cooper's Cave. South Africa.*The South African Archaeological Bulletin* 72(206): 156-161.

Schweigart, H. 1965. Genesis of the iron ores of the Pretoria Series, South Africa. *Economic Geology* 60(2): 269-298.

Tasker, D. (2017). A preliminary assessment of the open-air lithic assemblage from Elandsdrift farm, cradle of humankind, South Africa. Unpublished Honours dissertation. Johannesburg: University of the Witwatersrand

ten Bruggencate, R.E., Milne, S.B., Fayek, M., Park, R.W. and Stenton, D.R. 2015. Characterization of chert artifacts and two newly identified chert quarries on southern Baffin Island. *Lithic Technology* 40(3): 189-198.

ten Bruggencate, R.E., Milne, S.B., Fayek, M., Park, R.W., Stenton, D.R. and Hamilton, A.C. 2018. Characterizing southern Baffin Island chert: a cautionary tale for provenance research. *Journal of Archaeological Science: Reports* 22: 324-329.

Toth, N.P. 1982. The Stone Technologies of Early Hominids at Koobi Fora: An Experimental Approach. Unpublished PhD. dissertation. Berkeley: University of California.

Toth, N. and Schick, K. 1993. Early stone industries and inferences regarding language and cognition. *Tools, Language and Cognition in Human Evolution*: 346-362.

Toth, N. and Schick, K. 2019. Why did the Acheulean happen? Experimental studies into the manufacture and function of Acheulean artifacts. *L'Anthropologie* 123(4-5): 724-768.

Tykot, R. and Young, S. 1996. Archaeological applications of inductively coupled plasma-mass spectrometry. In: Orna, M.V. (eds.) *ACS Symposium Series 625 Archaeological Chemistry:* 116-130. Washington D.C.: American Chemical Society.

Van Riet Lowe, C. 1929. Fresh light on the prehistoric archaeology of South Africa. *Banthu Studies 3*: 388–389.

Vázquez, C., Palacios, O., Lué-Merú, M., Custo, G., Ortiz, M. and Murillo, M. 2011. Provenance study of obsidian samples by using portable and conventional X ray fluorescence spectrometers. Performance comparison of both instrumentations. *Journal of Radioanalytical and Nuclear Chemistry* 292(1):367-373.

Veldeman, I., Baele, J.M., Goemaere, E., Deceukelaire, M., Dusar, M. and De Doncker, H.W.J.A. 2012. Characterizing the hypersiliceous rocks of Belgium used in (pre-) history: a case study on sourcing sedimentary quartzites. *Journal of Geophysics and Engineering* 9(4): 118-128.

Wallace, I.J. and Shea, J.J. 2006. Mobility patterns and core technologies in the Middle Paleolithic of the Levant. *Journal of Archaeological Science* 33(9): 1293-1309.

Wang, W. and Bae, C.J. 2015. How old are the Bose (Baise) Basin (Guangxi, southern China) bifaces? The Australasian tektites question revisited. *Journal of Human Evolution* 80: 171-174.

Wess, T.J., Drakopoulos, M., Snigirev, A., Wouters, J., Paris, O., Fratzl, P., Collins, M., Hillier, J. and Nielsen, K. 2001. The use of small-angle X-ray diffraction studies for the analysis of structural features in archaeological samples. *Archaeometry* 43(1): 117-129.

Wilkins, J. 2017. Middle Pleistocene lithic raw material foraging strategies at Kathu Pan 1, Northern Cape, South Africa. *Journal of Archaeological Science: Reports* 11: 169-188.

Williams, P.R., Dussubieux, L. and Nash, D.J. 2012. Provenance of Peruvian Wari Obsidian: Comparing INAA, LA-ICP-MS, and Portable XRF. *Obsidian and ancient manufactured glasses*. Albuquerque: University of New Mexico Press.

Yamaguchi, K.E., Johnson, C.M., Beard, B.L. and Ohmoto, H. 2005. Biogeochemical cycling of iron in the Archean–Paleoproterozoic Earth: constraints from iron isotope variations in sedimentary rocks from the Kaapvaal and Pilbara Cratons. *Chemical Geology* 218(1-2): 135-169.

APPENDIX

Table 1. Technological analysis of LCTs

Accession#	Length	Width	Thick	Mass (g)	D Scars	Scar Dir	Edge Angle	Cortex %	Area (Meshlab)	Volume	Notes
4	151	109,1	34,2	598,1	15	4	accute	12	278,26	234,9	handaxe
22	136	64,4	42,5	438,8	18	6	obtuse	46	193,69	168,07	pick
51	117,2	86,6	38	389,1	7	4	obtuse	6	191,77	147,23	cleaver
179	132	75,5	27	367,1	10	5	obtuse	40	193,19	149,09	cleaver
205	111,6	72	38,3	368,35	22	7	obtuse	9	173,96	138,04	handaxe
236	120,8	68,3	47	380	25	5	obtuse	15	173,24	141,46	handaxe
311	162,3	85,3	49,5	516,58	9	3	obtuse	42	231,32	195,8	handaxe
328	120,3	69,5	36	327,83	13	4	obtuse	10	176,14	121,26	cleaver
415	123	76,5	32	325,84	8	3	accute	4	171,39	123,86	handaxe
1060p	175,7	99	46,9	752,41	43	7	accute	21	289,21	283,79	pick
1067p	127,1	76	42,4	400	17	4	accute	38	183,25	144,97	handaxe
1084p	186,8	104,3	45,6	866,77	20	4	accute	35	331,3	338,95	handaxe
1089p	162,3	93,8	56,3	705,29	17	3	accute	33	276,02	268,25	pick
128p	111,11	70,6	37,6	300	12	5	obtuse	8	150,45	110,89	handaxe
222p	163,8	105,2	59,5	1098,66	15	4	obtuse	30	358,97	428,07	cleaver
228m	112,6	69,2	35,7	347,37	21	5	obtuse	22	160,5	131,85	handaxe
348p	182,2	86,1	59,1	1088,42	20	4	accute	45	339,98	375,11	handaxe
499p	108,8	83,6	28,3	312,4	27	6	accute	22	161,29	118,83	handaxe
818p	146,5	52,7	44,7	316,41	22	4	obtuse	11	165,88	119,9	pick
823p	165,2	89,2	54	704,5	18	5	accute	10	274,57	270,84	handaxe
902p	110	68,3	41,5	366,4	15	3	obtuse	47	191,96	142,43	handaxe
AGT1m	119,2	68,4	46,4	319,75	19	5	obtuse	18	160,76	121,21	handaxe

Table 2. Technological analysis of cores

Accession#	Type	Length	Width	Thick	Mass (g)	Scars	Edge Angle	Cortex %	Area (Meshlab)	Volume	FSD
21	bsp	128,60	106,50	48,60	1054,26	7	accute	75	326,6	387,82	0,02143
32	bsp	78,60	67,30	38,70	234,65	19	accute	40	114,68	89,49	0,16568
44	uau1	130,60	63,60	40,30	613,61	9	obtuse	35	232,29	234,21	0,03874
48	mf	106,00	101,00	73,80	810,96	11	obtuse	50	251,95	312,39	0,04366
52	mf	94,70	74,30	66,00	508,97	31	obtuse	4	196,05	193,47	0,15812
57	bp	82,80	59,40	35,30	235,43	22	obtuse	20	121,64	89,06	0,18086
57(2)	mf	82,80	63,60	49,20	302,86	24	obtuse	15	139,88	115,1	0,17158
59	mf	65,20	45,30	21,60	86,71	9	accute	40	65,35	33,08	0,13772
67	mf	86,00	51,20	36,60	139,22	6	obtuse	35	95,48	55,64	0,06284
83	mf	93,60	57,30	39,70	215,95	17	obtuse	5	120,86	84,03	0,14066
87	mf	128,20	87,40	84,90	1172,83	18	obtuse	10	320,76	449,02	0,05612
105	bp	112,00	54,70	60,60	567,99	12	obtuse	28	203,07	210,26	0,05909
106	mf	125,60	108,20	57,60	1003,31	14	obtuse	42	304,09	394,32	0,04604
114	bsp	134,40	88,20	44,20	622,50	12	accute	36	250,71	235,7	0,04786
128	uau1	85,70	65,60	57,40	274,86	11	obtuse	90	128,99	110,83	0,08528
128B	uau1	90,40	63,90	58,40	481,63	4	obtuse	82	159,57	163,8	0,02507
131	mf	100,60	79,00	61,10	611,45	8	obtuse	65	206,82	226,83	0,03868
131B	mf	138,50	106,70	74,60	1231,61	3	obtuse	78	345,11	478	0,00869
141	mf	74,70	57,90	43,60	204,52	13	obtuse	42	103,31	76,12	0,12583
142	mf	102,00	79,30	51,80	386,12	11	obtuse	28	166,08	145,4	0,06623
147	bsp	110,00	82,80	50,10	496,00	9	accute	75	192,67	181,04	0,04671
162	mf	130,50	75,70	34,40	401,31	6	obtuse	15	206,58	150,02	0,02904
166	bsp	73,90	50,50	46,10	204,21	2	obtuse	60	105,16	79,5	0,01902
172	mf	78,10	65,60	46,00	223,63	3	obtuse	80	110,3	88,32	0,0272
173	mf	72,50	57,20	40,80	199,00	5	obtuse	80	98,02	75,1	0,05101
190B	mf	108,40	77,90	64,50	616,00	12	obtuse	54	177,41	165,39	0,06764
190	mf	105,30	72,50	49,20	425,78	6	obtuse	55	216,37	227,05	0,02773
191	mf	59,90	56,10	28,40	127,14	23	obtuse	13	75,04	46,59	0,3065
206	bsp	115,10	90,40	50,10	432,75	9	obtuse	40	194,91	160,51	0,04618
218	mf	97,90	81,00	41,10	361,23	9	obtuse	26	165,73	139,83	0,05431
231	bap	70,30	52,40	45,20	143,82	11	obtuse	10	87,44	57,58	0,1258
236	bsp	85,10	70,90	49,70	329,25	3	obtuse	90	144,13	126,91	0,02081
238	mf	130,70	76,20	59,40	612,15	8	obtuse	37	248,48	237,44	0,0322
239	uau1	120,20	70,80	58,70	599,16	3	obtuse	82	224,32	225,38	0,01337
242	mf	132,90	82,10	74,90	847,13	4	obtuse	69	261,32	323,97	0,01531
245	bsp	85,70	56,90	37,20	259,38	7	accute	60	116,22	93,15	0,06023
251	uau1	103,30	74,10	65,70	423,96	2	obtuse	60	180,21	161,95	0,0111
264	mf	85,10	54,10	49,30	314,61	18	obtuse	0	147,38	119,96	0,12213
272	bsp	100,60	76,20	57,10	447,34	11	accute	70	172,03	164,2	0,06394
273	usp	82,80	64,70	36,70	208,92	1	obtuse	90	113,87	81,88	0,00878
274	mf	91,40	70,50	50,90	533,97	13	obtuse	55	203,87	204,1	0,06377
276	usp	79,30	71,30	36,40	193,33	2	accute	80	110,25	78,84	0,01814
277	mf	63,10	59,40	43,40	169,43	19	obtuse	5	90,91	65,24	0,209
1080p	mf	136,80	67,00	52,40	683,61	22	obtuse	25	249,53	263,11	0,08817
191p	mf	92,70	73,10	56,00	405,50	22	obtuse	1	171,81	156,6	0,12805
250p	uc	101,70	58,50	33,70	206,89	25	accute	6	122,88	79,62	0,20345
334p	uc	87,50	50,00	31,00	115,70	19	obtuse	0	85,05	46,3	0,2234
349p	mf	172,80	89,50	63,30	909,39	21	obtuse	48	328,05	353,49	0,06401
497p	mf	76,50	56,60	37,50	174,96	33	accute	2	98,8	67,8	0,33401
501p	mf	137,80	85,00	50,80	594,27	27	accute	1	237,57	228,23	0,11365
504p	bsp	114,70	73,10	61,10	541,30	13	obtuse	40	207,01	204,43	0,0628
810p	mf	146,00	117,00	52,70	1076,39	16	obtuse	21	349,11	417,74	0,04583
8A	mf	95,50	65,50	57,10	412,48	2	obtuse	85	172,58	157,12	0,01159
901p	mf	63,50	55,30	48,00	223,44	22	obtuse	7	106,7	88,13	0,20619
903p	mf	59,60	51,20	42,40	182,27	33	obtuse	15	93,09	70,68	0,3545
U1p	mf	95,60	73,30	41,80	369,14	16	obtuse	17	153,71	132,14	0,10409
U2p	balp	120,20	105,80	42,80	625,29	10	obtuse	0	243,17	234,6	0,04112
U3p	uaut	60,30	65,30	52,70	233,52	4	obtuse	65	114,75	87,07	0,03486
U4p	mf	72,50	68,60	56,00	320,00	6	obtuse	65	132,62	121,56	0,04524
U5p	bsp	105,20	99,00	44,40	645,89	10	obtuse	80	233,52	243,45	0,04282

Table 3. AD-ICPMS raw data part 1

ppm	U1	U2	U4	U5	QM3 MILL	QM7 MILL	QM14	MOG1-3	MOG1-5	GO1-2	GO1-9 MIL	GO2-2	GO2-4	VMO1-3	VMO1-6	VMO1-11	FFIO1-2D(	FFIO1-2M	FFIO1-5	MIO1-3	MIO1-7	MIO2-3
Li	112,959	13,613	2,175	27,209	3,358	4,867	0,498	0,547	0,486	1,585	1,970	3,354	0,827	1,792	0,192	0,453	0,543	0,544	1,020	19,884	14,465	0,255
P	75,841	50,396	243,082	978,686	47,872	123,205	52,717	214,884	353,120	484,327	570,354	140,604	171,386	265,913	506,817	720,995	36,725	81,506	111,696	302,119	57,382	116,406
Sc	9,037	2,245	1,786	8,761	0,812	0,859	1,031	1,592	3,136	1,284	0,838	5,183	6,094	1,079	1,077	1,999	0,431	0,679	0,800	3,540	3,931	0,406
Ti	571,509	405,334	144,190	1424,194	99,229	90,954	113,649	112,339	70,131	73,510	94,015	870,279	870,855	89,044	40,233	108,328	59,742	65,696	76,111	951,328	837,523	75,471
V	130,258	37,810	45,161	116,298	24,873	22,778	31,814	44,581	23,870	27,942	18,129	36,213	36,512	24,002	12,490	83,953	6,282	19,665	6,565	54,093	65,685	9,300
Cr	242,791	158,374	102,389	567,439	18,195	15,582	9,161	90,792	20,713	15,777	17,800	44,130	56,588	19,510	9,941	20,650	8,471	16,753	16,530	82,899	144,501	20,750
Co	134,805	627,443	299,419	74,675	13,087	11,371	31,292	90,740	36,086	758,258	10,366	200,066	259,754	540,427	19,289	121,695	407,759	13,085	10,331	149,914	122,754	95,258
Ni	118,441	91,222	66,965	53,621	33,451	31,874	5,758	11,875	6,885	82,687	25,513	38,817	35,921	58,043	3,347	18,391	44,235	37,485	5,860	29,373	27,226	14,067
Cu	125,699	59,125	115,814	35,696	36,887	36,487	5,926	5,849	10,209	100,280	42,747	26,458	524,422	28,334	7,348	24,519	24,020	44,675	9,679	81,885	271,876	165,293
Zn	179,577	32,848	26,151	38,594	8,720	15,998	6,263	7,428	9,615	20,413	15,407	96,127	253,817	8,371	4,456	30,708	9,697	9,210	10,177	39,535	42,320	41,839
Ga	12,649	4,037	3,547	13,223	2,835	2,682	1,790	2,544	2,240	1,858	2,406	7,236	6,015	1,085	1,526	1,465	0,772	2,682	1,867	5,900	6,151	0,685
Rb	3,771	1,447	24,304	54,878	0,439	1,287	0,200	0,241	0,281	1,693	0,553	65,705	59,492	0,229	0,448	0,227	0,799	0,389	0,357	1,645	0,317	0,277
Sr	1,168	1,746	4,754	28,455	0,701	1,193	0,891	2,356	0,906	2,983	6,887	16,154	13,825	0,652	11,814	9,657	2,529	2,005	8,588	1,444	0,473	0,717
Y	4,512	2,193	1,798	12,395	1,335	1,264	1,354	1,271	1,247	1,598	1,564	7,430	9,446	1,209	0,948	2,064	1,063	1,317	1,984	2,325	1,771	0,945
Zr	58,538	25,749	20,144	158,908	15,722	16,547	16,594	16,972	22,900	14,843	16,060	44,977	59,528	16,356	13,681	16,022	11,365	12,212	20,503	62,299	47,234	12,351
Nb	2,166	2,493	1,497	5,428	0,658	0,556	0,508	0,860	0,391	1,958	0,587	2,931	4,000	1,893	0,152	0,946	1,343	0,377	0,426	3,294	2,310	0,192
Sn	5,644	1,753	2,839	5,708	1,724	1,597	1,131	1,953	1,692	2,875	1,595	3,105	2,804	1,292	0,923	1,551	0,730	1,392	1,315	3,353	71,294	0,788
Sb	0,662	0,210	1,532	1,698	0,366	0,365	0,161	1,041	0,439	4,510	1,477	3,622	2,568	0,147	0,160	0,493	0,195	0,503	0,410	0,304	0,179	0,047
Cs	0,390	0,235	0,874	4,061	0,052	0,104	0,032	0,031	0,038	0,106	0,065	6,628	6,108	0,040	0,058	0,065	0,075	0,046	0,061	0,234	0,066	0,042
Ba	15,857	10,123	38,225	192,477	5,415	8,500	3,545	4,927	4,747	14,989	36,408	184,994	252,124	3,226	25,754	17,552	64,243	24,464	52,112	19,751	3,181	2,632
La	3,904	3,027	6,547	55,497	4,021	3,664	2,345	3,543	6,120	6,737	4,306	12,371	4,087	2,327	5,416	5,974	2,487	3,292	14,613	4,835	2,864	3,188
Ce	7,352	5,175	10,378	78,410	6,809	6,195	3,749	6,231	11,803	11,066	7,201	21,157	7,084	4,152	9,698	10,074	4,280	5,490	17,776	8,157	5,224	5,297
Pr	0,852	0,691	1,076	11,123	0,815	0,707	0,502	0,698	0,590	1,193	0,778	2,517	1,006	0,487	0,986	1,061	0,447	0,598	1,828	1,100	0,616	0,561
Nd	3,027	2,612	3,785	39,825	3,008	2,584	1,934	2,633	2,203	4,285	2,853	9,209	4,067	1,880	3,328	3,772	1,675	2,231	5,371	4,172	2,372	2,024
Sm	0,649	0,550	0,654	7,132	0,575	0,483	0,390	0,474	0,416	0,705	0,512	1,652	1,032	0,376	0,531	0,649	0,321	0,417	0,836	0,826	0,553	0,352
Eu	0,185	0,137	0,121	1,457	0,102	0,072	0,075	0,085	0,069	0,152	0,124	0,382	0,281	0,065	0,092	0,111	0,057	0,073	0,164	0,193	0,123	0,065
Gd	0,685	0,511	0,505	5,655	0,429	0,344	0,327	0,352	0,310	0,492	0,417	1,583	1,450	0,305	0,377	0,507	0,269	0,352	0,656	0,597	0,421	0,279
Tb	0,125	0,080	0,067	0,745	0,051	0,043	0,050	0,049	0,038	0,061	0,058	0,228	0,250	0,044	0,046	0,074	0,034	0,046	0,083	0,085	0,058	0,037
Dy	0,909	0,560	0,462	3,956	0,343	0,316	0,360	0,324	0,274	0,396	0,400	1,426	1,762	0,333	0,292	0,513	0,257	0,312	0,523	0,567	0,400	0,256
Ho	0,198	0,111	0,089	0,691	0,064	0,061	0,073	0,069	0,058	0,079	0,079	0,291	0,385	0,068	0,053	0,107	0,049	0,060	0,098	0,118	0,085	0,049
Er	0,675	0,351	0,294	1,887	0,210	0,208	0,239	0,218	0,193	0,250	0,249	0,873	1,169	0,226	0,171	0,357	0,156	0,191	0,301	0,403	0,289	0,150
Tm	0,123	0,055	0,043	0,288	0,030	0,029	0,040	0,035	0,030	0,037	0,041	0,136	0,196	0,038	0,024	0,058	0,021	0,026	0,044	0,068	0,052	0,022
Yb	0,992	0,443	0,341	1,976	0,265	0,258	0,307	0,272	0,259	0,296	0,327	0,946	1,303	0,321	0,212	0,477	0,185	0,222	0,346	0,522	0,441	0,173
Lu	0,152	0,060	0,045	0,286	0,032	0,032	0,041	0,038	0,035	0,039	0,043	0,142	0,190	0,042	0,026	0,066	0,021	0,028	0,044	0,083	0,072	0,024
Hf	1,619	1,016	0,833	4,692	0,673	0,679	0,724	0,736	0,908	0,647	0,687	1,430	1,720	0,721	0,617	0,639	0,470	0,523	0,848	2,046	1,536	0,477
Ta	0,934	7,368	3,572	1,070	0,073	0,064	0,258	1,138	0,517	6,106	0,078	0,449	2,429	5,307	0,123	1,097	4,623	0,054	0,080	3,076	1,030	0,446
W	510,365	4367,259	2405,072	362,617	4,445	3,253	234,375	839,398	296,370	6220,971	7,882	212,175	2258,859	4771,372	145,559	1028,162	3496,752	8,855	75,555	813,604	489,280	148,288
Tl	0,023	0,015	0,155	0,334	0,006	0,008	0,008	0,010	0,008	0,012	0,011	0,497	0,443	0,007	0,006	0,007	0,012	0,008	0,006	0,009	0,001	0,001
Pb	14,302	4,002	18,456	44,219	2,556	1,250	0,976	2,785	2,481	3,383	4,632	12,889	7,382	0,702	1,439	5,962	11,786	11,307	11,342	16,441	5,567	2,796
Th	14,439	3,953	3,934	15,077	2,829	2,680	2,887	3,002	4,481	2,807	2,915	4,985	3,823	3,128	2,369	3,824	1,392	1,773	2,644	7,471	6,501	1,736
U	4,434	1,385	1,244	2,906	0,726	1,138	1,033	1,552	1,558	1,734	1,967	3,170	2,220	1,451	0,977	10,392	0,629	0,848	0,970	1,947	1,865	1,210

Table 5. AD-ICPMS raw data part 2

ppm	MIO2-6	MIO3-4 M	MIO3-5 M	MIO4-2	MIO4-4	MIO5-5 M	MIO5-6	8A	21	44	179	206	242	245	349P	504P	1080P	MGQ1-2	MGQ1-3	BCR2	BHVO2	BCR2	BHVO2
Li	0,079	4,640	2,385	123,534	46,960	2,837	0,436	12,474	37,037	2,844	2,827	56,612	4,564	2,296	2,502	23,450	0,789	4,208	28,675	9,866	5,021	9,9	5
P	58,440	84,091	151,755	622,942	175,987	137,880	89,838	200,769	4931,860	246,695	316,726	229,878	299,421	348,385	369,312	369,221	100,492	237,575	122,521	1539,625	1202,772	1571	1178
Sc	0,498	1,124	0,850	9,345	8,809	0,795	1,169	4,945	10,291	2,935	4,525	8,383	3,123	3,486	5,565	6,089	0,910	1,572	2,295	32,062	30,941	32	31
Ti	57,460	164,064	140,009	1020,656	856,316	139,612	138,487	881,961	1095,976	171,180	625,577	2099,536	208,846	449,659	116,412	619,814	167,432	238,199	349,711	########	########	13005	15621
V	9,025	22,248	22,772	129,435	168,521	19,515	19,225	103,079	48,369	59,692	71,471	82,036	66,120	132,153	44,228	65,865	28,802	25,380	37,190	415,354	327,936	414	329
Cr	18,403	19,244	26,603	62,697	109,665	21,759	19,453	403,180	163,337	144,691	329,430	208,257	376,283	394,873	158,102	240,709	165,451	23,476	43,000	10,864	285,000	17	285
Co	403,008	5,141	15,701	64,988	30,744	12,443	22,476	352,788	76,454	307,217	34,706	65,829	1136,191	104,881	121,022	203,439	328,215	239,685	170,320	37,234	45,257	35,8	47
Ni	55,030	11,262	40,746	127,890	37,250	33,630	6,813	74,764	97,968	58,052	22,952	68,187	187,812	22,874	29,216	49,394	51,625	32,929	44,119	10,903	112,000	12,7	112
Cu	41,366	14,851	54,997	6,002	80,861	45,839	11,408	50,305	52,149	35,486	44,688	49,660	161,418	26,686	49,769	49,981	167,121	20,066	33,423	17,876	155,237	19,4	142
Zn	7,801	11,008	10,792	265,142	72,071	8,096	5,832	31,942	169,537	9,943	18,464	83,924	49,992	21,009	8,879	41,187	59,700	12,432	38,891	142,446	110,534	147	107
Ga	0,757	1,953	3,097	13,758	8,715	2,847	1,850	6,697	15,164	3,685	7,124	12,408	4,212	4,510	4,809	7,971	1,570	3,431	3,683	22,435	21,252	22,7	21
Rb	0,104	0,295	0,379	1,401	11,902	0,649	0,564	2,091	12,559	7,027	17,638	0,466	6,350	2,387	3,253	8,685	1,056	3,769	0,751	49,867	9,927	49	10,1
Sr	0,533	6,058	1,832	7,825	7,068	4,967	1,513	3,266	282,618	1,674	9,350	10,718	7,399	3,295	9,402	13,487	1,193	6,925	3,191	322,932	379,729	321	382
Y	0,935	1,647	1,308	11,639	6,723	1,490	1,627	6,799	34,632	1,956	2,858	12,127	3,221	3,405	4,499	10,382	1,693	3,262	3,207	31,312	22,773	31	23
Zr	12,469	21,934	18,722	79,854	89,750	19,501	20,487	107,831	89,524	25,497	73,127	345,078	31,420	57,702	20,202	154,403	17,747	32,977	59,911	183,738	169,465	194	160
Nb	0,781	0,993	0,642	4,642	3,944	0,680	0,432	3,559	5,772	1,743	1,867	6,575	2,146	1,559	0,643	2,802	1,472	1,099	1,842	11,868	17,798	12,8	16,4
Sn	0,780	1,621	1,835	5,027	6,433	1,532	1,460	2,736	3,167	1,849	3,165	7,204	1,935	3,000	1,452	3,872	1,796	1,921	2,524	3,473	1,935	2,1	2,7
Sb	0,054	0,265	0,413	0,545	0,637	0,373	0,313	0,437	0,693	0,456	1,070	0,361	0,412	2,379	0,469	0,448	1,211	0,255	0,274	0,504	0,208	0,62	0,16
Cs	0,024	0,037	0,050	0,906	1,675	0,082	0,090	0,205	2,674	0,551	0,826	0,067	0,443	0,191	0,308	0,805	0,232	0,197	0,346	1,215	0,106	1,17	0,11
Ba	1,486	11,271	8,735	37,737	34,312	60,376	17,322	29,512	668,988	22,257	60,922	34,299	54,210	8,656	46,401	49,357	6,993	43,322	13,485	668,212	123,664	641	128,7
La	3,551	4,057	3,688	13,920	7,704	5,347	5,076	6,619	120,347	8,573	16,596	25,802	18,207	7,104	24,307	31,242	3,612	14,471	7,886	25,758	14,874	24,5	15,6
Ce	6,184	7,162	6,607	19,653	17,541	9,267	9,930	10,111	90,221	14,873	24,604	47,481	19,380	14,380	22,203	56,549	5,849	20,625	14,269	51,062	36,597	50,5	37
Pr	0,627	0,713	0,708	2,961	1,971	0,922	1,005	1,335	19,825	1,587	2,712	5,038	2,734	1,558	6,902	6,827	0,620	3,534	1,604	6,336	4,971	6,3	5
Nd	2,252	2,678	2,621	11,156	7,621	3,310	3,720	5,235	71,493	5,713	9,333	18,322	9,257	5,807	26,819	25,265	2,286	13,343	6,030	27,628	23,468	27	24
Sm	0,409	0,516	0,502	2,427	1,358	0,603	0,693	1,306	12,652	0,952	1,545	3,636	1,397	1,055	4,931	4,752	0,444	2,441	1,282	6,276	5,822	6,3	5,8
Eu	0,074	0,119	0,085	0,563	0,360	0,108	0,130	0,342	2,977	0,171	0,317	0,730	0,273	0,222	0,986	1,222	0,092	0,512	0,311	1,925	1,984	1,91	2
Gd	0,304	0,539	0,386	2,484	1,082	0,470	0,512	1,499	12,837	0,663	1,117	2,883	1,137	0,763	3,782	4,037	0,448	1,886	1,131	6,475	5,923	6,5	5,9
Tb	0,040	0,080	0,055	0,402	0,184	0,060	0,069	0,266	1,727	0,088	0,142	0,401	0,151	0,112	0,443	0,576	0,065	0,241	0,153	0,959	0,852	0,95	0,86
Dy	0,262	0,501	0,356	2,708	1,385	0,378	0,455	1,805	9,728	0,564	0,824	2,552	0,921	0,782	2,153	3,272	0,467	1,269	0,935	5,984	4,914	6	4,9
Ho	0,050	0,096	0,072	0,541	0,319	0,074	0,090	0,364	1,685	0,112	0,153	0,542	0,177	0,165	0,330	0,591	0,090	0,207	0,174	1,203	0,908	1,2	0,91
Er	0,159	0,302	0,228	1,545	1,105	0,221	0,274	1,074	4,089	0,347	0,460	1,700	0,529	0,545	0,764	1,569	0,272	0,548	0,534	3,301	2,300	3,3	2,3
Tm	0,022	0,048	0,036	0,232	0,204	0,032	0,041	0,166	0,534	0,056	0,073	0,281	0,078	0,088	0,088	0,227	0,036	0,073	0,083	0,469	0,294	0,46	0,3
Yb	0,175	0,351	0,265	1,527	1,558	0,248	0,294	1,163	3,158	0,409	0,554	2,029	0,572	0,675	0,558	1,510	0,276	0,546	0,632	3,319	1,950	3,2	2,02
Lu	0,025	0,050	0,038	0,233	0,264	0,035	0,042	0,176	0,437	0,061	0,087	0,325	0,082	0,101	0,069	0,224	0,035	0,076	0,092	0,471	0,260	0,47	0,26
Hf	0,512	0,841	0,676	2,650	2,606	0,720	0,813	3,377	2,637	0,952	2,423	9,656	1,043	1,638	0,742	4,634	0,731	1,122	1,799	4,790	4,289	5	4,1
Ta	2,776	0,230	0,081	0,517	0,482	0,082	0,134	5,745	1,205	4,908	0,403	1,038	6,323	0,859	2,001	3,006	2,749	2,027	2,069	0,701	1,058	0,78	0,94
W	788,129	2,680	1,599	63,050	69,499	1,124	57,565	1730,760	168,119	1411,526	142,129	76,472	758,271	130,115	205,307	401,828	542,474	337,615	346,385	0,464	0,257	0,44	0,27
Tl	-0,001	0,002	0,001	0,003	0,062	0,002	0,005	0,025	0,076	0,028	0,150	0,010	0,014	0,014	0,018	0,061	0,008	0,011	0,006	0,300	0,014	0,3	0,058
Pb	4,197	4,037	9,219	2,127	32,649	2,956	3,557	5,473	32,031	5,737	30,206	5,990	6,164	125,852	18,125	27,378	9,753	8,702	4,148	9,532	1,635	10,9	1,4
Th	1,850	3,492	2,760	9,772	16,986	2,425	3,539	7,145	8,422	4,369	7,747	14,180	4,867	7,819	3,355	9,087	2,090	3,996	4,585	5,643	1,151	5,5	1,18
U	1,069	3,696	4,360	6,277	7,894	0,961	1,640	4,311	15,217	2,103	3,918	6,013	1,115	3,216	3,599	2,139	1,315	2,040	2,189	1,750	0,435	1,73	0,44

Table 5. AD-ICPMS raw data part 2

| Reading No | Time | Type | Duration | Units | Sequence | Flags | SAMPLE | LOCATION | INSPECTOR | MISC | NOTE | Al2O3 | Al2O3 Error | FeO | FeO Error | MgO | MgO Error | CO2 | CO2 Error | Mg | Mg Error | Al | Al Error | Ba | Ba Error | Si | Si Error | P | P Error | S | S Error | Cl | Cl Error | K | K Error | Ca | Ca Error | Ti | Ti Error | V | V Error | Cr | Cr Error | Mn | Mn Error | Fe | Fe Error | Co | Co Error | Ni | Ni Error | Cu | Cu Error | Zn | Zn Error | As | As Error | Se | Se Error | Rb | Rb Error | Sr | Sr Error | Zr | Zr Error | Nb | Nb Error | Mo | Mo Error | Pd | Pd Error | Ag | Ag Error | Cd | Cd Error | Sn | Sn Error | Sb | Sb Error | Ba | Ba Error | W | W Error | Au | Au Error | Pb | Pb Error | Bi | Bi Error |
|---|---|---

Table 6. GPS points

Waypoint	Latitude	Longitude	Waypoint	Latitude	Longitude	Waypoint	Latitude	Longitude	Waypoint	Latitude	Longitude	Waypoint	Latitude	Longitude
001	-25,95145	27,67831	101	-25,97140	27,68995	201	-25,97200	27,66686	301	-25,98079	27,66834	401	-25,97374	27,66599
002	-25,95158	27,67839	102	-25,97137	27,69001	202	-25,97187	27,66667	302	-25,98108	27,66821	402	-25,97395	27,66587
003	-25,95152	27,67844	103	-25,97129	27,69004	203	-25,97179	27,66635	303	-25,98135	27,66823	403	-25,97411	27,66579
004	-25,95136	27,67863	104	-25,97118	27,69015	204	-25,97174	27,66623	304	-25,98171	27,66822	404	-25,97415	27,66562
005	-25,95124	27,67866	105	-25,97126	27,69015	205	-25,97180	27,66611	305	-25,98206	27,66813	405	-25,97423	27,66557
006	-25,95114	27,67872	106	-25,97142	27,69015	206	-25,97156	27,66611	306	-25,98233	27,66835	406	-25,97432	27,66550
007	-25,95128	27,67873	107	-25,97149	27,69017	207	-25,97169	27,66647	307	-25,98268	27,66848	407	-25,97435	27,66535
008	-25,95141	27,67878	108	-25,97151	27,69027	208	-25,97169	27,66693	308	-25,98291	27,66853	408	-25,97410	27,66538
009	-25,95146	27,67871	109	-25,97155	27,69035	209	-25,97140	27,66736	309	-25,98309	27,66823	409	-25,97408	27,66545
010	-25,95167	27,67863	110	-25,97166	27,69038	210	-25,97130	27,66777	310	-25,98309	27,66811	410	-25,97407	27,66557
011	-25,95138	27,67835	111	-25,97173	27,69043	211	-25,97103	27,66813	311	-25,98282	27,66796	411	-25,97395	27,66571
012	-25,95142	27,67825	112	-25,97182	27,69038	212	-25,97065	27,66842	312	-25,98250	27,66779	412	-25,97382	27,66573
013	-25,95129	27,67828	113	-25,97191	27,69030	213	-25,97024	27,66863	313	-25,98231	27,66775	413	-25,97366	27,66575
014	-25,95112	27,67832	114	-25,97199	27,69015	214	-25,97006	27,66882	314	-25,98213	27,66781	414	-25,97358	27,66570
015	-25,95091	27,67840	115	-25,97201	27,69011	215	-25,96983	27,66862	315	-25,98182	27,66788	415	-25,97361	27,66582
016	-25,95076	27,67851	116	-25,95941	27,67669	216	-25,96913	27,66929	316	-25,98144	27,66794	416	-25,97368	27,66590
017	-25,95061	27,67855	117	-25,95962	27,67650	217	-25,96899	27,66940	317	-25,98111	27,66795	417	-25,97371	27,66595
018	-25,95054	27,67862	118	-25,95979	27,67633	218	-25,96902	27,66958	318	-25,98081	27,66792	418	-25,97587	27,66394
019	-25,95074	27,67882	119	-25,95988	27,67617	219	-25,96883	27,66972	319	-25,98058	27,66810	419	-25,97556	27,66363
020	-25,95098	27,67898	120	-25,96001	27,67599	220	-25,96865	27,66971	320	-25,98028	27,66811	420	-25,97556	27,66363
021	-25,95136	27,67896	121	-25,96021	27,67572	221	-25,96850	27,66947	321	-25,98005	27,66806	421	-25,97562	27,66325
022	-25,95155	27,67900	122	-25,96047	27,67531	222	-25,96816	27,66977	322	-25,98088	27,66807	422	-25,97573	27,66338
023	-25,95179	27,67893	123	-25,96063	27,67502	223	-25,96797	27,66995	323	-25,98079	27,66816	423	-25,97590	27,66315
024	-25,95194	27,67888	124	-25,96081	27,67473	224	-25,96772	27,67018	324	-25,98047	27,66814	424	-25,97595	27,66316
025	-25,95214	27,67876	125	-25,96102	27,67455	225	-25,96743	27,67057	325	-25,98038	27,66814	425	-25,97595	27,66316
026	-25,95231	27,67852	126	-25,96117	27,67446	226	-25,96724	27,67094	326	-25,98035	27,66815	426	-25,97596	27,66319
027	-25,95247	27,67833	127	-25,96143	27,67427	227	-25,96701	27,67115	327	-25,97583	27,66306	427	-25,97596	27,66319
028	-25,95252	27,67797	128	-25,96155	27,67420	228	-25,96651	27,67139	328	-25,97572	27,66322	428	-25,97596	27,66319
029	-25,95259	27,67781	129	-25,96171	27,67409	229	-25,96627	27,67154	329	-25,97564	27,66372	429	-25,97596	27,66319
030	-25,95276	27,67771	130	-25,96189	27,67395	230	-25,96606	27,67171	330	-25,97558	27,66358	430	-25,97596	27,66319
031	-25,95294	27,67766	131	-25,96207	27,67386	231	-25,96555	27,67192	331	-25,97553	27,66375	431	-25,97596	27,66319
032	-25,95327	27,67764	132	-25,96220	27,67389	232	-25,96533	27,67203	332	-25,97547	27,66389	432	-25,97596	27,66319
033	-25,95349	27,67764	133	-25,96247	27,67358	233	-25,96503	27,67227	333	-25,97561	27,66397	433	-25,97596	27,66319
034	-25,95374	27,67761	134	-25,96264	27,67358	234	-25,96470	27,67243	334	-25,97575	27,66383			
035	-25,95399	27,67785	135	-25,96280	27,67360	235	-25,96434	27,67254	335	-25,97580	27,66367			
036	-25,95440	27,67777	136	-25,96294	27,67359	236	-25,96401	27,67264	336	-25,97592	27,66350			
037	-25,95464	27,67778	137	-25,96309	27,67357	237	-25,96361	27,67272	337	-25,97608	27,66333			
038	-25,95483	27,67774	138	-25,96318	27,67364	238	-25,96305	27,67295	338	-25,97719	27,66442			
039	-25,95508	27,67774	139	-25,96331	27,67361	239	-25,96275	27,67296	339	-25,97706	27,66456			
040	-25,95536	27,67777	140	-25,96379	27,67344	240	-25,96244	27,67282	340	-25,97692	27,66464			
041	-25,95542	27,67774	141	-25,96401	27,67337	241	-25,96214	27,67296	341	-25,97683	27,66481			
042	-25,95538	27,67745	142	-25,96423	27,67330	242	-25,96177	27,67303	342	-25,97683	27,66503			
043	-25,95518	27,67747	143	-25,96454	27,67320	243	-25,96134	27,67329	343	-25,97703	27,66494			
044	-25,95490	27,67741	144	-25,96473	27,67315	244	-25,96110	27,67330	344	-25,97717	27,66472			
045	-25,95465	27,67743	145	-25,96519	27,67292	245	-25,96073	27,67315	345	-25,97722	27,66453			
046	-25,95433	27,67745	146	-25,96521	27,67289	246	-25,96028	27,67302	346	-25,97797	27,66796			
047	-25,95412	27,67744	147	-25,97928	27,66473	247	-25,95997	27,67301	347	-25,97797	27,66800			
048	-25,95380	27,67744	148	-25,97932	27,66481	248	-25,95970	27,67316	348	-25,97805	27,66804			
049	-25,95345	27,67751	149	-25,97941	27,66486	249	-25,95967	27,67323	349	-25,97813	27,66799			
050	-25,95311	27,67730	150	-25,97946	27,66484	250	-25,95951	27,67353	350	-25,97822	27,66807			
051	-25,95281	27,67709	151	-25,97951	27,66492	251	-25,95941	27,67395	351	-25,97831	27,66813			
052	-25,95236	27,67699	152	-25,97963	27,66491	252	-25,95944	27,67414	352	-25,97788	27,66799			
053	-25,95219	27,67724	153	-25,97959	27,66488	253	-25,95955	27,67451	353	-25,97793	27,66797			
054	-25,95206	27,67763	154	-25,97954	27,66487	254	-25,95959	27,67474	354	-25,97802	27,66795			
055	-25,95209	27,67787	155	-25,97948	27,66485	255	-25,95974	27,67517	355	-25,97812	27,66794			
056	-25,95191	27,67802	156	-25,97943	27,66485	256	-25,95982	27,67546	356	-25,97822	27,66794			
057	-25,95178	27,67817	157	-25,97936	27,66481	257	-25,95981	27,67562	357	-25,97832	27,66796			
058	-25,95164	27,67824	158	-25,97932	27,66474	258	-25,95979	27,67579	358	-25,97836	27,66814			
059	-25,95146	27,67829	159	-25,97925	27,66468	259	-25,95969	27,67624	359	-25,97826	27,66816			
060	-25,95145	27,67828	160	-25,97925	27,66477	260	-25,95958	27,67635	360	-25,97815	27,66817			
061	-25,97105	27,68920	161	-25,97927	27,66482	261	-25,95945	27,67648	361	-25,97805	27,66820			
062	-25,97105	27,68919	162	-25,97931	27,66490	262	-25,95934	27,67658	362	-25,97793	27,66816			
063	-25,97076	27,68954	163	-25,97940	27,66492	263	-25,95913	27,67685	363	-25,97785	27,66807			
064	-25,97091	27,68991	164	-25,97947	27,66491	264	-25,95896	27,67703	364	-25,97446	27,66623			
065	-25,97099	27,68980	165	-25,97952	27,66492	265	-25,95890	27,67709	365	-25,97450	27,66628			
066	-25,97104	27,68974	166	-25,97957	27,66493	266	-25,95870	27,67725	366	-25,97448	27,66626			
067	-25,97107	27,68965	167	-25,97964	27,66490	267	-25,95836	27,67736	367	-25,97462	27,66636			
068	-25,97116	27,68953	168	-25,96519	27,67285	268	-25,95810	27,67740	368	-25,97473	27,66634			
069	-25,97127	27,68926	169	-25,96546	27,67265	269	-25,95763	27,67734	369	-25,97488	27,66639			
070	-25,97140	27,68904	170	-25,96576	27,67243	270	-25,95732	27,67731	370	-25,97514	27,66646			
071	-25,97119	27,68914	171	-25,96605	27,67231	271	-25,95714	27,67725	371	-25,97434	27,66617			
072	-25,97105	27,68916	172	-25,96623	27,67222	272	-25,95675	27,67710	372	-25,97448	27,66609			
073	-25,97088	27,68935	173	-25,96645	27,67213	273	-25,95658	27,67711	373	-25,97471	27,66621			
074	-25,97071	27,68955	174	-25,96655	27,67199	274	-25,95595	27,67730	374	-25,97491	27,66624			
075	-25,97067	27,68969	175	-25,96691	27,67187	275	-25,95578	27,67741	375	-25,97509	27,66626			
076	-25,97076	27,68981	176	-25,96710	27,67172	276	-25,95549	27,67756	376	-25,97525	27,66627			
077	-25,97097	27,68994	177	-25,96725	27,67150	277	-25,95547	27,67778	377	-25,97537	27,66633			
078	-25,97105	27,68973	178	-25,96740	27,67143	278	-25,95574	27,67782	378	-25,97526	27,66650			
079	-25,97122	27,68958	179	-25,96767	27,67122	279	-25,95614	27,67771	379	-25,97508	27,66656			
080	-25,97140	27,68957	180	-25,96780	27,67109	280	-25,95645	27,67762	380	-25,97487	27,66654			
081	-25,97143	27,68943	181	-25,96799	27,67076	281	-25,95695	27,67764	381	-25,97469	27,66646			
082	-25,97140	27,68905	182	-25,96829	27,67033	282	-25,95716	27,67761	382	-25,97452	27,66636			
083	-25,97069	27,68961	183	-25,96841	27,67019	283	-25,95739	27,67770	383	-25,97437	27,66622			
084	-25,97120	27,69011	184	-25,96885	27,66994	284	-25,95771	27,67774	384	-25,97388	27,66649			
085	-25,97124	27,69012	185	-25,96899	27,67000	285	-25,95803	27,67774	385	-25,97397	27,66635			
086	-25,97135	27,69011	186	-25,96917	27,66988	286	-25,95837	27,67767	386	-25,97395	27,66629			
087	-25,97146	27,69008	187	-25,96928	27,66962	287	-25,95862	27,67754	387	-25,97398	27,66618			
088	-25,97154	27,69012	188	-25,96952	27,66945	288	-25,95889	27,67737	388	-25,97384	27,66630			
089	-25,97160	27,69024	189	-25,96964	27,66936	289	-25,95911	27,67718	389	-25,97392	27,66610			
090	-25,97171	27,69029	190	-25,96990	27,66921	290	-25,95918	27,67709	390	-25,97406	27,66609			
091	-25,97199	27,69014	191	-25,97025	27,66898	291	-25,95933	27,67692	391	-25,97413	27,66619			
092	-25,97194	27,69019	192	-25,97042	27,66882	292	-25,95944	27,67671	392	-25,97414	27,66636			
093	-25,97192	27,69026	193	-25,97077	27,66863	293	-25,95987	27,67627	393	-25,97409	27,66652			
094	-25,97185	27,69029	194	-25,97084	27,66853	294	-25,95993	27,67611	394	-25,97369	27,66583			
095	-25,97179	27,69032	195	-25,97106	27,66839	295	-25,95978	27,67619	395	-25,97371	27,66583			
096	-25,97165	27,69026	196	-25,97126	27,66828	296	-25,95977	27,67612	396	-25,97385	27,66578			
097	-25,97159	27,69020	197	-25,97146	27,66821	297	-25,98001	27,66804	397	-25,97389	27,66579			
098	-25,97156	27,69007	198	-25,97180	27,66796	298	-25,98009	27,66815	398	-25,97398	27,66574			
099	-25,97154	27,68991	199	-25,97203	27,66732	299	-25,98025	27,66826	399	-25,97405	27,66558			
100	-25,97144	27,68988	200	-25,97207	27,66711	300	-25,98058	27,66837	400	-25,97421	27,66543			

Table 7. Macroscopic lithological traits of geological samples and artefacts

SAMPLE#	GRAIN VIS	COLOUR	TEXTURE	BANDING	SAMPLE#	GRAIN VIS	COLOUR	TEXTURE	BANDING
MIO2-8	y	10R7/6	medium fine	yes	MP-818p	no	Grey 1 5GY 4/	f	n
MIO2-9	y	10R8/2	coarse med	no	MP-1067p	no	Gey 2 5B 5/1	f	n
MIO1-2	y	5B4/1	coarse med	yes	MP-902p	yes	2.5YR 5/8	m	n
MIO1-9	y	5B5/1 = 5G6/1	medium fine	y C	MP-499p	yes	5YR6/1	M-f	n
MIO1-4	n	5G6/1 + N4	fine	y C	MP-128p	yes	2.5YR4/6	m	n
MIO1-5	n	7.5R 4/8 + 5G 7/1	fine	y C	MP-1089p	yes	Grey1 10Y6/1	m	n
MIO1-6	n	5B4/1	fine	no	MP-823p	yes	10R5/4 + 10R	M-c	Y
MIO2-2	y	10R7/4	Med-coarse	no	MP-348p	yes	Grey 2 10B4/	F-m	n
MIO1-3	y	10R5/4	medium fine	y C	MP-1084p	yes	7.5YR6/6	M-c	n
MIO2-3	y	7.5R7/4	Med-coarse	y C	MP-222p	no	5YR7/6	F-m	n
MIO2-6	y	10R7/4	Med-coarse	y C	MP-903p	yes	10R8/2	M-f	n
MIO2-1	y	10R5/6	Med-coarse	y C	MP-191p	yes	10R8/3	M-c	n
MIO2-5	y	10R7/6	Med-coarse	y C	MP-501p	yes	10R7/2	M-c	n
MIO2-4	y	10R6/6 + 10R5/6 + 10R7/8	medium fine	y C	MP-349p	yes	10R8/3	m	n
MIO2-10	y	10R5/6	med	y C	MP-U2p	yes	10R3/4 + 10R	M-c	y
MIO2-7	y	10R6/6	med	yes	MP-1080p	yes	10R4/1	m	y
MIO1-8	n	5B4/1	fine	y C	MP-U5p	yes	5YR7/6	M-f	y
MIO1-1	y	5B4/1 + 10R6/6	fine	no	MP-497p	yes	5YR7/6	F-m	n
MIO1-7	n	5B4/1 + 7.5R8/2	Fine-med	yes	MP-901p	yes	7.5YR8/6	M-c	n
MIO5-11	n	Grey 1 7/1+ 10R7/4	fine	y C	MP-334p	yes	Grey 2 5B4/1	m	n
MIO5-10	y	10R5/6	fine	y C	MP-U3p	yes	Grey 2 5B4/1	M-c	n
MIO5-7	y	Grey 2 3/1	Fine-med	yes	MP-U4p	no	10R6/4	f	n
MIO5-5	n	Grey 2 3/1	Fine-med	no	MP-U1p	yes	Grey 2 5B5/1	M-c	n
MIO5-15	n	Grey 2 3/1	fine	no	MP-504p	no	Grey2 10BG6/	f	n
MIO5-9	y	10R86/8	med	no	MP-250p	no	10R7/3	f	n
MIO5-8	y	10R4/6	med	no	MP-810p	no	10R7/3	f	n
MIO5-14	y	10R6/3	Fine-med	no	MP-4	yes	Grey 2 5B3/1	M-f	n
MIO5-12	y	10R7/3	med	no	MP-236	no	7.5YR7/6	f	n
MIO5-1	y	10R5/2	Fine-med	no	MP-228m	yes	7.5YR7/6	M-f	y
MIO5-3	y	10R5/8	med	no	MP-51	no	5YR6/4	f	n
MIO5-2	y	10R7/2	med	yes	MP-AGT1m	no	5YR6/4	f	n
MIO5-4	y	Grey 2 4/1	med	no	MP-415	yes	7.5YR7/6	M-c	y
MIO4-3	y	Grey 2 4/1 + Grey 1 5/1 + 10R	Coarse/fine-me	y C	MP-205	yes	5YR5/4	F-m	n
MIO5-6	y	10R6/3	Med-coarse	no	MP-328	yes	Grey 2 5B4/1	F-m	n
MIO3-5	y	10R6/3 + Grey 2 6/1	Med-fine	no	MP-22	yes	5YR4/4	c	n
MIO4-7	y	10R5/1	Med-coarse	no	MP-179	yes	2.5YR4/6	M-c	n
MIO4-6	y	Grey 2 4/1 +10R6/6	coarse	y C	MP-311	no	2.5YR5/6	f	n
MIO5-13	y	10R6/8	med	no	MP-191	yes	2.5YR6/6	m	n
MIO4-1	y	Grey 2 4/1	coarse	no	MP-273	yes	7.5YR7/6	M-c	n
MIO4-5	y	Grey 1 7/1+ 10R5/3	Coarse-med	no	MP-264	yes	7.5YR7/4	F-m	y
MIO4-2	y	Grey 2 5-1 + 10 R5/2	Fine-med	no	MP-272	yes	5YR3/1	m	n
MIO4-4	y	10R6/1 + 10R6/2	med	no	MP-147	yes	10R5/6	m	n
MIO3-2	y	10R6/4 + Grey 2 6/1	med	no	MP-21	yes	2.5YR7/8	c	n
MIO3-4	y	Grey 2 4/1	Med-coarse	no	MP-206	no	2.5YR 2.5/1	f	n
MIO3-3	y	Grey 2 6/1	Med-coarse	no	MP-114	no	10R 2.5/1	f	n
MIO3-1	y	10R6/4	med	no	MP-52	yes	7.5YR3/2	M-f	n
MIO3-6	y	10R4/8	med	no	MP-128	yes	Grey 2 10B2.5	M-c	n
GO1-2	y	7.5R7/6 + N2.5	Med-fine	yes	MP-44	yes	2.5YR6/6	m	n
G02-1	n	10R4/2 + 10R4/2	fine	no	MP-83	yes	2.5YR6/6	F-m	n
G01-5	y	10R6/6 + N2.5	Med-coarse	yes	MP-274	yes	2.5YR7/6	m	n
GO1-7	n	10R4/6 + N2.5	fine	no	MP-173	yes	Grey 2 10B4/	m	n
G02-5	n	10R6/4 + 10YR6/4	fine	no	MP-238	yes	2.5YR5/4 + 2.	M-c	n
GO2-6	y	10R7/4 + N8	med	no	MP-105	yes	2.5YR4/4	m	n
GO1-1	y	10R6/6 N2.5	med	yes	MP-106	yes	2.5YR4/4	m	n
GO1-4	n	10R5/6	med	yes	MP-57	yes	5YR 7/6	M-c	n
GO2-3	y	7.5R8/2	course	no	MP-131	yes	Grey 2 10B4/	C-m	n
GO2-2	n	10R6/2 + N8	fine	no	MP-67	yes	7.5YR7/6	C-m	n
GO1-9	n	N2.5	fine	no	MP-242	yes	5YR3/4	m	n
GO1-10	y	5YR6/6 + N2.5	med-coarse	no	MP-162	yes	5YR3/2	M-f	y
GO2-7	y	7.5R7/4 + N8	med-coarse	no	MP-245	yes	10YR7/6	c	n
GO1-3	y	N2.5	fine-med	no	MP-59	yes	5YR4/2	m	n
G01-8	y	N2.5	fine-med	yes	MP-190	yes	5YR4/3	m	n
GO1-6	y	7.5R6/6 + 5G7/2	med-coarse	yes	MP-48	yes	5YR3/3 + 5YR	M-c	n
VMO1-11	y	N2.5 + 7.5R6/6	med-coarse	yes	MP-231	yes	10R5/6	m	n
VMO1-6	n	7.5R4/8	fine	no	MP-131	yes	2.5YR3/4	M-f	n
VMO1-4	y	7.5R5/8 + N2.5	fine-med	no	MP-190	yes	5YR7/6 + Gre	m	n
VMO1-7	n	7.5R6/8	fine	no	MP-276	yes	2.5YR5/6	M-c	n
VMO1-2	y	10R6/4	Coarse-med	no	MP-8A	yes	2.5YR3/4	M-c	n
VMO1-9	n	7.5R6/6 + N2.5	fine	no	MP-251	yes	5YR 4/3	M-c	n
VMO1-3	y	2.5YR7/6 + 7.5YR8/4	med	no	MP-128	yes	2.5YR 4/3	M-f	n
VMO1-1	y	7.5YR + 5B4/1 + N8	med	no	MP-239	yes	Grey 2 10BG	C-m	n
VMO1-10	y	7.5R7/4 + 7.5R5/8	coarse	no	MP-142	no	5YR3/2	f	n
VMO1-5	y	7.5R5/6	med-coarse	yes	MP-172	yes	5YR5/4	M-f	n
VMO1-8	y	7.5R7/4	coarse	no	MP-166	yes	5YR7/6	m	n
QM01-1	y	7.5R7/4	Med-fine	no	MP-87	yes	5YR5/4	M-f	n
QM01-2	y	7.5R6/4	coarse	no	MP-236	yes	5YR5/4	M-f	n
QM01-3	n	5B8/1	fine	no	MP-277	yes	5YR6/4	C-m	n
QM01-6	y	10R3/6	med	no	MP-32	no	Grey2 5B5/1	f	n
QM01-7	n	N6	fine	no	MP-57	yes	5YR6/4	M-f	n
QM01-8	y	5B5/1	med-fine	yes	MP-218	no	7.5YR8/6 + 5Y	f	n
QM01-10	y	7.5R5/4	coarse	no	MP-141	yes	5YR 7/6	f	n
QM01-11	n	7.5R6/4	fine	no			141	yes	5YR 7/6
QM01-12	y	10R4/2	coarse	no					
QM01-13	y	7.5R6/4	med	no					
QM01-14	y	7.5R5/6	coarse	no					
QM01-15	y	7.5R6/6	med	no					
QM01-16	n	7.5R5/8	fine	no					
FFIO1-1	y	7.5R7/4	med	no					
FFIO1-2	y	7.5R7/4	med-course	no					
FFIO1-3	y	7.5R8/2	med-course	no					
FFIO1-4	y	7.5R7/4	med-course	no					
FFIO1-5	y	5YR8/2	course	no					
G02-4	n	7.5R2.5/4	fine	no					
FFIO2-1	y	7.5R5/4	med	no					
FFIO2-2	y	7.5R6/4	course	no					
FFIO2-3	y	7.5R4/6	med-course	no					
FFIO2-4	y	7.5R6/6	med-fine	no					
FFIO2-5	y	7.5R6/6	course	no					
MGQ01-1	n	5B4/1	fine	n					
MGQ01-2	n	5B4/1	fine	n					
MGQ01-3	y	5GY8/8	medium	y					
MGQ01-4	n	5B4/1	fine	n					
MGQ01-5	y	5B4/1	medium	n					

Table 8. Pearson correlations for AD-ICPMS data

Pearson Correlation Matrix

	FFIO	FFIO	VMO	VMO	VMO	GO1	GO2	GO2	GO3	QM	QM	QM	MOG	MOG	MGQ	MGQ	MIO1	MIO1	MIO2	MIO2	MIO3	MIO3	MIO4	MIO4	MIO5	MIO5
FFIO	1,000	0,521	0,769	0,521	0,906	0,927	0,851	0,769	0,863	0,952	0,898	0,870	0,875	0,924	0,921	0,955	0,893	0,800	0,860	0,668	0,525	0,733	0,853	0,907	0,461	0,821
FFIO	0,521	1,000	0,827	0,419	0,347	0,468	0,200	0,554	0,390	0,349	0,364	0,526	0,726	0,414	0,406	0,384	0,186	0,416	0,178	0,334	0,786	0,381	0,130	0,202	0,358	0,191
VMO	0,769	0,827	1,000	0,530	0,591	0,742	0,519	0,559	0,661	0,620	0,662	0,698	0,835	0,708	0,613	0,594	0,547	0,679	0,547	0,522	0,868	0,606	0,509	0,572	0,463	0,499
VMO	0,521	0,419	0,530	1,000	0,140	0,206	0,166	0,151	0,169	0,317	0,783	0,829	0,284	0,192	0,525	0,455	0,205	0,907	0,125	0,651	0,433	0,947	0,141	0,268	0,985	0,149
VMO	0,906	0,347	0,591	0,140	1,000	0,961	0,916	0,839	0,929	0,974	0,691	0,632	0,871	0,974	0,860	0,892	0,941	0,504	0,934	0,508	0,372	0,413	0,924	0,931	0,088	0,912
GO1	0,927	0,468	0,742	0,206	0,961	1,000	0,867	0,767	0,936	0,947	0,714	0,633	0,905	0,993	0,817	0,880	0,941	0,569	0,945	0,476	0,489	0,466	0,926	0,936	0,138	0,873
GO2	0,851	0,200	0,519	0,166	0,916	0,867	1,000	0,753	0,819	0,887	0,680	0,634	0,732	0,911	0,805	0,834	0,908	0,519	0,897	0,529	0,329	0,437	0,894	0,911	0,118	0,831
GO2	0,769	0,554	0,559	0,151	0,839	0,767	0,753	1,000	0,723	0,782	0,514	0,615	0,891	0,781	0,823	0,736	0,642	0,373	0,618	0,471	0,455	0,316	0,594	0,650	0,105	0,646
GO3	0,863	0,390	0,661	0,169	0,929	0,936	0,819	0,723	1,000	0,936	0,697	0,586	0,842	0,938	0,763	0,814	0,885	0,519	0,907	0,628	0,545	0,418	0,888	0,881	0,160	0,959
QM	0,952	0,349	0,620	0,317	0,974	0,947	0,887	0,782	0,936	1,000	0,821	0,739	0,848	0,956	0,907	0,942	0,950	0,655	0,930	0,630	0,399	0,576	0,927	0,950	0,277	0,934
QM	0,898	0,364	0,662	0,783	0,691	0,714	0,680	0,514	0,697	0,821	1,000	0,936	0,644	0,718	0,864	0,860	0,754	0,962	0,699	0,789	0,457	0,934	0,713	0,793	0,755	0,705
QM	0,870	0,526	0,698	0,829	0,632	0,633	0,634	0,615	0,586	0,739	0,936	1,000	0,683	0,639	0,857	0,797	0,612	0,927	0,540	0,775	0,537	0,918	0,546	0,650	0,790	0,566
MOG	0,875	0,726	0,835	0,284	0,871	0,905	0,732	0,891	0,842	0,848	0,644	0,683	1,000	0,893	0,827	0,782	0,739	0,538	0,731	0,495	0,662	0,454	0,698	0,745	0,216	0,717
MOG	0,924	0,414	0,708	0,192	0,974	0,993	0,911	0,781	0,938	0,956	0,718	0,639	0,893	1,000	0,839	0,879	0,955	0,564	0,957	0,497	0,467	0,461	0,941	0,952	0,128	0,886
MGQ	0,921	0,406	0,613	0,525	0,860	0,817	0,805	0,823	0,763	0,907	0,864	0,857	0,827	0,839	1,000	0,901	0,816	0,764	0,760	0,648	0,388	0,720	0,764	0,847	0,474	0,735
MGQ	0,955	0,384	0,594	0,455	0,892	0,880	0,834	0,736	0,814	0,942	0,860	0,797	0,782	0,879	0,901	1,000	0,903	0,742	0,861	0,602	0,316	0,686	0,866	0,912	0,394	0,809
MIO1	0,893	0,186	0,547	0,205	0,941	0,941	0,908	0,642	0,885	0,950	0,754	0,612	0,739	0,955	0,816	0,903	1,000	0,594	0,992	0,466	0,251	0,502	0,995	0,995	0,145	0,893
MIO1	0,800	0,416	0,679	0,907	0,504	0,569	0,519	0,373	0,519	0,655	0,962	0,927	0,538	0,564	0,764	0,742	0,594	1,000	0,530	0,731	0,478	0,991	0,544	0,646	0,871	0,500
MIO2	0,860	0,178	0,547	0,125	0,934	0,945	0,897	0,618	0,907	0,930	0,699	0,540	0,731	0,957	0,760	0,861	0,992	0,530	1,000	0,441	0,277	0,428	0,998	0,983	0,073	0,906
MIO2	0,668	0,334	0,522	0,651	0,508	0,476	0,529	0,471	0,628	0,630	0,789	0,775	0,495	0,497	0,648	0,602	0,466	0,731	0,441	1,000	0,642	0,720	0,440	0,508	0,711	0,648
MIO3	0,525	0,786	0,868	0,433	0,372	0,489	0,329	0,455	0,545	0,399	0,457	0,537	0,662	0,467	0,388	0,316	0,251	0,478	0,277	0,642	1,000	0,423	0,228	0,283	0,439	0,387
MIO3	0,733	0,381	0,606	0,947	0,413	0,466	0,437	0,316	0,418	0,576	0,934	0,918	0,454	0,461	0,720	0,686	0,502	0,991	0,428	0,720	0,423	1,000	0,447	0,558	0,917	0,411
MIO4	0,853	0,130	0,509	0,141	0,924	0,926	0,894	0,594	0,888	0,927	0,713	0,546	0,698	0,941	0,764	0,866	0,995	0,544	0,998	0,440	0,228	0,447	1,000	0,987	0,090	0,902
MIO4	0,907	0,202	0,572	0,268	0,931	0,936	0,911	0,650	0,881	0,950	0,793	0,650	0,745	0,952	0,847	0,912	0,995	0,646	0,983	0,508	0,283	0,558	0,987	1,000	0,211	0,882
MIO5	0,461	0,358	0,463	0,985	0,088	0,138	0,118	0,105	0,160	0,277	0,755	0,790	0,216	0,128	0,474	0,394	0,145	0,871	0,073	0,711	0,439	0,917	0,090	0,211	1,000	0,155
MIO5	0,821	0,191	0,499	0,149	0,912	0,873	0,831	0,646	0,959	0,934	0,705	0,566	0,717	0,886	0,735	0,809	0,893	0,500	0,906	0,648	0,387	0,411	0,902	0,882	0,155	1,000

Table 9. Pearson correlations for P-XRF data

Pearson Correlation Matrix																									
	FFIO	FFIO	VMO	VMO	VMO	GO1	GO2	GO2	GO3	QM	QM	QM	MOG	MOG	MGQ	MGQ	MIO1	MIO1	MIO2	MIO2	MIO3	MIO3	MIO4	MIO4	MIO5	MIO5
FFIO	1,000	0,999	0,973	0,994	0,998	0,993	0,996	0,956	0,976	0,995	0,994	0,998	0,987	0,990	0,998	0,994	0,985	0,983	0,999	0,999	0,997	0,991	0,951	0,826	0,996	0,999
FFIO	0,999	1,000	0,976	0,994	1,000	0,994	0,998	0,960	0,978	0,997	0,997	0,999	0,987	0,992	0,999	0,996	0,987	0,985	1,000	1,000	0,999	0,994	0,956	0,833	0,998	1,000
VMO	0,973	0,976	1,000	0,992	0,979	0,993	0,987	0,998	1,000	0,990	0,990	0,984	0,996	0,996	0,983	0,992	0,998	0,999	0,974	0,974	0,980	0,992	0,997	0,933	0,988	0,979
VMO	0,994	0,994	0,992	1,000	0,994	1,000	0,997	0,982	0,993	0,998	0,998	0,996	0,999	0,998	0,996	0,999	0,998	0,997	0,992	0,992	0,994	0,997	0,978	0,884	0,997	0,995
VMO	0,998	1,000	0,979	0,994	1,000	0,994	0,999	0,964	0,981	0,998	0,998	1,000	0,987	0,994	1,000	0,997	0,989	0,987	1,000	1,000	1,000	0,996	0,961	0,840	0,999	0,999
GO1	0,993	0,994	0,993	1,000	0,994	1,000	0,997	0,983	0,994	0,999	0,998	0,997	0,999	0,999	0,997	0,999	0,998	0,997	0,992	0,992	0,994	0,998	0,980	0,887	0,998	0,995
GO2	0,996	0,998	0,987	0,997	0,999	0,997	1,000	0,975	0,989	1,000	1,000	1,000	0,992	0,998	0,999	0,999	0,995	0,994	0,997	0,997	0,999	0,999	0,973	0,864	1,000	0,998
GO2	0,956	0,960	0,998	0,982	0,964	0,983	0,975	1,000	0,997	0,978	0,979	0,970	0,988	0,987	0,968	0,982	0,992	0,993	0,957	0,957	0,966	0,983	1,000	0,954	0,975	0,963
GO3	0,976	0,978	1,000	0,993	0,981	0,994	0,989	0,997	1,000	0,991	0,991	0,985	0,996	0,996	0,985	0,993	0,999	0,999	0,976	0,976	0,982	0,993	0,995	0,928	0,989	0,981
QM	0,995	0,997	0,990	0,998	0,998	0,999	1,000	0,978	0,991	1,000	1,000	0,999	0,995	0,999	0,999	1,000	0,997	0,996	0,996	0,996	0,998	0,999	0,976	0,873	1,000	0,998
QM	0,994	0,997	0,990	0,998	0,998	0,998	1,000	0,979	0,991	1,000	1,000	0,999	0,994	0,999	0,999	1,000	0,997	0,996	0,996	0,996	0,998	1,000	0,977	0,874	1,000	0,997
QM	0,998	0,999	0,984	0,996	1,000	0,997	1,000	0,970	0,985	0,999	0,999	1,000	0,991	0,996	1,000	0,998	0,993	0,991	0,999	0,999	1,000	0,998	0,967	0,853	1,000	0,999
MOG	0,987	0,987	0,996	0,999	0,987	0,999	0,992	0,988	0,996	0,995	0,994	0,991	1,000	0,997	0,991	0,996	0,998	0,998	0,985	0,985	0,987	0,994	0,985	0,905	0,993	0,989
MOG	0,990	0,992	0,996	0,998	0,994	0,999	0,998	0,987	0,996	0,999	0,999	0,996	0,997	1,000	0,996	0,999	0,999	0,999	0,991	0,991	0,994	0,999	0,985	0,895	0,998	0,993
MGQ	0,998	0,999	0,983	0,996	1,000	0,997	0,999	0,968	0,985	0,999	0,999	1,000	0,991	0,996	1,000	0,998	0,992	0,990	0,999	0,999	0,999	0,997	0,965	0,850	0,999	1,000
MGQ	0,994	0,996	0,992	0,999	0,997	0,999	0,999	0,982	0,993	1,000	1,000	0,998	0,996	0,999	0,998	1,000	0,998	0,997	0,995	0,995	0,997	1,000	0,979	0,881	0,999	0,996
MIO1	0,985	0,987	0,998	0,998	0,989	0,998	0,995	0,992	0,999	0,997	0,997	0,993	0,998	0,999	0,992	0,998	1,000	1,000	0,986	0,986	0,990	0,997	0,990	0,910	0,995	0,989
MIO1	0,983	0,985	0,999	0,997	0,987	0,997	0,994	0,993	0,999	0,996	0,996	0,991	0,998	0,999	0,990	0,997	1,000	1,000	0,983	0,983	0,988	0,997	0,992	0,915	0,994	0,987
MIO2	0,999	1,000	0,974	0,992	1,000	0,992	0,997	0,957	0,976	0,996	0,996	0,999	0,985	0,991	0,999	0,995	0,986	0,983	1,000	1,000	0,999	0,994	0,953	0,827	0,997	1,000
MIO2	0,999	1,000	0,974	0,992	1,000	0,992	0,997	0,957	0,976	0,996	0,996	0,999	0,985	0,991	0,999	0,995	0,986	0,983	1,000	1,000	0,999	0,993	0,953	0,827	0,997	1,000
MIO3	0,997	0,999	0,980	0,994	1,000	0,994	0,999	0,966	0,982	0,998	0,998	1,000	0,987	0,994	0,999	0,997	0,990	0,988	0,999	0,999	1,000	0,997	0,963	0,844	0,999	0,999
MIO3	0,991	0,994	0,992	0,997	0,996	0,998	0,999	0,983	0,993	0,999	1,000	0,998	0,994	0,999	0,997	1,000	0,997	0,997	0,994	0,993	0,997	1,000	0,981	0,883	0,999	0,995
MIO4	0,951	0,956	0,997	0,978	0,961	0,980	0,973	1,000	0,995	0,976	0,977	0,967	0,985	0,985	0,965	0,979	0,990	0,992	0,953	0,953	0,963	0,981	1,000	0,957	0,973	0,959
MIO4	0,826	0,833	0,933	0,884	0,840	0,887	0,864	0,954	0,928	0,873	0,874	0,853	0,905	0,895	0,850	0,881	0,910	0,915	0,827	0,827	0,844	0,883	0,957	1,000	0,865	0,839
MIO5	0,996	0,998	0,988	0,997	0,999	0,998	1,000	0,975	0,989	1,000	1,000	1,000	0,993	0,998	0,999	0,999	0,995	0,994	0,997	0,997	0,999	0,999	0,973	0,865	1,000	0,998
MIO5	0,999	1,000	0,979	0,995	0,999	0,995	0,998	0,963	0,981	0,998	0,997	0,999	0,989	0,993	1,000	0,996	0,989	0,987	1,000	1,000	0,999	0,995	0,959	0,839	0,998	1,000

Table 10. PCA scores for AD-ICPMS samples

Sample	Outcrop	PC 1	PC 2	PC 3	PC 4	PC 5
MIO1-3	MIO1	62,315	-35,631	22,629	2,4332	48,132
MIO1-7	MIO1	-161,92	105,09	166,34	-55,664	143
MIO2-3	MIO2	-125,46	34,957	61,395	-64,897	21,44
MIO2-6	MIO2	-11,42	294,59	-105,05	9,8591	10,507
MIO3-4	MIO3	-200,18	-53,55	-53,672	-0,0469	-8,8638
MIO3-5	MIO3	-138,46	-71,491	-19,406	-29,689	3,6133
MIO4-2	MIO4	312,64	-298,57	113,38	187,58	26,522
MIO4-4	MIO4	-99,466	-77,945	71,57	98,206	96,814
MIO5-5	MIO5	-151,64	-65,345	-12,337	-17,199	-37,222
MIO5-6	MIO5	-186,71	-41,981	-59,735	-2,3855	-14,643
MGQ1-2	MGQ	54,146	64,176	-63,177	7,3918	-20,752
MGQ1-3	MGQ	-76,928	64,078	-40,191	42,462	21,781
QM3	QM	-226,9	-24,21	-43,473	-8,9352	0,54728
QM7	QM	-163,85	-64,268	-34,663	-15,42	-5,6311
QM14	QM	-212,58	-18,283	-72,859	5,6559	-5,5956
MOG1-3	MOG	-45,335	-53,546	-58,498	5,6677	34,855
MOG1-5	MOG	42,391	-167,51	-46,896	-36,032	-7,8437
GO1-2	GO1	536,99	380,74	-74,595	-33,847	23,882
GO1-9	GO1	211,43	-291,43	8,7536	-80,432	-32,603
GO2-2	GO2	-41,078	90,659	34,899	104,36	-121
GO2-4	GO2	22,333	226,66	514,35	-36,77	-69,319
VMO1-3	VMO	237,08	297,98	-120,51	5,3289	15,059
VMO1-6	VMO	162,21	-258,65	-35,05	-65,598	-37,057
VMO1-11	VMO	401,34	-286,18	-5,9891	-53,622	2,9203
FFIO1-2	FFIO	-26,373	310,44	-101,29	32,113	-41,612
FFIO1-5	FFIO	-174,58	-60,769	-45,926	-0,51257	-46,922
8A	8A	-432,02	139,07	-15,63	-6,9176	-2,8296
21	21	4356,9	-62,929	3,0353	10,956	4,861
44	44	-385,87	-127,74	-23,237	-60,398	20,413
179	179	-311,88	63,263	-32,635	-37	-5,0513
206	206	-396,56	21,23	275,29	-6,6549	-11,851
242	242	-330,85	77,095	-91,16	63,132	-66,997
245	245	-288,91	136,06	-71,366	-41,794	91,913
349P	349P	-260,34	-117,13	-34,658	-57,738	4,4132
504P	504P	-258,43	2,5106	76,973	-33,31	-4,4777
1080P	1080P	-532,66	-133,84	-45,036	47,785	-48,7
U1	U1	-553,16	-28,349	21,347	167,8	65,395
U2	U2	-581,48	-123,87	-22,281	-25,415	3,4784
U4	U4	-386,96	-177,62	-26,324	-10,504	-18,894
U5	U5	362,25	332,24	-14,315	-9,9405	-31,674

Table 11. PCA scores for p-XRF samples

Samples	Outcrops	PC 1	PC 2	PC 3	PC 4	PC 5
FFIO1-2	FFIO	-9,0053	-4,8888	0,027734	-0,04594	-0,0206
FFIO1-5	FFIO	-9,8198	-0,32406	0,021007	0,071904	-0,0615
VMO1-11	VMO	8,9259	0,33966	0,39649	0,054712	0,053398
VMO1-3	VMO	1,0499	-5,4884	0,13	-0,0655	-0,09547
VMO1-6	VMO	-9,2415	1,9104	-0,11605	0,065148	-0,12544
GO1-2	GO1	1,1261	-4,2737	-0,11545	-0,30271	-0,39994
GO1-9	GO2	-5,2067	2,4714	0,12637	0,093535	0,037106
GO2-2	GO2	14,226	0,74856	-1,547	0,15264	0,21654
GO2-4	GO3	8,6704	-1,5396	-1,9389	0,040728	0,034861
QM3	QM	-3,089	0,41111	0,29794	0,16963	0,19907
QM7	QM	-3,0865	1,7573	0,025365	-0,84926	0,42158
QM14	QM	-6,9018	1,322	0,083832	0,10903	0,051106
MOG1-3	MOG	4,9974	-6,1975	0,57716	0,19535	0,26247
MOG1-5	MOG	0,97955	1,006	0,44156	0,11952	0,19812
MGQ1-2	MGQ	-6,6589	-0,53693	-0,03156	-0,02371	-0,10774
MGQ1-3	MGQ	-1,5391	0,46418	0,12422	-0,02555	-0,0971
MIO1-3	MIO1	4,2981	-0,64991	0,1556	-0,0201	-0,10486
MIO1-7	MIO1	5,2268	-0,1288	0,23411	0,020321	-0,02867
MIO2-3	MIO2	-11,247	0,68851	0,04863	0,088522	0,072302
MIO2-6	MIO2	-10,787	-0,32339	-0,21036	-0,10249	-0,19393
MIO3-4	MIO3	-9,2678	3,709	-0,03512	0,085582	-0,00018
MIO3-5	MIO3	-2,1602	4,1089	0,081438	0,029975	-0,07957
MIO4-2	MIO4	14,573	3,779	0,066883	-0,09453	-0,36551
MIO4-4	MIO4	37,299	0,83287	0,83376	-0,00092	0,010742
MIO5-5	MIO5	-5,0522	2,4576	0,12212	0,070098	-0,02155
MIO5-6	MIO5	-8,3088	-1,6555	0,20025	0,16402	0,14476
8a	8a	-1,8552	1,6408	-0,13188	-0,0468	-0,00384
21	21	11,016	-0,78602	-1,0928	0,44318	0,18628
44	44	-4,8069	-2,3778	0,29537	-0,07936	0,061594
179	179	5,2571	-0,76578	0,09173	0,35259	-0,42482
206	206	5,229	0,7175	0,11582	-0,11489	0,047221
242	242	-6,0991	-0,33991	-1,0279	-0,53143	-0,13927
245	245	17,495	-1,3916	0,55624	-0,34571	0,031575
349p	349p	-7,2005	-0,22248	0,52036	0,20457	0,053455
504p	504p	-3,7839	0,059993	0,19606	0,040338	0,058975
1080p	1080p	-10,638	-1,0831	0,081165	0,045475	0,062881
u1	u1	7,7765	2,6063	0,17506	-0,04444	-0,01143
u2	u2	-7,9662	0,43674	-0,11692	-0,0139	-0,00856
u4	u4	-7,7058	1,0746	0,17512	0,15914	0,014819
u5	u5	3,2827	0,43067	0,16264	-0,06876	0,071122